SPATIAL MODELING AND ANALYSIS OF VEHICULAR NETWORKS

A Dissertation

Submitted to the Graduate School
of the University of Notre Dame
in Partial Fulfillment of the Requirements
for the Degree of

Doctor of Philosophy

by

Jeya Pradha Jeyaraj

Martin Haenggi, Director

Graduate Program in Electrical Engineering
Notre Dame, Indiana
December 2021

SPATIAL MODELING AND ANALYSIS OF VEHICULAR NETWORKS

Abstract

by

Jeya Pradha Jeyaraj

Through vehicle-to-vehicle communication (V2V), vehicles can exchange information required for safety alerting other vehicles in their vicinity. Due to the mission-critical nature of safety applications, high reliability is a key requirement of V2V systems. Reliability is the probability that a V2V link can sustain a certain target data rate. It depends on the locations of transmitting and receiving vehicles and interferers, street geometry, and wireless medium. The reliability results obtained by conducting a large number of trials in the real world fail to provide crisp insights into the effects of network design parameters on reliability despite their high costs. We aim to complement/reduce these large-scale experiments by applying mathematical tools from stochastic geometry to (i) model vehicular networks, and (ii) analyze the reliability of V2V communication. In particular, we introduce the notion of model equivalence, which shows that the number of models can be drastically reduced to only a few classes. Also, we prove that many existing models can be substantially simplified to the proposed transdimensional models with virtually no loss in accuracy. Furthermore, we investigate the meta distribution (MD) of the signal-to-interference ratio (SIR), which is a much sharper performance metric than the SIR distribution that is usually studied. The SIR MD answers questions such as 'what fraction of the V2V links are 99% reliable if the target data rate is 10 Mbps?' This metric is the key towards designing V2V networks with guaranteed reliability.

With respect to the broadcast communication, we formulate the binned meta distribution of the SIR, which answers questions like 'what fraction of the V2V links that are in the distance range of 100-200 m are 99% reliable if the target data rate is 10 Mbps?' The binned variant of the MD provides insights into the effective range for reliable broadcast communication. Having the binned SIR MD as the performance metric, we compare different stochastic geometry models to system-level simulations. The Poisson point process-based vehicular networks rank the highest in terms of analytical tractability with loose approximations to system-level simulations; the Matérn hard-core process-based models provide tight approximations but are highly intractable; the determinantal point process-based models rank the highest in terms of accuracy with good tractability.

To Sanket

ACKNOWLEDGMENTS

The last five years have been a personal journey as much as a professional one. My Ph.D. was a roller coaster ride with the deepest downfalls in my life so far. I was sick so often due to the different weather conditions from my homeland and lifestyle. I got very anxious that I was losing time recuperating from sickness and wasting the opportunity to do great work. My self-doubt increased over the years, and I started feeling like an impostor. Fortunately, some people pushed me to ride upward and eventually finish the Ph.D. I would like to acknowledge those wonderful people here.

I express my sincerest gratitude to my advisor, Prof. Martin Haenggi, for his consistent support and guidance. He taught me the importance of doing fundamental research and identifying one, using mathematics to describe ideas clearly and improve the quality of writing. I gratefully acknowledge his patience in providing crisp comments on multiple versions of an article or a paper. Sometimes, irrespective of any number of drafts I wrote, I would not be sure whether it was good enough. Many thanks to him for asking for the status updates. If not for them, the journal articles would have taken even longer to get published. I appreciate the conversations with him over the years and his constructive directions, which have shaped my thought process and provided different perspectives on research areas.

Thanks to my committee members Prof. Nicholas Laneman, Prof. Yih-Fang Huang, and Prof. Christian Poellabauer for their encouragement and insightful comments during the candidacy and defense.

I gratefully acknowledge the National Science Foundation and Toyota Motor North America for funding my research.

I enjoyed the classes and exams at Notre Dame, particularly, those of Prof. Ken Sauer, Prof. Martin Haenggi, and Prof. Bertrand Hochwald in the EE department, and Prof. Jun Li and Prof. Hyungsak Tak in the ACMS department. I am grateful to them for providing a wonderful learning experience and asking concept-oriented insightful questions. Special thanks to Prof. Li for his teaching style that nurtured my interest in applied mathematics and statistics, and assignments that were more like fun real-world data puzzles than mundane homework problems.

I cherished my summer internships, thanks to my colleagues—Hongsheng Lu, Ahmed Hamdi Sakr, and John Kenny at Toyota Infotech Labs, and Gabi Sarkis and Dan Vassilovski at Qualcomm. Working with them helped me to get the bigger picture of the vehicular network industry as well as the nuances between academia and industry. Their words of appreciation for my internship work have boosted my morale to do good research and eschew any reservations I had in my mind about my capabilities.

I gratefully acknowledge the assistance from Christine Broadbent Landaw, EE graduate studies coordinator. I could always rely on her for any administrative queries and the right directions to complete the work.

Outside academics, a person who had a profound impact on me is my gym instructor, Indiana. I am indebted to her for the motivation and positivity she brings in her classes and afterward. She says 'Don't quit on me' towards the last set of the exercises. I could barely breathe at times but would still pull through for her. Those words echoed in my ears not only during gym sessions but also during my hard times.

Thanks to the nurses and doctors in the University health center for being very kind and caring. They have reminded me that if we can show love for someone else during their difficult times, we can love ourselves too in our bad times. I am grateful for the positive impact coronavirus brought in my life, how much ever insane it might sound. It gave me time to know and love myself better.

I had great pleasure in my pastimes with my friends Uma, Keerthi, Krishna, Etika, Obaid, Soumyadip, Atul, and Shinjini. Thanks for having kept me sane with all our crazy game nights and fun-filled chats. I am particularly grateful to Keerthi, Uma, and Vijay, for being like a family and filling me with yummy Indian food. Many thanks to Ke Feng and Wei Zheng for being supportive and our conversations about the research lifestyles that have pointed me to the areas I need to improve. I appreciate my colleagues and mentors from the graduate society of women engineers and orientation committee for enriching my experiences at Notre Dame with thought-provoking seminars and initiatives.

I express my deepest gratitude to Sanket, my husband, for believing in my potential more than me. If not for his kindness, positivity, and encouragement, I would not have completed my Ph.D. Thanks to my wonderful family for showering me with love and affection and being my pillars of strength.

CONTENTS

Acknowledgments iii

List of Figures ix

List of Tables xiv

Acronyms and Notation xv

Chapter 1: Introduction 1
1.1 Spatial Modeling 2
1.2 Outline of the Thesis 3

Chapter 2: Vehicular Networks on Orthogonal Street Systems 7
2.1 Network Model 7
2.2 Success Probability 12
2.2.1 Interference from the Same Street 12
2.2.2 Interference from a Different Street 13
2.2.3 Success Probabilities for General and Intersection Users 14
2.3 Understanding Vehicular Network Behavior 15
2.3.1 Asymptotic Reliability Analysis 15
2.3.2 Comparison to Poisson Point Processes 18
2.4 Results and Discussion 20
2.5 Conclusions 21

Chapter 3: Cox Models for Vehicular Networks 24
3.1 System Model 26
3.1.1 General Framework 26
3.1.2 Vehicular Network Models 27
3.1.3 Performance Metric and Types of Vehicles 29
3.1.4 Equivalence 32
3.1.5 Further Notation 32
3.2 Properties of Vehicular Networks 33
3.3 Success Probabilities 38
3.4 Equivalence of Spatial Models 43
3.4.1 OG-PPP and PLP-PPP 43

3.4.2 PSP-PPP and PLP-PPP . . . 43
3.4.3 PLM-PPP and PSP-PPP . . . 45
3.4.4 Equivalence Under Random Link Distances . . . 49
3.4.4.1 PLP-PPP vs. OG-PPP . . . 49
3.4.4.2 PSP-PPP vs. PLP-PPP . . . 49
3.4.4.3 PLM-PPP vs. PSP-PPP . . . 50
3.5 Conclusions . . . 51

Chapter 4: Transdimensional Models for Vehicular Networks . . . 52
4.1 The Transdimensional Poisson Point Process . . . 52
4.2 SIR Meta Distribution . . . 55
4.2.1 Related Work . . . 55
4.2.2 Formulation . . . 57
4.3 The Transdimensional Approach to the PLP-PPP . . . 58
4.3.1 Derivation of Moments . . . 58
4.3.2 First-Order Moment Analysis for the PLP-PPP . . . 61
4.3.3 Comparison of First-Order Moments . . . 62
4.3.4 Comparison of Higher-Order Moments and SIR Meta Distributions . . . 67
4.3.5 Presence of Shadowing . . . 70
4.3.6 Beta Approximation of the SIR Meta Distribution . . . 71
4.4 The Transdimensional Approach to the PSP-PPP . . . 74
4.4.1 First-Order Moments: PSP-PPP vs. TPPP . . . 74
4.4.2 SIR Meta Distribution: PSP-PPP vs. TPPP . . . 75
4.5 Application to Congestion Control . . . 77
4.5.1 Success Probability-Based Congestion Control . . . 77
4.5.2 Beta Approximation-Based Congestion Control . . . 79
4.6 Extension to Non-Poisson Point Processes . . . 82
4.6.1 The Transdimensional Approach to the PLP-MHCP . . . 84
4.6.2 The Transdimensional Approach to the PSP-MHCP . . . 86
4.7 Conclusions . . . 86

Chapter 5: Determinantal Point Processes for Vehicular Networks: Modeling, Analysis, and System-level Simulations . . . 89
5.1 Related Work . . . 91
5.2 ns-3 and Stochastic Geometry . . . 92
5.3 Baseline Network Models and Determinantal Point Processes . . . 95
5.3.1 Poisson Point Processes . . . 96
5.3.2 Matérn Hard-Core Processes . . . 96
5.3.3 Determinantal Point Processes . . . 96
5.4 Properties and Construction of DPPs . . . 99
5.4.1 Properties . . . 99
5.4.2 Construction of L-Matrix . . . 100
5.4.2.1 Quality Factor . . . 101

5.4.2.2 Similarity Matrix . . . 102
5.5 Binned Meta Distribution of the SINR . . . 102
5.5.1 Signal-to-Interference-plus-Noise Ratio . . . 103
5.5.2 Conditional Success Probability . . . 103
5.5.3 Formulation of the Binned Meta Distribution of the SINR . . . 103
5.6 Key Results . . . 104
5.7 Results and Discussion . . . 107
5.7.1 ns-3 vs. DPP . . . 108
5.7.1.1 Distance to the n-th Nearest Transmitter . . . 110
5.7.1.2 Binned SINR MD . . . 110
5.7.2 ns-3 vs. Baseline Models . . . 110
5.8 2D DPPs for Vehicular Networks . . . 112
5.9 Conclusions . . . 117

Chapter 6: Summary and Future Work . . . 118
6.1 Summary . . . 118
6.2 Future Directions . . . 121

Appendix A: Proofs of Chapter 3 . . . 123
A.1 Proof of Lemma 3.4 . . . 123
A.2 Proof of Lemma 3.5 . . . 125
A.3 Proof of Lemma 3.6 . . . 126
A.4 Proof of Theorem 3.1 . . . 126
A.5 Proof of Proposition 3.1 . . . 128
A.6 Proof of Proposition 3.2 . . . 130
A.7 Proof of Proposition 3.3 . . . 131
A.8 Proof of Proposition 3.4 . . . 132
A.9 Proof of Lemma 3.8 . . . 133
A.10 Proof of Lemma 3.9 . . . 134

Appendix B: Proofs of Chapter 4 . . . 135
B.1 Proof of Theorem 4.1 . . . 135
B.2 Proof of Corollary 4.2 . . . 137
B.3 Proof of Theorem 4.3 . . . 138
B.4 Proof of Theorem 4.4 . . . 139

Appendix C: Proofs of Chapter 5 . . . 142
C.1 Proof of Lemma 5.1 . . . 142
C.2 Proof of Lemma 5.2 . . . 142

Bibliography . . . 144

LIST OF FIGURES

1.1 A section of (a) Manhattan (b) Boston shot using Google Earth. Streets are highlighted in blue. 2
1.2 Snapshots of (a) regular point process (b) cluster point process (c) PPP on orthogonal grid (d) PPP on Poisson line process. Lines represent streets and 'o' represent vehicles. 4

2.1 A snapshot of the SG-PPP. Lines represent streets and 'o' represent vehicles. $\lambda = 1$, and $s = 1$. 9
2.2 Nearest neighbor distance distributions $G(r)$ for SG-PPP and 2D PPP. The equation number is given in the parentheses. $\lambda = 2$, $p = 1$, and $s = 1$. 19
2.3 Success probabilities of the typical general and intersection vehicles in the SG-PPP. The equation number of the success probability is given in the parentheses in the legend. 20
2.4 Success probability of the (a) typical general vehicle and (b) typical intersection vehicle in the SG-PPP vs. success probability of the typical vehicle in 1D and 2D PPPs. The equation numbers of the success probabilities are given in the parentheses in the legends. 22

3.1 Part of Rome's city center. Visual inspection shows a mean street length of about 250 m and many T-junctions. 25
3.2 Snapshots of vehicular networks: (a) OG-PPP (b) PLP-PPP (c) PSP-PPP and (d) PLM-PPP. Lines or sticks denote the streets, and '$\circ$' denote the vehicles. The stick lengths in (c) are Rayleigh distributed with parameter 2. 30
3.3 (a) Fitting $h\hat{f}_H(h)/\mathbb{E}[H]$ to the half-lengths of the streets that pass through the typical vehicle in the PLM. (b) Mean and variance of number of neighbors to the typical general vehicle in the PLM-PPP vs. PSP-PPP with $f_H(h) = \hat{f}_H(h) = 2bh\exp(-bh^2)$. $\mu = 0.01$ and $\lambda = 0.3$. The value of b corresponding to $\mu = 0.01$ is 0.0103. The intensity of 2D PPP is $2\lambda\mu\mathbb{E}[H]$, which is the 2D intensity of the PLM-PPP/PSP-PPP. 35
3.4 Comparison of (a) mean distance from the typical general vehicle to its n-th nearest neighbor and (b) nearest-neighbor distance distributions in the PLM-PPP and PSP-PPP given by (3.10) with $f_H(h) = \hat{f}_H(h) = 2bh\exp(-bh^2)$, where $b = 1.04$ for $\mu = 1$, and 0.0103 for $\mu = 0.01$. $\lambda = 0.3$. 37

3.5 Success probabilities of the typical general and intersection/T-junction vehicles in the (a) PLP-PPP (b) PSP-PPP and (c) PLM-PPP. $\lambda p = 0.3, D = 0.25$, $\alpha = 4$, $\mu = 2$, 0.1, and 0.3 for the PLP, PSP, and PLM, respectively. $f_H^{\mathrm{PSP}}(h) = \delta(h-10)$. The equation numbers are given in parentheses in the legends. 42
3.6 Reparametrization of the PSP. The stick $S(y, \varphi, h) \in \Xi_{\mathrm{S}}$ is extended to form a line $S'(r, \phi, q)$. The perpendicular from the extended stick is at a distance r from o and forms an angle ϕ with the $x-$axis. . . . 44
3.7 Success probability of the typical general vehicle in the PLM-PPP vs. that in the PSP-PPP-based approximation given by (19) with $f_H(h) = 2bh\exp(-bh^2)$, where $b = 1.04$ for $\mu = 1$, and 0.0103 for $\mu = 0.01$. $\lambda p = 0.3$, $D = 0.25$, and $\alpha = 4$. 46
3.8 Success probability of the typical general vehicle in the (a) PSP-PPP (b) PLM-PPP (c) PLP-PPP vs. that of the typical vehicle in 1D and 2D PPPs. $\lambda p = 0.3, D = 0.25$, $\alpha = 4$, $\mu = 0.1$, 0.3, and 2 for the PSP, PLM, and PLP, respectively. $f_H^{\mathrm{PSP}}(h) = \delta(h-10)$. The equation numbers are given in parentheses in the legends. 48
3.9 Success probabilities of the typical general vehicle that receives a message from its nearest neighbor. $\lambda p = 0.5$ and $\alpha = 4$. $f_H(h) = \hat{f}_H(h) = 2bh\exp(-bh^2)$, where $b = 1.04$ for $\mu = 1$, and 0.0103 for $\mu = 0.01$. . . 50

4.1 Snapshot of the TPPP with respect to the typical vehicle in the PLP-PPP is shown in (a), where $m\lambda/2 = \lambda_2 = 0.1$. Snapshots of the TPPP with respect to the typical general and intersection vehicles in the PSP-PPP are shown in (b) and (c), respectively, where $\lambda = 0.3$, $\mu = 0.01$, $f_H(h) = 2ch\exp(-ch^2)$ with $c = 0.01$, and $\lambda_2 = 2\lambda\mu\mathbb{E}[H]$. Line/stick denotes a street and 'o' denotes a vehicle. 54
4.2 The histogram of the empirical probability density function of the link success probability for transmit probabilities $p = 1/10$ and $p = 1$. Both cases have the same mean success probability of 0.5944, but we see a different distribution of link success probabilities for different values of λ and p. For $p = 1/10$, the link success probabilities mostly lie between 0.4 and 0.8 (concentrated around their mean), while for $p = 1$, they are spread much more widely. Taken from [1]. 56
4.3 Comparison of success probabilities of the (a) typical general vehicle and (b) typical intersection vehicle in the PLP-PPP to that of the typical vehicle in 1D and 2D PPPs. $\mu = 2$, $\lambda = 1$, $p = 0.3$, $D = 0.25$, and $\alpha = 4$. The equation numbers are given in the parentheses in the legends. 63
4.4 Comparison of normalized mean squared distances to the n-th nearest neighbor from the typical general vehicle at the origin in the PLP-PPP and TPPP. $\lambda = \mu = 1$. 65

4.5 Difference between the success probabilities of the typical general vehicle in the PLP-PPP (4.7) and TPPP (4.10) as a function of λp and $D^2\theta^\delta$. $\mu = 0.204$, $\delta = 2/\alpha$, and $\alpha = 4$. The maximum difference of 0.0404 corresponding to the pair $(0.12, 10.1)$ is highlighted using a red filled circle. 66
4.6 Outage probabilities of the typical general vehicle in the PLP-PPP, TPPP, and that of the typical vehicle in a 1D PPP. $\mu = 1$ and $\alpha = 4$. The equation numbers corresponding to the success probability are given in the parentheses in the legend. 66
4.7 Moments of the conditional success probabilities for different SIR thresholds. $\mu = 1$, $\lambda = 1$, $p = 0.3$, $D = 0.25$, and $\alpha = 4$. The equation numbers of the moments M_b are given in the parentheses in the legends. 68
4.8 SIR meta distributions for different reliabilities. $\mu = 1$, $\lambda = 1$, $p = 0.3$, and $D = 0.25$. The equation numbers of the moments required to evaluate $\bar{F}_{P_m}(\theta, x)$ are given in the parentheses in the legends. 69
4.9 SIR meta distributions for the PLP-PPP, TPPP and their beta approximations. $\mu = 1$, $\lambda = 1$, $p = 0.3$, $\alpha = 4$, and $D = 0.25$. The transition at $x = 1-p$ is highlighted by the dashed line. The equation numbers in the parentheses in the legends either refer to the moments or expression of $\bar{F}_{P_2}(\theta, x)$. 73
4.10 Success probabilities of the typical general ((a) and (b)) and intersection ((c) and (d)) vehicles in the PSP-PPP (3.18) and the corresponding TPPP (4.20). $f_H(h) = 2ch\exp(-ch^2)$ with $c = \mu$, $D = 0.25$, and $\alpha = 4$. 76
4.11 Comparison of exact SIR meta distribution for the PSP-PPP and its approximations. $f_H(h) = 2ch\exp(-ch^2)$ with $c = 1$, $\mu = 1$, $\lambda = 1$, $p = 0.3$, $\alpha = 4$, and $D = 0.25$. The transition at $x = 1 - p$ is highlighted by the dotted line. The beta approximation to $\bar{F}_{P_2}(\theta, x)$ is given by (4.19). 77
4.12 (a) Pairs of $(1/\lambda, p)$ such that $p_2(\lambda, p) = q$ for $q = 0.1, 0.5, 0.8, 0.9$ in the TPPP. $\theta = 0$ dB, $D = 0.25$, $\mu = 1$, and $\alpha = 4$. The equation numbers of p_2 are given in the parentheses in the legends. (b) Histograms of conditional link success probabilities for different combinations of $(1/\lambda, p)$ that yield $p_2 = 0.9$ in (a). 78
4.13 Pairs $(1/\lambda, p)$ such that $\bar{F}_{P_2}(1, x, \lambda, p) = q$ for $q = 0.1, 0.4, 0.7$, and 0.9. $D = 0.25$, $\mu = 1$, and $\alpha = 4$. 80
4.14 Pairs of $(1/\lambda, p)$ that satisfy the target performance given in the legends. The range of p_2 listed for each combination $(\bar{F}_{P_2}, x)$ is obtained by finding the success probabilities for different values of $(1/\lambda, p)$ sampled along the contour that satisfies $\bar{F}_{P_2}(1, x, \lambda, p) = 0.9$ for a given x. $D = 0.25$, $\mu = 1$, and $\alpha = 4$. 81

4.15 Comparison of exact SIR MD for the PLP-PPP and beta-approximated SIR MD for the TPPP. For each λ, p is chosen according to the beta approximation-based congestion control scheme such that the SIR MD for the TPPP equals 0.9. $\mu = 1$, $D = 0.25$, and $\alpha = 4$. The equation numbers in the parentheses in the legends either refer to the moments or expression of $\bar{F}_{P_2}$. 82
4.16 Realizations of the (a) PLP-MHCP with $\mu = \lambda = 0.3$ (b) PSP-MHCP with $\mu = 0.01$, and $\lambda = 0.1$. $r_{\mathrm{M}} = 2$. Lines/sticks represent streets, and 'o' represent vehicles. The disks around the vehicles are of radius $r_{\mathrm{M}}/2$. 84
4.17 Snapshots of the TNPP with respect to the a) typical general vehicle and b) typical intersection vehicle in the PLP-MHCP. $\lambda = \mu = 0.3$, and $r_{\mathrm{M}} = 2$. The estimated 2D intensity is $\lambda_2 = 0.035$. Lines represent streets, and 'o' represent vehicles. The disks around the vehicles are of radius $r_{\mathrm{M}}/2$. 85
4.18 Comparison of success probabilities of the typical general vehicle in the PLP-MHCP, and the corresponding TNPP-I and TNPP-II. $r_{\mathrm{M}} = 0.5$. The estimated 2D intensities of the PLP-MHCP for $\mu = 0.5$, and $\lambda = 0.15, 0.3, 0.6$, and 2 are $0.067, 0.117$, 0.193, and 0.324, respectively. When $\mu = 2$, $\lambda_2 = 0.248, 0.42, 0.632$, and 0.872. 85
4.19 Snapshots of the PSP-MHCP with respect to the a) typical general vehicle and b) typical intersection vehicle at the origin. $\mu = 0.01$, $\lambda = 0.1$ and $r_{\mathrm{M}} = 2$. $f_H(h) = 2bh\exp(-bh^2)$ with $b = 0.0103$. The estimated 2D intensity is $\lambda_2 = 0.013$. Sticks represent streets, and 'o' represent vehicles. The disks around the vehicles are of radius $r_{\mathrm{M}}/2$. 87
4.20 Comparison of success probabilities of the typical general vehicle in the PSP-MHCP, and the corresponding TNPP-I and TNPP-II. $f_H(h) = 2bh\exp(-bh^2)$. The values of b corresponding to $\mu = 1$ and 0.01 are 1.08 and 0.0103, respectively. $r_{\mathrm{M}} = 0.5$. The estimated 2D intensities of the PSP-MHCP for $\mu = 0.01$, and $\lambda = 0.15, 0.3$, and 2 are $0.023, 0.044$, and 0.133, respectively. When $\mu = 1$, $\lambda_2 = 0.218, 0.375$, and 0.893. 87

5.1 Comparison of different similarity kernels. $\sigma = 100$. 101
5.2 (a) n-th nearest-transmitter distance distributions (b) Mean number of transmitters within distance r of the typical vehicle (c) Comparison of the SINR MDs for ns-3 and DPP for different bin indices. S is Gaussian. $\sigma^* = 200$ and $\boldsymbol{\upsilon}^* = [-1.5543, 0.0011]$. They are obtained by optimizing (5.26). The distance bin is of length 50 m. The conditional success probability required to evaluate the binned SINR MD/success probability for the DPP is given by (5.19). 111

5.3 ns-3 vs. DPP. Figs. (a)-(c) show the binned SINR MD and (d) shows the binned success probability for different N and bin indices. S is Gaussian. The DPP parameters that match the SINR MD in ns-3 for (a) $N = 500$ are $\nu = -0.8501$ and $\sigma = 395$, (b) $N = 250$ are $\nu = -1.1945$ and $\sigma = 415$, and (c) $N = 50$ are $\nu = 280$ and $\sigma = -1.4263$. The distance bin is of length 50 m. The unit of intensity λ is per meter. The conditional success probability required to evaluate the binned SINR MD/success probability for the DPP is given by (5.19). 113

5.4 ns-3 vs. PPP. Figs. (a)-(c) show the binned SINR MD and (d) shows the binned success probability for different traffic intensities and bin indices. The transmit probability is $p = 0.0055$. The distance bin is of length 50 m. The unit of intensity λ is per meter. The equation numbers corresponding to the binned SINR MD and success probability are given in the parentheses in the legends. 114

5.5 ns-3 vs. MHCP. Figs. (a)-(c) show the binned SINR MD and (d) shows the binned success probability for different traffic intensities and bin indices. The distance bin is of length 50 m. The hard-core distance r_{M} that approximates ns-3 are 425.1 m, 718.3 m, and 1349.7 m for $\lambda = 1/8, 1/16$, and $1/32$ per meter, respectively. 115

5.6 PLP-PPP vs. 2D DPP. Figs. (a) and (b) show the binned SINR MD and success probability, respectively. The distance bin is of length 50 m. $\alpha = 2.5$. $N = 1000$. Similarity matrix is Gaussian with $\sigma = 100$, $\nu = -1.8526$. The rest of the parameters are given in Table 5.1. . . . 116

A.1 Fitting the (a) CCDF and (b) PDF of the half-lengths to that of the Rayleigh distribution. $\mu = 0.01$. 124

A.2 Realizations corresponding to cases (1a), (1b), (2a), and (2b). The midpoints of the streets are highlighted using filled '$\circ$'. The points of intersection of the street on $b(o, r)$ are at distances u_i, $i \in \{1, 2\}$, from the midpoint of the street. u_i in the cases (1b) and (2b) refers to u_1 or u_2. 127

LIST OF TABLES

3.1 Conditions for Equivalence between the Spatial Models 47

5.1 Simulation Parameters 109

ACRONYMS AND NOTATION

CSMA/CA	Carrier-sense multiple access with collision avoidance
DPP	Determinantal point process
DSRC	Dedicated short-range communications
LBT	Listen before talk
LTE	Long-term evolution
MD	Meta distribution
NR	New radio
PLP	Poisson line process
PLM	Poisson lilypond model
PPP	Poisson point process
PSP	Poisson stick process
PLP-DPP	DPP on a PLP
PLP-PPP	PPP on a PLP
PLM-PPP	PPP on a PLM
PSP-PPP	PPP on a PSP
SG-PPP	PPP on a square grid
SIR	Signal-to-interference ratio
SINR	Signal-to-interference-plus-noise ratio
TPPP	Transdimensional Poisson point process
TNPP	Transdimensional non-Poisson point process
V2V	Vehicle-to-vehicle
V2X	Vehicle-to-everything

Φ_d	d-dimensional PPP
λ_d	Intensity of Φ_d
D	Distance between the typical vehicle and its transmitter
m	Order of the typical vehicle
θ	SIR/SINR threshold
p	Transmit probability
α	Path-loss exponent
p_m	Success probability
H	Half-length of the street in the PSP
$\mathcal{S}$	Street system
μ	Street intensity
λ	Vehicle intensity on each street
$\mathcal{V}$	Vehicular point process
$\mathcal{V}_o^m$	Vehicular point process on the typical vehicle's streets
$\mathcal{V}_!$	Vehicular point process on all but typical vehicle's streets
I	Total interference with respect to $\mathcal{V}$
I_o^m	Interference with respect to $\mathcal{V}_o^m$
$I_!$	Interference with respect to $\mathcal{V}_!$
P_m	Conditional success probability
$M_{b,m}$	bth moment of P_m
$\bar{F}_{P_m}$	SIR/SINR MD
x	SIR/SINR MD reliability threshold
$\mathcal{B}_u$	u-th bin

CHAPTER 1

INTRODUCTION

Nearly 1.3 million fatalities occur in road crashes each year, with 90% caused due to human errors [2]. National highway traffic safety administration (NHTSA) of the United States estimates that the vehicle-to-vehicle (V2V) communication can eliminate 80% of the accidents [3]. V2V can alert vehicles about the events happening in their vicinity that even the best sensors in vehicles may fail to detect. This promising technology can support road safety services such as safer autonomous driving, broadcasting hazard warnings and roadblocks, cooperative adaptive cruise control, platooning, and infotainment services.

Due to the mission-critical nature of safety applications, high reliability is a key requirement of V2V systems. In this context, an important question is 'what is the maximum density of vehicles on the street that can achieve a certain reliability?' The answer depends on the street geometry, relative locations of vehicles and infrastructure nodes, and the wireless signal propagation. The answer is hard to determine using system-level simulations and large-scale experiments as they require conducting multiple trials with a large number of vehicles in different traffic scenarios for different street systems. Hence designing and planning V2V systems only based on extensive system-level simulations or experiments fails to provide insights into the key dependencies and trade-offs between the network parameters.

The goal of our research is to analyze the behavior of reliable vehicular networks and obtain crisp insights that serve as an alternative or companion to large-scale simulations and experiments. To this end, we need spatial models that closely capture

(a) (b)

Figure 1.1: A section of (a) Manhattan (b) Boston shot using Google Earth. Streets are highlighted in blue.

different street systems and uncertainties in the locations of vehicles.

1.1 Spatial Modeling

Some street systems are more regular as in Manhattan, while some are less regular as in Boston (Fig. 1.1). Furthermore, the vehicle locations are subject to considerable uncertainty. As a result, studying a specific instance of the network (traffic pattern) is insufficient to analyze and design the vehicular network. It would be helpful if we could make statistical statements about classes of likely network realizations. In essence, we need spatial models that can characterize different street systems with varying levels of regularity and uncertain (random) vehicle locations.

Stochastic geometry [4] provides the mathematical toolsets that permits the modeling and analysis of random spatial patterns. It yields statistical features of the ensembles of vehicular network realizations and analytical results that can be evaluated quickly to get useful design insights. To be concrete, below we give a few examples of the mathematical tools from stochastic geometry to model vehicle locations and streets.

A point process is a random collection of points, where a point can represent a vehicle, pedestrian, an infrastructure node, or any other node. A realization of a

point process of vehicles can be considered equivalent to a traffic pattern at a time instant. There exist different types of point processes pertaining to the characteristics of point patterns (alternatively, different traffic patterns). For example, Fig. 1.2 shows snapshots of three different point processes: (a) a regular point process, (b) a cluster point process, and (c) a Poisson point process (PPP). In a regular point process, there is a minimum spacing between two points, which can be used to represent vehicle locations on a highway during heavy traffic. In a cluster point process, points tend to attract each other, which can be used to characterize the vehicle locations near intersections.

A PPP corresponds to a point pattern which is in between those produced by regular and cluster point processes. The advantage of the PPP is its analytical tractability. It has been widely used in the modeling of cellular, device-to-device (D2D), and machine-to-machine (M2M) networks [5]. Real-world wireless networks are hard to describe using mathematical models, let alone analyze. PPPs with their appealing feature of analytical tractability come in handy in those situations, and they were shown to provide lower bounds on the network performance in many cases, even though they cannot exactly characterize the real-world wireless networks [5, 6, 7].

A city with a regular street system like Manhattan (Fig 1.1a) can be depicted by an orthogonal grid with variable spacing between the streets Fig. 1.2c. The Poisson line process used to model the lines (streets) in Fig. 1.2d can be used for cities with irregular street systems. We discuss further modeling of vehicular networks in the following chapters in detail along with the analyses.

1.2 Outline of the Thesis

In Chapter 2 [8, 9], we debunk the claim in [10] that the vehicles can be modeled as random points on a 2D plane using PPPs. We highlight the need for modeling the street geometry and show that without it, we will not be able to fully understand the

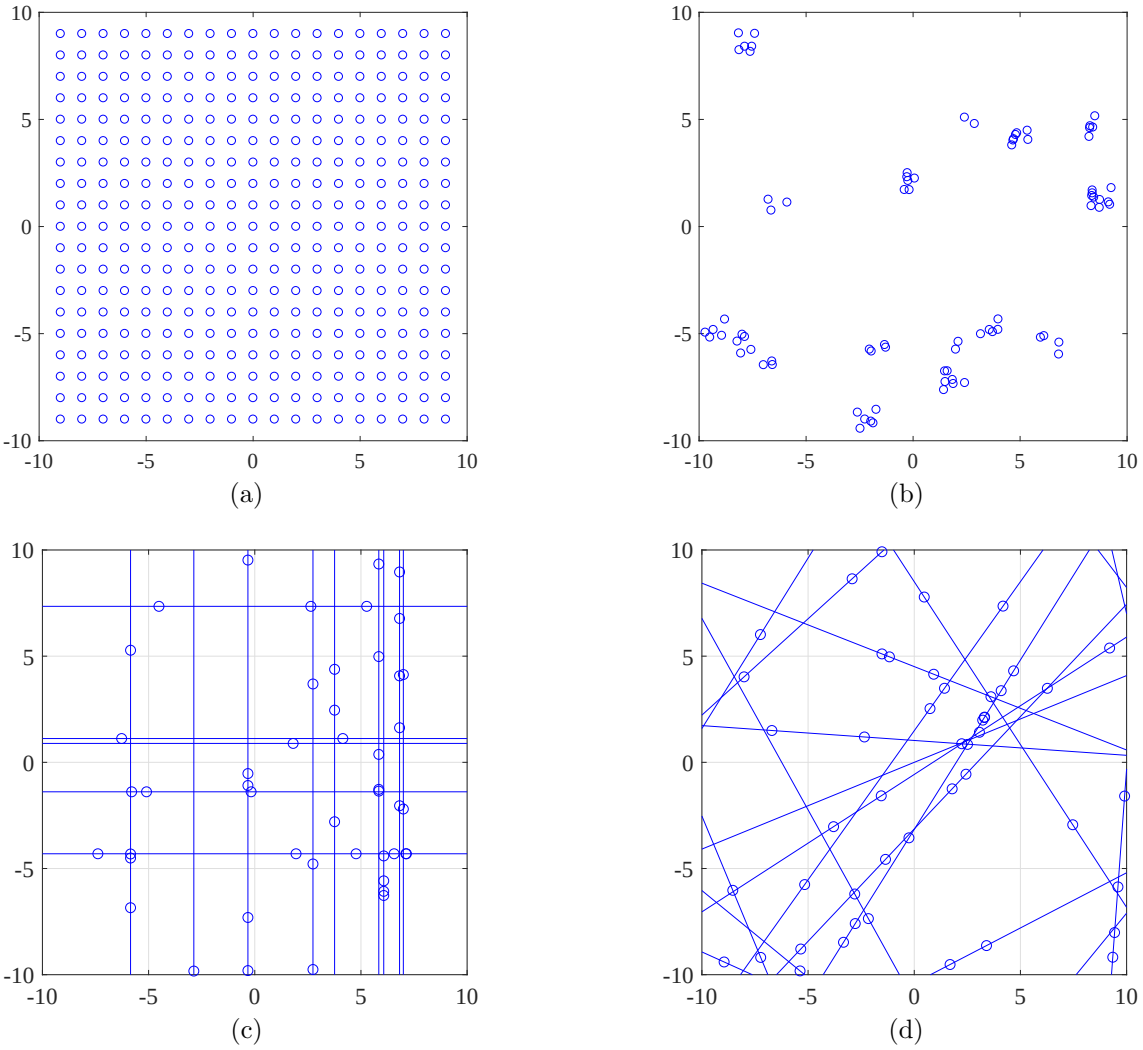

Figure 1.2: Snapshots of (a) regular point process (b) cluster point process (c) PPP on orthogonal grid (d) PPP on Poisson line process. Lines represent streets and 'o' represent vehicles.

vehicular network behavior.

We introduce a general framework for modeling vehicular networks in Chapter 3 [11]. This framework enables us to model street systems in different geographical regions where the streets can be of different lengths and orientations and form intersections and T-junctions. We evaluate the probability that a vehicle at a general location, intersection, or a T-junction can successfully receive a message from a transmitter at a certain distance. Further, we introduce the notion of equivalence. Instead of analyzing a distinct street geometry for each city, we can find the street systems that behave qualitatively the same way and can thus be investigated jointly. By establishing such equivalence between the street systems, we can focus on a specific subset of street systems, which will significantly reduce the computation time and costs associated with designing and planning.

The calculations of the performance metrics can become unwieldy at times especially due to the random modeling of streets as well as vehicle locations. In Chapter 4 [12, 13], we introduce transdimensional models that are an alternative for the established more complicated vehicular network models. The transdimensional models focus only on certain aspects of the vehicular networks but can provide insights into the network behavior as well as the complicated (much less tractable) models. The key advantage is that the transdimensional models lend themselves to simpler and tractable analytical expressions.

The Poisson-based vehicular networks provide loose approximations or lower bounds to system-level simulations. Here, the transmitting vehicles can be arbitrarily close. The hard-core models guarantee a minimum distance between the transmitting vehicles but they are difficult to analyze. In Chapter 5, we explore a middle route between PPPs and hard-core point processes for modeling vehicular networks. In particular, we investigate determinantal point processes whose structure facilitates *simalysis* [14], a blend of simulation and analysis, to study the vehicular network

behavior. Further, we revisit the question of whether we need to model the streets if we model the locations of transmitting vehicles using determinantal point processes.

CHAPTER 2

VEHICULAR NETWORKS ON ORTHOGONAL STREET SYSTEMS

Some of the prior works in the literature [15, 16, 17, 18, 19] focus on analyzing the vehicular communication on a single street with one or multiple lanes. Though the insights into the vehicular network behavior provided by the single-street models are certainly useful, they are insufficient to understand the overall network behavior especially in dense urban areas, and at intersections. It is shown in [20] that the proximity of a vehicle to an intersection reduces the chances of successful packet reception, emphasizing the need to model intersections. Another approach is to model the vehicle locations as random points on the plane using a 2D PPP neglecting the street geometry [10]. The analysis of GPS traces of taxis in Beijing performed by [21] demonstrates that the taxi locations do not form a 2D PPP, invalidating the model in [10]. The pertinent question is whether we need a vehicular network model that accounts for the street geometry or whether a 1D model is sufficient to understand the vehicular network behavior. In this chapter, we focus on answering this question through a simple model—an orthogonal grid-based vehicular network.

2.1 Network Model

We consider a vehicular network model that consists of a square (orthogonal) grid formed by horizontally and vertically oriented streets. The transmitting vehicles on each street form independent 1D homogeneous PPPs with intensity λ. Each vehicle broadcasts with probability p following the slotted ALOHA protocol. Then

the intensity of active transmitters on each street in each time slot is λp. We formally define the *PPP on a square grid* (SG-PPP) below.

Definition 2.1 (SG-PPP)**.** *Let*

$$L(\ell, \varphi) \triangleq \{(x, y) \in \mathbb{R}^2 \colon x \cos\varphi + y \sin\varphi = \ell\}$$

denote a line in $\mathbb{R}^2$*, where* $\ell \in \mathbb{R}$ *is the location and* $\varphi \in [0, \pi)$ *is the direction of the line. For example, the* x *axis* $(\mathbb{R}, 0)$ *is* $L_0^{\pi/2}$*, and the* y *axis* $(0, \mathbb{R})$ *is* L_0^0*.*

Let $\mathcal{P}_\ell^\varphi$ *denote a 1D PPP of intensity* λ *on the line* $L(\ell, \varphi)$*. For different* ℓ *or* φ*, the processes are independent. Then*

$$\mathcal{P}_{\mathbb{Z}} \triangleq \bigcup_{k \in \mathbb{Z}} \mathcal{P}_k^0 \cup \mathcal{P}_k^{\pi/2}$$

is a union of horizontally and vertically oriented 1D PPPs, such that exactly one of the coordinates of each point is an integer.

To make the model stationary and of variable intensity with respect to the inter-street spacing s*, the SG-PPP model is defined as*

$$\mathcal{V} \triangleq s(\mathcal{P}_{\mathbb{Z}} + U),$$

where $s > 0$ *and* U *is uniform on* $[0, 1)^2$*.*

Fig. 2.1 depicts the model. We can also obtain a grid of 1D PPPs by quantizing either of the coordinates of each point of a 2D PPP with equal probability.

Definition 2.2 (SG-PPP—Alternate Definition)**.** *Let* $q_{\mathbb{Z}} \colon \mathbb{R}^2 \mapsto \mathbb{R}^2$ *be the random quantization function defined as*

$$q_{\mathbb{Z}}((u, v)) \triangleq Q_{(u,v)}(u, \lfloor v \rfloor) + (1 - Q_{(u,v)})(\lfloor u \rfloor, v),$$

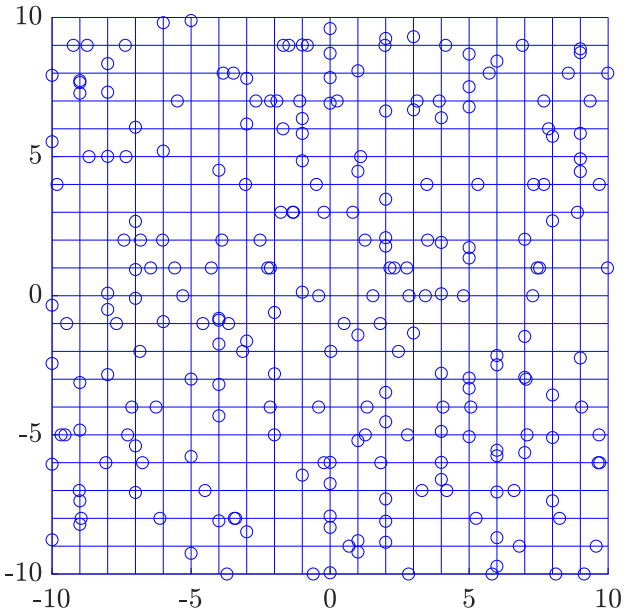

Figure 2.1: A snapshot of the SG-PPP. Lines represent streets and 'o' represent vehicles. $\lambda = 1$, and $s = 1$.

where Q_x, $x \in \mathbb{R}^2$, *is a random field of independent Bernoulli random variables with mean* $1/2$ *and* $\lfloor z \rfloor$ *is the largest integer smaller than or equal to* z.

Let $\mathcal{P} \subset \mathbb{R}^2$ *be a stationary 2D PPP of intensity* λ_2 *and define*

$$\mathcal{P}_{\mathbb{Z}} \triangleq q_{\mathbb{Z}}(\mathcal{P}).$$

The SG-PPP follows as

$$\mathcal{V} \triangleq s(\mathcal{P}_{\mathbb{Z}} + U),$$

as in the first definition.

We also define the (scaled) quantization function $q \colon \mathbb{R}^2 \mapsto \mathbb{R}^2$ *as*

$$q(x) \triangleq s(q_{\mathbb{Z}}(x) + U).$$

The quantization levels correspond to the streets, which are integers for the model shown in Fig. 2.1. For example, given integer quantization levels, $U = (0, 0)$, and

$s = 1$, a point $(4.93, 1.16)$ in a 2D PPP $\mathcal{P}$ can be quantized either as $(5, 1.16)$, displacing the point to a vertical street or as $(4.93, 1)$, displacing it to a horizontal street. On quantizing a 2D PPP $\mathcal{P}$ defined on $[0, M]^2$, we obtain M horizontal and M vertical streets, each of length M. Random translation U does not affect the number of streets and their lengths. Scaling by a factor s results in a square grid of size sM. The intensity of active transmitters in $\mathcal{P}$ is $\lambda_2 p$. Equating the total expected number of active transmitters in $\mathcal{P}$ and its scaled quantized version $\mathcal{V}$, we obtain

$$\lambda p \times 2M \times sM = \lambda_2 p \times (sM)^2, \tag{2.1}$$

which implies $\lambda = \lambda_2 s/2$. For $s = 1$, displacing each of the points of a 2D PPP to either horizontal or vertical streets results in streets each with transmitters at half the intensity of a 2D PPP.

Performance Metric and the Typical Vehicle Our metric of interest is the success probability or reliability, which is the probability of successfully receiving the message at a distance D from the transmitter. If a transmitter can communicate to a receiver at a distance D, then the other receivers within distance D are also highly likely to receive the message.

To define a meaningful network-wide metric, we focus on the success probability of a representative vehicle (receiver) whose performance corresponds to the average of that of all vehicles. In point process theory, this representative vehicle is called 'the typical point.' In our context, it is 'the typical vehicle.' As vehicles are located on the street(s), having a vehicle at the origin implies that at least one street passes through the origin. Under expectation over the SG-PPP, a vehicle conditioned to be at the origin becomes the typical vehicle. Note that we can condition the typical vehicle to be at any location since the vehicular network is stationary owing to the underlying stationary street system (see Definition 1) and the homogeneity of the

PPP. The typical vehicle's transmitter is assumed to be at a distance D from the origin. The transmitter can be another vehicle, a roadside unit, a pedestrian, or any other node.

In the SG-PPP, we consider two types of typical vehicles: the typical general vehicle and the typical intersection vehicle. For the typical general vehicle, we condition on the translation $U = (u_1, u_2)$ such that the origin is not an intersection, *i.e.,* $u_1 = 0, u_2 \in (0, 1)$. In the case of the typical intersection vehicle, the intersection falls at the origin, *i.e.*, $u_1 = u_2 = 0$. Note that the term 'typical vehicle' refers to both the general and intersection vehicles, unless otherwise stated. Let r_j denotes the distance between the typical vehicle and the nearest location on the jth street, *i.e.*, the perpendicular distance. Without loss of generality, we order the perpendicular distances r_j such that $r_0 \leq r_1 \leq \ldots$, where $r_0 = 0$.

Signal-to-Interference Ratio The received signal power S at the origin with respect to some transmitter x is $g_x \ell(x)$, where the channel power gain g_x is exponentially distributed with mean 1 (Rayleigh fading) and $\ell(w) = \|w\|^{-\alpha}$ is the standard path loss function with exponent α. Let D denote the distance between the typical vehicle and its desired transmitter, and g denote the corresponding channel power gain. The received interference power at the origin is the sum of all the interference powers from the other transmitters on the same as well as the different streets. Let I_j denote the interference from the street at perpendicular distance r_j from the typical vehicle. Thus the total interference power is $I = \sum_{j \in \mathbb{N}_0} I_j$, where $\mathbb{N}_0 = \mathbb{N} \cup \{0\}$. Accordingly, the signal-to-interference ratio SIR at the typical vehicle is

$$\mathsf{SIR} = \frac{S}{\sum\limits_{j \in \mathbb{N}_0} I_j} = \frac{g D^{-\alpha}}{\sum\limits_{j \in \mathbb{N}_0} \sum\limits_{z \in V_j} g_z \|z\|^{-\alpha} B_z}, \tag{2.2}$$

where V_j represents the point process of vehicles on the jth street at a time instant and $\mathcal{V} = \bigcup_{j \in \mathbb{N}_0} V_j$. B_z is a Bernoulli random variable with mean p, the transmit

probability. The transmission is considered successful when the SIR exceeds a certain threshold θ which parametrizes the data rate.

2.2 Success Probability

In this section, we derive the success probabilities of (i) the typical general vehicle, which equals the average fraction of vehicles who achieve SIR greater than θ, and (ii) the typical intersection vehicle, which equals the average fraction of vehicles who achieve SIR greater than θ when they are at intersections.

The success probability (reliability) of the typical vehicle is defined as

$$p_{\mathrm{s}} \triangleq \mathbb{P}(\mathsf{SIR} > \theta) = \mathbb{P}(S > I\theta) \tag{2.3}$$

$$= \mathbb{P}(g > \theta D^{\alpha} I) = \mathbb{E}_I(\exp(-\theta D^{\alpha} I)) \tag{2.4}$$

$$\overset{(a)}{=} \prod_{j \in \mathbb{N}_0} \mathbb{E}_{I_j}(\exp(-\theta D^{\alpha} I_j)) \overset{(b)}{=} \prod_{j \in \mathbb{N}_0} \mathcal{L}_{I_j}(\theta D^{\alpha}) \tag{2.5}$$

where (a) follows from the independence of the 1D PPPs and (b) follows from the definition of Laplace transform. First, we will find the interference from the same street and from a different street. Using the results obtained, we will evaluate the success probabilities of the typical general and intersection vehicles.

2.2.1 Interference from the Same Street

Based on our ordering of perpendicular distances, I_0 denotes the interference from the same street where the typical general vehicle lies. The Laplace transform of the interference from the same street is

$$\begin{aligned}\mathcal{L}_{I_0}(\theta D^{\alpha}) &= \mathbb{E}_{I_0}(\exp(-\theta D^{\alpha} I_0)) \\ &= \mathbb{E}\left[\prod_{z \in \mathcal{V}_0 : B_z = 1} \mathbb{E}\left(\exp\left(-\theta D^{\alpha} g_z \|z\|^{-\alpha}\right)\right) \right]\end{aligned}$$

$$
\begin{aligned}
&= \mathbb{E}\left[\prod_{z\in\mathcal{V}_0:B_z=1}\frac{1}{1+\theta D^{\alpha}|z|^{-\alpha}}\right]\\
&\overset{(c)}{=} \exp\left(-\lambda p\int_{-\infty}^{\infty}\frac{1}{1+\left(\frac{u^2}{D^2\theta^{\delta}}\right)^{1/\delta}}\mathrm{d}u\right)\\
&\overset{(d)}{=} \exp\left(-\lambda pD\theta^{\delta/2}\int_{0}^{\infty}\frac{1}{(1+v^{1/\delta})\sqrt{v}}\mathrm{d}v\right)\\
&= \exp(-2\lambda pD\theta^{\delta/2}\Gamma(1+\delta/2)\Gamma(1-\delta/2)),
\end{aligned}
\tag{2.6}
$$

where $\delta = 2/\alpha$, (c) follows from the probability generating functional (PGFL) of the PPP, and (d) results from the change of variable $v = \frac{u^2}{D^2\theta^{\delta}}$. For the typical intersection vehicle, $r_0 = r_1 = 0$. Then $I_0 = I_1$ in distribution, and the Laplace transform of the interference from both the streets is

$$
\prod_{j=0}^{1}\mathcal{L}_{I_j}(\theta b^{\alpha}) = \mathcal{L}_{I_0}^{2}(\theta D^{\alpha}) = \exp(-4\lambda pD\theta^{\delta/2}\Gamma(1+\delta/2)\Gamma(1-\delta/2)). \tag{2.7}
$$

2.2.2 Interference from a Different Street

The Laplace transform of the interference from a different street for the typical general/intersection vehicle is given by

$$
\begin{aligned}
\mathcal{L}_{I_j}(\theta D^{\alpha}) &= \mathbb{E}_{I_j}(\exp(-\theta D^{\alpha}I_j))\\
&= \mathbb{E}\left[\prod_{z\in V_j:B_z=1}\mathbb{E}\left(\exp\left(-\theta D^{\alpha}g_z\|z\|^{-\alpha}\right)\right)\right]\\
&= \mathbb{E}\left[\prod_{z\in V_j:B_z=1}\frac{1}{1+\theta D^{\alpha}\|z\|^{-\alpha}}\right]\\
&\overset{(e)}{=} \exp\left(-\lambda p\int_{-\infty}^{\infty}\frac{1}{1+\left(\frac{r_j^2+u^2}{D^2\theta^{\delta}}\right)^{1/\delta}}\mathrm{d}u\right)
\end{aligned}
$$

$$\stackrel{(f)}{=} \exp\left(-\lambda p D \theta^{\delta/2} \int\limits_{\frac{r_j^2}{D^2\theta^\delta}}^{\infty} \frac{1}{(1+v^{1/\delta})\sqrt{v-\frac{r_j^2}{D^2\theta^\delta}}} \mathrm{d}v \right), \tag{2.8}$$

where $\delta = 2/\alpha$, (e) applies the PGFL of the PPP, and (f) is due to the change of variable $v = \frac{r_j^2+u^2}{D^2\theta^\delta}$. Note that (2.6) can be obtained from (2.8) by setting $r_j = 0$. For $\alpha = 2$ and 4, (2.8) simplifies to

$$\mathcal{L}_{I_j}(\theta D^2) = \exp\left(\frac{-\pi\lambda D^2 \theta}{\sqrt{r_j^2 + D^2\theta}} \right),$$

and

$$\mathcal{L}_{I_j}(\theta D^4) = \exp\left(\frac{-\pi\lambda D^2 \sqrt{\theta} \sin\left(\frac{1}{2}\arctan\left(\frac{D^2\sqrt{\theta}}{r_j^2}\right)\right)}{\left(r_j^4 + D^4\theta\right)^{\frac{1}{4}}} \right),$$

respectively.

2.2.3 Success Probabilities for General and Intersection Users

Now, we can express the success probabilities of the typical general and intersection vehicles using (2.5) as shown in Lemma 2.1.

Lemma 2.1. *The success probability of the typical general/intersection vehicle in the SG-PPP is given by*

$$\begin{aligned} p_{\mathrm{s}} =& \exp(-m\lambda p D \theta^{\delta/2} \Gamma(1+\delta/2)\Gamma(1-\delta/2)) \\ & \times \prod_{j \geq m/2} \exp\left(-\lambda p D \theta^{\delta/2} \int\limits_{\frac{r_j^2}{D^2\theta^\delta}}^{\infty} \frac{1}{(1+v^{1/\delta})\sqrt{v-\frac{r_j^2}{D^2\theta^\delta}}} \mathrm{d}v \right), \end{aligned} \tag{2.9}$$

where $\delta = 2/\alpha$, $m = 2$ for the typical general vehicle and 4 for the typical intersection vehicle.

Proof. Substituting the Laplace transform of the interference from the same street(s) (2.6), and (2.7), and from a different street (2.8) in (2.5), we obtain the result (2.9). □

2.3 Understanding Vehicular Network Behavior

We learned that the closed-form expression for (2.9) exists only for specific modeling parameters. To gain insights on the impact of interference from different streets on p_{s}, we focus on the asymptotic regimes $\theta \to 0$ and $\theta \to \infty$.

2.3.1 Asymptotic Reliability Analysis

First, we will study how the interferers affect p_{s} as $\theta \to 0$, which corresponds to the high-reliability regime.

Theorem 2.1. *As $\theta \to 0$, the SG-PPP behaves as*

$$1 - p_{\mathrm{s}} \sim m\lambda p D \theta^{\delta/2} \Gamma(1+\delta/2)\Gamma(1-\delta/2),$$

where $\delta = 2/\alpha$, $m = 2$ for the typical general vehicle and 4 for the typical intersection vehicle.

Proof. Let $K = \Gamma(1+\delta/2)\Gamma(1-\delta/2)$ and $\forall j \geq 0$,

$$F_j(\theta) = \exp\left(-\lambda p D \theta^{\delta/2} \int_{\frac{r_j^2}{D^2\theta^\delta}}^{\infty} \frac{1}{\left(1+v^{1/\delta}\right)\sqrt{v - \frac{r_j^2}{D^2\theta^\delta}}} \mathrm{d}v \right).$$

Note that $\prod_{j<m/2} F_j(\theta) = \exp(-m\lambda p D \theta^{\delta/2} K)$. Then we can express (2.9) as

$$p_{\mathrm{s}} = \exp\left(-m\lambda p D \theta^{\delta/2} K - \sum_{j \geq m/2} \ln F_j(\theta) \right). \tag{2.10}$$

For small θ, we can approximate (2.10) using Taylor's series as

$$\lim_{\theta\to 0}\frac{1-p_{\mathrm{s}}}{\theta^{\delta/2}} = m\lambda pDK + \lim_{\theta\to 0}\sum_{j\geq m/2}\frac{\ln F_j(\theta)}{\theta^{\delta/2}} \tag{2.11}$$

Observe that $\frac{\ln F_j(\theta))}{\theta^{\delta/2}} \to 0$ as $\theta \to 0$ since the lower limit of the integral $\frac{r_j^2}{D^2\theta^{\delta}} \to \infty$. Hence the limit (2.11) reduces to

$$\lim_{\theta\to 0}\frac{1-p_{\mathrm{s}}}{\theta^{\delta/2}} = m\lambda pbK,$$

and thus

$$p_{\mathrm{s}} \sim 1 - m\lambda pD\theta^{\delta/2}\Gamma(1+\delta/2)\Gamma(1-\delta/2), \quad \theta \to 0. \tag{2.12}$$

This completes the proof. □

The success probability of the typical vehicle in a d-dimensional PPP is [4, Sec. 5.2]

$$p_{\mathrm{s}} = \exp(-c_d\lambda_d D^d\theta^{\delta'}\Gamma(1+\delta')\Gamma(1-\delta')), \tag{2.13}$$

where c_d denotes the volume of a d-dimensional unit ball, D is the link distance between each transmitter and its receiver, λ_d is the transmitter intensity, $\delta' = d/\alpha$ and α is the path loss exponent. Note that $c_1 = 2$ and $c_2 = \pi$.

We can approximate the success probability of the typical vehicle in a d-dimensional PPP (2.13) using Taylor's series as

$$p_{\mathrm{s}} \sim 1 - c_d\lambda_d D^d\theta^{\delta'}\Gamma(1+\delta')\Gamma(1-\delta'), \quad \theta \to 0. \tag{2.14}$$

Comparing (2.12) and (2.14), we observe that $\lambda_1 = \lambda p$, $d = 1$ ($c_1 = 2$), $\delta' = \delta/2 = 1/\alpha$, and $m = 2$ since a 1D PPP refers to a single street. For the typical intersection vehicle, as it lies at the intersection of two streets, and the vehicles on each street

form independent 1D PPPs, we have $m = 4$, and

$$p_{\mathrm{s}} \sim 1 - 4\lambda p D \theta^{\delta/2} \Gamma(1+\delta/2)\Gamma(1-\delta/2), \quad \theta \to 0. \tag{2.15}$$

Remark 2.1. *The SG-PPP behaves like a 1D PPP as $\theta \to 0$. In this regime, the effect of the interference from different streets ($r_j \neq 0$) is negligible, and it is sufficient to consider only the interference from the same street(s) as seen from* (2.12)-(2.15).

Next, we analyze the low-reliability regime, where $\theta \to \infty$.

Theorem 2.2. *As $\theta \to \infty$, the success probability of the typical vehicle in the SG-PPP behaves as*

$$p_{\mathrm{s}} \sim \exp(-\pi \lambda_2 D^2 \theta^{\delta} \Gamma(1+\delta)\Gamma(1-\delta)),\ \theta \to \infty, \tag{2.16}$$

where $\lambda_2 = 2\lambda p/s$, and $\delta = 2/\alpha$.

Proof. The success probability of the typical general/intersection vehicle in the SG-PPP from (2.2) and (2.4) is

$$p_{\mathrm{s}} = \mathbb{P}\bigg(g > D^{\alpha} \sum_{z \in \mathcal{V}} g_z \|\theta^{-1/\alpha} z\|^{-\alpha}\bigg). \tag{2.17}$$

If $q(\cdot)$ denotes the quantized version of each point of a 2D PPP $\mathcal{P}$ (see Def. 2), then (2.17) can be equivalently written as

$$p_{\mathrm{s}} = \mathbb{P}\bigg(g > D^{\alpha} \sum_{z \in \mathcal{P}} g_z \|\theta^{-1/\alpha} q(z)\|^{-\alpha} B_z\bigg). \tag{2.18}$$

Similarly, for a stationary 2D PPP $\mathcal{P}$, the success probability of the typical vehicle at the origin p'_{s} can be expressed as

$$p'_{\mathrm{s}} = \mathbb{P}\bigg(g > D^{\alpha} \sum_{z \in \mathcal{P}} g_z \|\theta^{-1/\alpha} z\|^{-\alpha} B_z\bigg). \tag{2.19}$$

Each point in $\mathcal{P}$ is displaced at most by $s/2$, where s is the spacing between the streets. Using the Cauchy-Schwarz inequality, we can obtain the lower bound $|\|z\|-\|q(z)\|| \leq \|z-q(z)\| \leq s/2$ on the distance between the point and its quantized version. On multiplying by $\theta^{-1/\alpha}$, we obtain

$$|\|\theta^{-1/\alpha}z\| - \|\theta^{-1/\alpha}q(z)B_z\|| \to 0, \quad \theta \to \infty. \tag{2.20}$$

Applying (2.20) to (2.18) and (2.19), we infer that the interference experienced by the typical general/intersection vehicle in the SG-PPP tends to that of in a 2D PPP as $\theta \to \infty$. Note that the type of vehicle does not matter since the quantization does not affect the points of $\mathcal{P}$ as $\theta \to \infty$, *i.e.*, there is no difference between a general vehicle and an intersection vehicle. Hence the success probability in the SG-PPP tends to that in a 2D Poisson network $\mathcal{P}$. From (2.1), we find the intensity of active transmitters in $\mathcal{P}$ as $2\lambda p/s$. Setting $d = 2$ ($c_2 = \pi$), $\lambda_2 = 2\lambda p/s$, and $\delta' = \delta = 2/\alpha$ in (2.13), we obtain (2.16). □

Remark 2.2. *The SG-PPP behaves like a 2D PPP as $\theta \to \infty$.*

2.3.2 Comparison to Poisson Point Processes

From our asymptotic analysis, we infer that the vehicular network shares some properties of both 1D and 2D PPPs. Here, we provide heuristic arguments that generalize the behavior of the vehicular network for all θ.

The success probability p_{s} in (2.9) is the product of the Laplace transforms of the interference from the same and different streets. As $0 \leq p_{\mathrm{s}} \leq 1$, we can infer that p_{s} is less than or equal to the Laplace transform of the interference from the same street(s), *i.e.*, $p_{\mathrm{s}} \leq \exp(-m\lambda p D\theta^{\delta/2}\Gamma(1+\delta/2)\Gamma(1-\delta/2))$, which is the success probability of the typical vehicle in a 1D PPP of intensity $m\lambda p/2$ (see (2.13)).

Due to the quantization (see Definition 2), the SG-PPP is a Cox process [4, Sec.

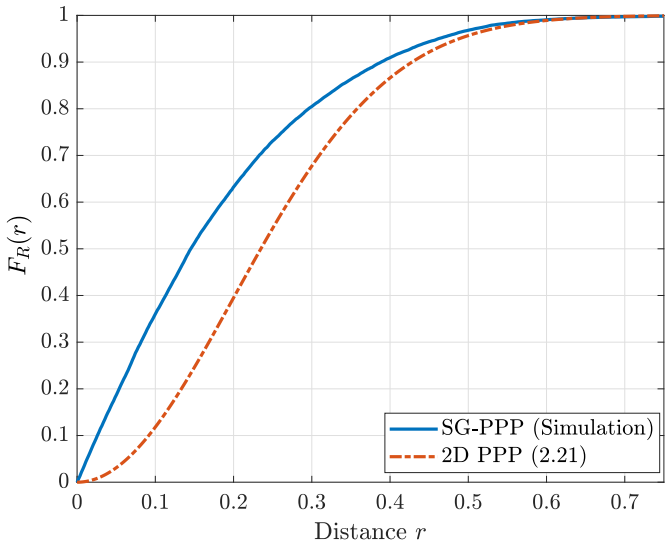

Figure 2.2: Nearest neighbor distance distributions $G(r)$ for SG-PPP and 2D PPP. The equation number is given in the parentheses. $\lambda = 2$, $p = 1$, and $s = 1$.

3.3] and thus exhibits clustering behavior, which means that the probability of finding a n-th nearest neighbor at a distance r is higher in the SG-PPP than in a PPP. For a 2D PPP $\mathcal{P}$ of intensity λ_2, the probability that the nearest neighbor is within a distance r is [4]

$$F_R^{\mathcal{P}}(r) = 1 - \exp(-\lambda_2 \pi r^2). \tag{2.21}$$

Fig. 2.2 shows the nearest neighbor distance distribution curves ($n = 1$) for the 2D PPP and the SG-PPP (obtained through simulations), which supports our clustering argument. For the same channel distribution, as the number of neighbors to the typical vehicle within a distance r is higher in the SG-PPP, the interference to the typical vehicle is higher than in a PPP. Let I' denote the interference to the typical vehicle in $\mathcal{P}$. Using (2.4), for $I \geq I'$, we get

$$\mathbb{E}_I(\exp(-\theta D^\alpha I)) \leq \mathbb{E}_{I'}(\exp(-\theta D^\alpha I')),$$

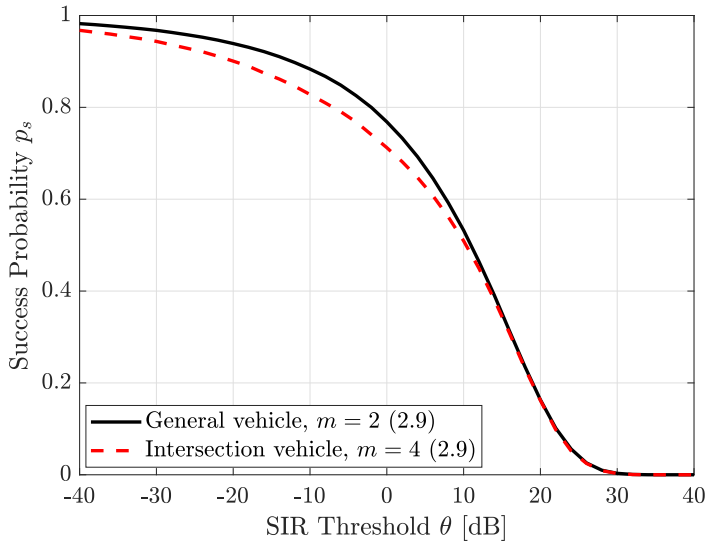

Figure 2.3: Success probabilities of the typical general and intersection vehicles in the SG-PPP. The equation number of the success probability is given in the parentheses in the legend.

which implies that the success probability in the SG-PPP is less than or equal to that in a 2D PPP. Hence the success probability of the typical vehicle in the SG-PPP is upper bounded by that in the 1D and 2D PPPs.

Remark 2.3. *The success probability of the typical vehicle in the SG-PPP is upper bounded by the minimum of the success probabilities of the typical vehicle in the 1D and 2D PPPs. As* $\theta \to 0$*, and* $\theta \to \infty$*, the bound gets tight.*

2.4 Results and Discussion

In this section, we present the numerical evaluations of the success probabilities of the typical general and intersection vehicles, and validate the asymptotic analysis. We assume $\lambda = 1$, $p = 0.3$, $D = 0.25$, $s = 1$, and $\alpha = 4$.

Fig. 2.3 shows the success probabilities of the typical general and intersection vehicles. The success probability of the typical general vehicle is higher than that of the typical intersection vehicle. As two streets pass through the intersection, the probability that the nearest interferer is within a distance r is higher for the intersection

vehicle than the general vehicle. This results in lower success probability for the typical intersection vehicle. Asymptotically, as $\theta \to \infty$, the success probabilities of the typical general and intersection vehicles match in accordance with our low-reliability analysis.

Figs. 2.4a and 2.4b compare the success probabilities of the typical general and intersection vehicles to that of the typical vehicle in 1D and 2D PPPs. At low SIR threshold θ, the success probabilities of the typical general and intersection vehicles match that of the 1D PPP with intensity $\lambda_1 = \lambda p \times m/2 = 0.15m$, for $m = 2$ and 4, respectively. At high SIR threshold, the SG-PPP matches 2D PPP with intensity $\lambda_2 = 0.6 = 2\lambda p$ for both types of vehicles, consistent with our asymptotic analysis. Hence the upper bound on the success probability of the typical vehicle is tight at the asymptotic regimes. The bound is least tight when the success probabilities of the 1D and 2D PPPs are the same, which happens when $\theta = -2$ dB in Fig. 2.4a and $\theta = 10$ dB in Fig. 2.4b.

2.5 Conclusions

In this chapter, we analyzed an orthogonal street system with vehicles on each street forming 1D PPPs. Using tools from stochastic geometry, we have derived exact analytical expressions for the success probabilities of the typical general vehicle, which characterizes the average performance of all the vehicles, and of the typical intersection vehicle, which characterizes the performance of the vehicles at intersections.

Our asymptotic analysis reveals that in the high-reliability regime, the interferers from the same streets as that of the typical receiver dominate the interference and the orthogonal street system behaves like a 1D PPP. On the other hand, in the low-reliability regime, the orthogonal street system behaves like a 2D PPP. Also, it is shown that the success probability of the typical general/intersection vehicle is upper

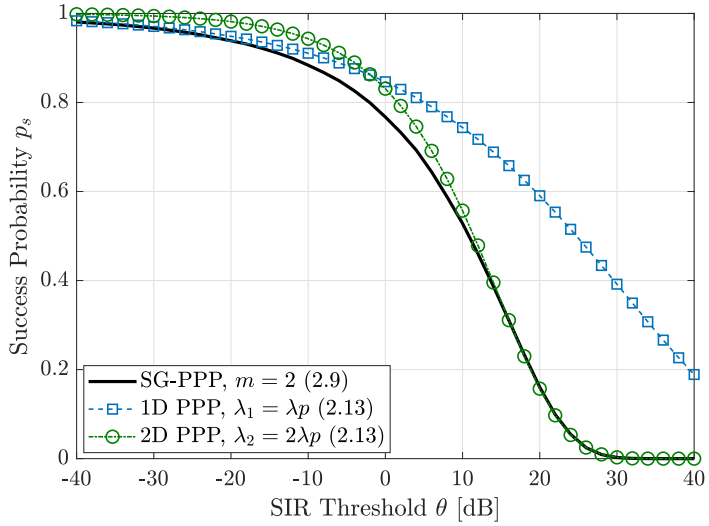

(a)

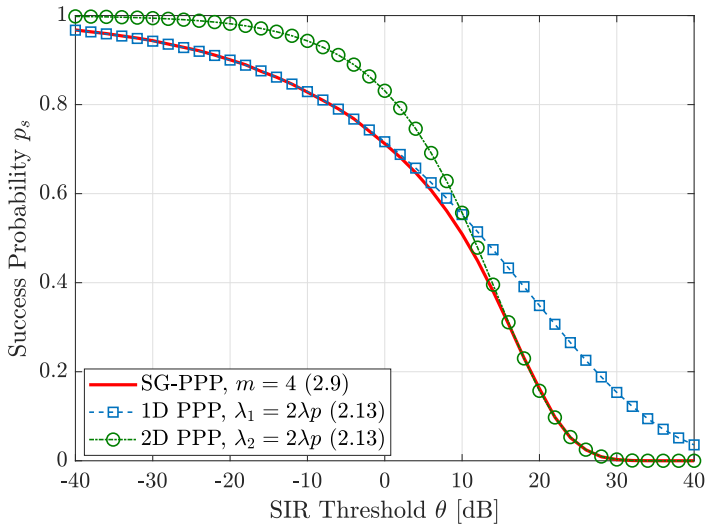

(b)

Figure 2.4: Success probability of the (a) typical general vehicle and (b) typical intersection vehicle in the SG-PPP vs. success probability of the typical vehicle in 1D and 2D PPPs. The equation numbers of the success probabilities are given in the parentheses in the legends.

bounded by the minimum of the success probabilities of the typical vehicle in the 1D and 2D PPPs, and that the bound gets tight in the asymptotic regimes. Hence the vehicles on the streets cannot be completely characterized by 1D PPPs and accurately modeled as 2D PPPs and and that the street geometry is essential in modeling the vehicular networks.

CHAPTER 3

COX MODELS FOR VEHICULAR NETWORKS

The street systems in different geographical regions may differ in their structure, street lengths, and degree of regularity. Crucitti et al. in [22] studied the street systems of 18 cities in different parts of the world. They divide the street systems into two classes—(i) self-organized patterns that are formed historically without the control of any central agency, and (ii) planned regular grid-like patterns. Cities such as Ahmedabad (India), Cairo (Egypt), and Venice (Italy) are examples of self-organized patterns with unimodal street length distributions. Los Angeles, Richmond, and San Francisco in the United States are examples of grid-like patterns with multimodal street length distributions. It is worth noting that that even in the cities containing grid-like street patterns, the street lengths are finite and vary significantly.

In the literature [23, 24, 25, 26, 27, 28, 29], street systems are most commonly modeled as a random collection of lines with uniform orientations using Poisson line processes (PLPs). While assuming that all streets are infinitely long may lead to useful results, it either overestimates the total interference or underestimates the local density of vehicles. For example, a street in a city that is 2 km long may have a density of 50 cars per km. But extending it to an infinite street would mean such a high car density extends to very remote rural regions far outside the city, which is not realistic. Further, in the PLP, each pair of streets forms an intersection and there are no T-junctions. Fig. 3.1 shows a part of Rome as an example, where few streets are long enough to be approximated by infinite streets, and there exist many T-junctions.

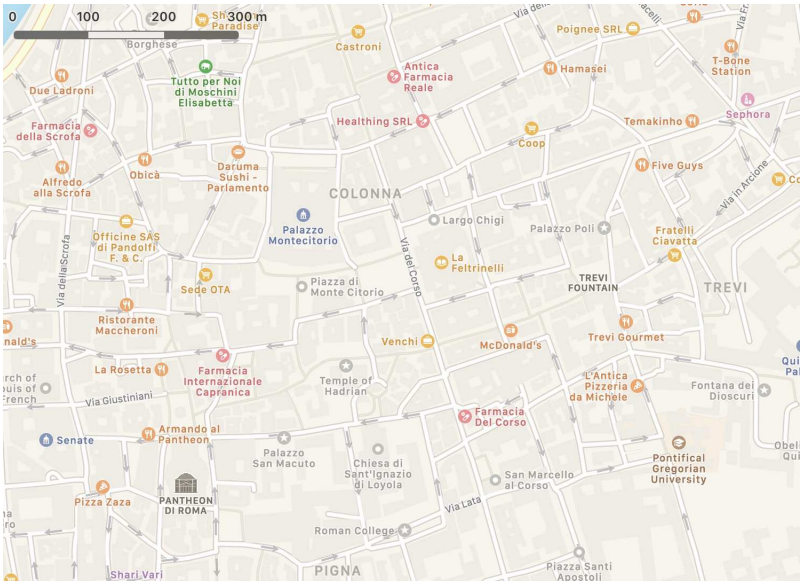

Figure 3.1: Part of Rome's city center. Visual inspection shows a mean street length of about 250 m and many T-junctions.

Consequently, we need street models that can characterize finite variations in the street lengths, and intersections and T-junctions. The edges of Poisson-Voronoi tessellation, Poisson-Delaunay tessellation, and Poisson line tessellation are considered to model streets of finite lengths in [30]. Estimators for the probability densities of the inter-node distances are derived for these tessellations owing to their intractability. A simpler alternative is to use line segments or sticks as we show later. In this chapter, we introduce a general framework for the modeling and analysis of vehicular networks. Under this framework, we develop models that represent street systems varying from regular grid-like patterns to irregular hodgepodges and characterize the uncertainty in the vehicle locations on the streets. In particular, the street lengths can be infinitely long or varying finitely and mutually independent or dependent resulting in intersections or T-junctions.

An important question is whether we need a different spatial model for each region. Alternatively, does there exist an equivalence between the models such that a single model is sufficient to analyze two different regions? If yes, a representative

subset can be used to analyze a larger set of models, reducing the computation time and costs associated with network design and planning. In this chapter, we show that some models developed within the framework are equivalent, in a precise sense defined later.

3.1 System Model

We will use the definitions and notations presented in this section for the rest of the report unless otherwise stated. Let $b(x, r)$ denote a disk of radius r centered at x, and $o \triangleq (0, 0)$ denote the origin. Let $|\cdot|_d$ denote the Lebesgue measure in d dimensions.

3.1.1 General Framework

Definition 3.1 (Street System)**.** *A street system $\mathcal{S}$ is a stationary random closed subset of $\mathbb{R}^2$ with $|\mathcal{S}|_2 = 0$ that contains no singletons or isolated points. Due to the stationarity,*

$$\mathbb{E}|\mathcal{S} \cap \mathcal{B}|_1 = \tau|\mathcal{B}|_2 \quad \textit{for Borel sets } \mathcal{B} \subset \mathbb{R}^2, \tag{3.1}$$

where τ is the mean total street length per unit area.

$|\mathcal{S}|_2 = 0$ in Definition 3.1 implies that $\mathcal{S}$ is a random 1D subset of the plane consisting of lines, line segments or sticks, curved segments or arcs, that characterize the streets. Let $\Xi = \{\xi_1, \xi_2, \ldots\}$ be a collection of 1D subsets in $\mathbb{R}^2$ such that for $i \neq j$, $|\xi_i \cap \xi_j|_1 = 0$ and $\xi_i \cup \xi_j$ is not a 1D subset. The street system $\mathcal{S}$ is the union of 1D subsets, *i.e.,*

$$\mathcal{S} \triangleq \bigcup_{\xi \in \Xi} \xi. \tag{3.2}$$

The elements of $\mathcal{S}$ are points in $\mathbb{R}^2$ but those of Ξ are 1D subsets, which are sets themselves, and hence $\mathcal{S} \neq \Xi$. Further, $\mathcal{S}$ uniquely characterizes Ξ and vice-versa,

i.e., there exists a one-to-one correspondence between $\mathcal{S}$ and Ξ. Any street system $\mathcal{S}$ can be partitioned as follows.

Definition 3.2 (Street System Decomposition)**.** *Let* $\mathcal{P}_m \triangleq \{z \in \mathbb{R}^2 : |\mathcal{S} \cap b(z,r)|_1 \sim mr, r \to 0\}$ *denote the set of points of order* $m \in \mathbb{N}$ *in the street system* $\mathcal{S}$*.*

The sets $\mathcal{P}_m$ are disjoint, and their union equals $\mathcal{S}$, *i.e.,* $\{\mathcal{P}_m\}_{m\in\mathbb{N}}$ is a partition of $\mathcal{S}$. For $m \neq 2$, the sets $\mathcal{P}_m$ are countable and form simple and stationary point processes. $\mathcal{P}_2$ is the only set with $|\mathcal{P}_2|_1 > 0$, in fact, $|\mathcal{P}_2|_1 = \infty$. We have $\mathcal{P}_2 = \mathcal{S}$ almost everywhere, *i.e.,* $\mathcal{P}_2$ is an open set and $\mathcal{S} = \mathrm{cl}(\mathcal{P}_2)$, where cl denotes the closure. $\mathcal{P}_1$ are endpoints, $\mathcal{P}_3$ are T-junctions, $\mathcal{P}_4$ are intersections, $\mathcal{P}_5$ are intersections with a T-junction, $\mathcal{P}_6$ are three-way intersections (three streets intersecting at one point), etc. Let

$$\mathcal{M} \triangleq \{m \in \mathbb{N} : \mathbb{P}(\mathcal{P}_m = \emptyset) = 0\} \tag{3.3}$$

denote the index set of the non-empty components. Then $\mathcal{S} = \bigcup_{m\in\mathcal{M}} \mathcal{P}_m$ is called an $\mathcal{M}-$indexed street system. Using $\mathcal{M}$, we can categorize different street systems. For example, a $(2,4)-$street system refers to a street geometry without endpoints and T-junctions but with intersections.

Definition 3.3 (Vehicular Point Process)**.** *A vehicular point process* $\mathcal{V} \subset \mathbb{R}^2$ *is a Cox process with random intensity measure* $\Upsilon(\mathcal{B}) = \lambda|\mathcal{S} \cap \mathcal{B}|_1$*.*

Equivalently, $\Upsilon(\mathcal{B}) = \lambda|\mathcal{P}_2 \cap \mathcal{B}|_1$ since a.s. $\mathcal{V} \subset \mathcal{P}_2$. This implies that the vehicles form independent 1D PPPs on each street. By Definition 1, the 2D intensity measure of $\mathcal{V}$ is $\mathbb{E}[\Upsilon(\mathcal{B})] = \lambda\mathbb{E}[|\mathcal{S} \cap \mathcal{B}|_1] = \lambda\tau|\mathcal{B}|_2$.

3.1.2 Vehicular Network Models

Here, we present a few models that fall under our framework. A street system may include curves or circles. We focus only on street systems formed by lines or sticks.

A line (an infinitely long street) L can be represented as

$$L(x,\varphi) = \{(a,b) \in \mathbb{R}^2 : a\cos\varphi + b\sin\varphi = x\}, \tag{3.4}$$

where $(|x|,\varphi)$ are the polar coordinates of the foot of the perpendicular from the origin o to L.

Definition 3.4 (Line-based Poisson Street System)**.** *Consider a marked point process on $\mathbb{R}\times\Omega$, whose ground process is a PPP Φ_1 of intensity μ on $\mathbb{R}$ and marks are i.i.d. on $\Omega \subseteq [0,\pi)$. Let ν denote the distribution of Ω. The collection of lines $\Xi_{\mathrm{L}} = \{L(x,\varphi) : (x,\varphi) \in \Phi_1 \times \Omega\}$ with the intensity measure $\Lambda_{\Xi}(\mathrm{d}x\,\mathrm{d}\varphi) = \mu\mathrm{d}x \times \mathrm{d}\nu(\varphi)$ forms*

- *an orthogonal grid with exponential spacing (OG) if $\mathrm{d}\nu(\varphi) = 0.5\delta_0 + 0.5\delta_{\pi/2}$,*
- *a Poisson line process (PLP) if $\mathrm{d}\nu(\varphi) = \mathrm{d}\varphi/\pi$.*

The line-based Poisson street system is $\mathcal{S} = \bigcup_{L\in\Xi_{\mathrm{L}}} L$.

The OG and PLP inherently form intersections and hence are classified as $(2,4)$-street systems. Streets of varying finite lengths can be represented using sticks. A stick S is defined by its midpoint y, orientation φ, and half-length h, and represented as a closed set as

$$S(y,\varphi,h) = [y - hu(\varphi), y + hu(\varphi)], \tag{3.5}$$

where $u(\varphi) = (\cos\varphi, \sin\varphi)$. Alternatively, $S(y,\varphi,h) = y + \mathrm{rot}_{\varphi}([-h,h])$, where rot_{φ} denotes the rotation by φ around o. Now, we are ready to define the stick-based street system.

Definition 3.5 (Stick-based Poisson Street System)**.** *Let $\mathcal{Q} = \{(y_i, \boldsymbol{t}_i)\}$, $i \in \mathbb{N}$, denote an i.i.d. marked point process with the ground process $\{y_i\}$ forming a 2D PPP*

Φ_2 *of intensity* μ*. Associate with* y_i *a 2D mark* $\boldsymbol{t}_i = (\varphi_i, h_i)$*, where the orientation* φ_i *is i.i.d. on* $[0, \pi)$*, and* h_i *is the half-length. The countable collection of sticks* $\Xi_{\mathrm{S}} = \{S(y_i, \varphi_i, h_i)\}$ *forms*

- *a Poisson stick process (PSP) if the half-lengths are i.i.d. with some distribution* F_H*.*
- *a Poisson lilypond model (PLM)*[1] *if each stick grows from zero length at a constant rate on both sides until one of its endpoints hits another stick, thereby forming a T-junction.*

Then $\mathcal{S} = \bigcup_{S \in \Xi_{\mathrm{S}}} S$ *defines the stick-based Poisson street system.*

Let $y_i \equiv (\gamma_i, \phi_i)$ in polar coordinates, where $\gamma_i \in \mathbb{R}^+$, and $\phi_i \in [0, 2\pi)$. The PSP has no T-junctions a.s., thus forming a $(1, 2, 4)-$street system, whereas the PLM has no intersections a.s. due to its touch-and-stop growth mechanism, thus forming a $(1, 2, 3)-$street system.

We only consider the street systems containing points of order up to 4. The analyses shown in this chapter can be extended to higher-order street systems as well.

We refer to the vehicular point processes formed by the OG, PLP, PSP, and PLM as the OG-PPP, PLP-PPP, PSP-PPP, and PLM-PPP, respectively. Fig. 3.2 depicts sample realizations.

3.1.3 Performance Metric and Types of Vehicles

Each vehicle broadcasts with probability p following the slotted ALOHA protocol. Then the intensity of transmitting vehicles on each street in each time slot is λp. Our metric of interest is the success probability or reliability, which is the probability of a vehicle successfully receiving the message from a transmitter at distance D. If a

[1]The PLM is denoted as LM-I in [31]. We note that the other model, LM-II in [31], has similar properties as the PLM.

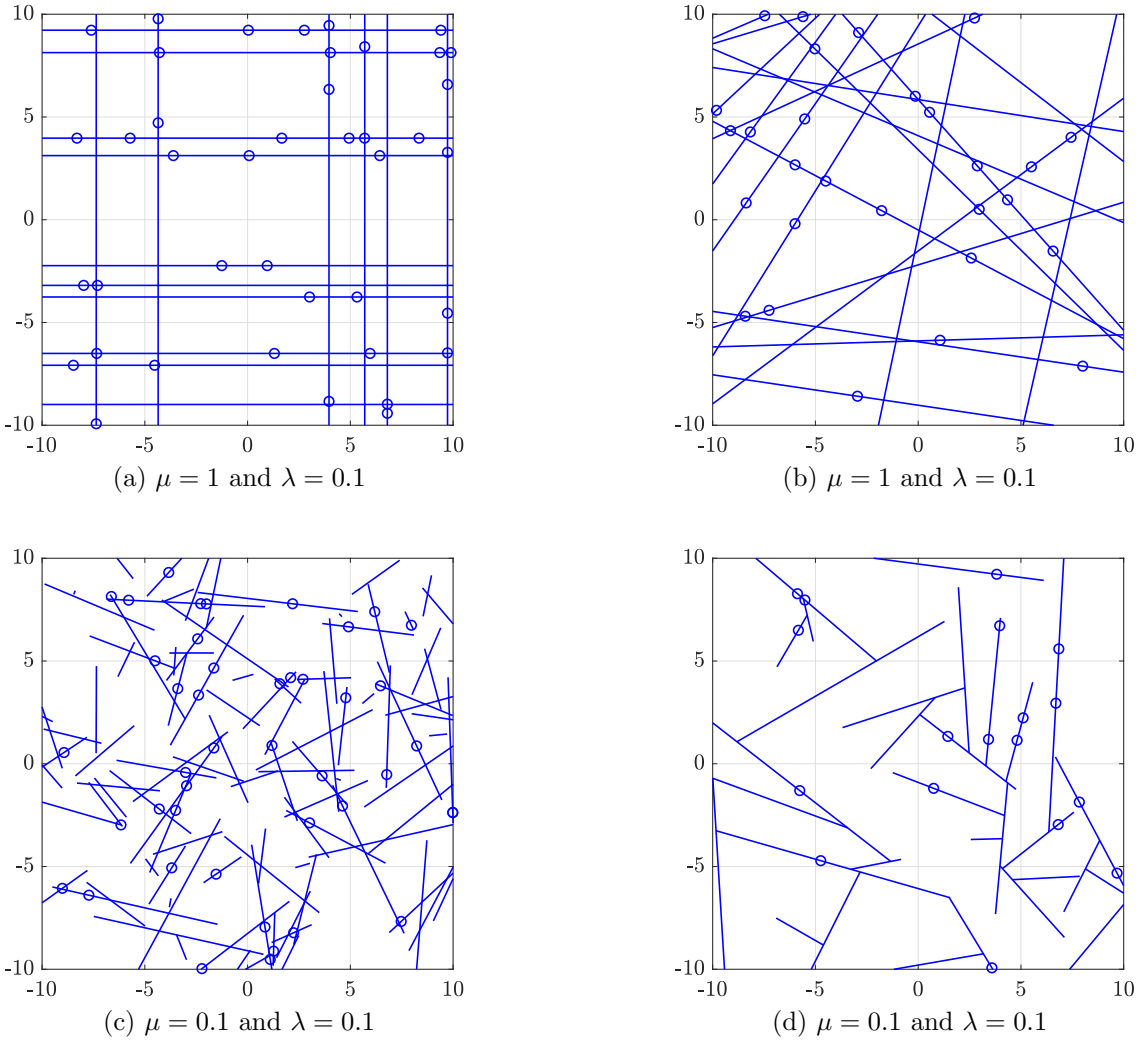

(a) $\mu = 1$ and $\lambda = 0.1$

(b) $\mu = 1$ and $\lambda = 0.1$

(c) $\mu = 0.1$ and $\lambda = 0.1$

(d) $\mu = 0.1$ and $\lambda = 0.1$

Figure 3.2: Snapshots of vehicular networks: (a) OG-PPP (b) PLP-PPP (c) PSP-PPP and (d) PLM-PPP. Lines or sticks denote the streets, and '$\circ$' denote the vehicles. The stick lengths in (c) are Rayleigh distributed with parameter 2.

transmitter can communicate to a receiver at a distance D, then the other receivers within distance D are also highly likely to receive the message. This model can be extended to analyze any form of vehicle-to-everything (V2X) communication since the transmitter is only specified by its distance D to the typical vehicle at the origin. The transmitter can be a vehicle, a roadside unit, a pedestrian, or any other infrastructure node, *i.e.,* the transmitter is the 'X' in V2X.

As in Chapter 2, we focus on the typical vehicle at the origin to evaluate the success probability. Note that we can condition the typical vehicle to be at any location since the vehicular network is stationary owing to the underlying stationary street system (Definition 1) and the homogeneity of the PPP. The typical vehicle's transmitter is assumed to be at a distance D from the origin.

The performance of vehicular communication at intersections and T-junctions is crucial as they are more prone to accidents. In view of this, we evaluate the success probabilities of three kinds of vehicles: (i) *the typical general vehicle* whose order is 2; (ii) *the typical intersection vehicle* whose order is 4; and (iii) *the typical T-junction vehicle* whose order is 3. The term *typical vehicle* refers to all the three types of typical vehicles unless otherwise stated. Mathematically, the success probability of the typical vehicle of order m at o is defined as

$$p_m(\theta) = \mathbb{P}(\mathsf{SIR} > \theta \mid o \in \mathcal{P}_m), \;\; m = 2, 3, 4, \tag{3.6}$$

where SIR is the signal-to-interference ratio measured at o and θ parametrizes the target rate. The SIR for the typical vehicle with its transmitter at distance D is given by

$$\mathsf{SIR} = \frac{gD^{-\alpha}}{\sum_{z\in\mathcal{V}} g_z \|z\|^{-\alpha} B_z}, \tag{3.7}$$

where $I = \sum_{z\in\mathcal{V}} g_z \|z\|^{-\alpha}$ is the total interference power at the origin. The channel power gains g and g_z are exponentially distributed with mean 1 (Rayleigh fading),

and α is the path-loss exponent. $(B_z)_{z\in\mathcal{V}}$ is an i.i.d. sequence of Bernoulli random variables with mean p, the probability that the transmitter z is active. Equipped with the performance metric, we next define the equivalence of spatial models.

3.1.4 Equivalence

Definition 3.6 (Equivalence)**.** *Two spatial models* A *and* B *are said to be ϵ-equivalent with respect to the typical vehicle of order m if the total variation distance of their SIR distributions is at most ϵ, i.e., $\max_{\theta} |p_m^{\mathrm{A}}(\theta) - p_m^{\mathrm{B}}(\theta)| = \epsilon$, $0 \le \epsilon \le 1$. If this holds with $\epsilon = 0$, we call them strictly equivalent. Model* A *is said to be asymptotically equivalent to model* B *in the lower regime of θ if $(1 - p_m^{\mathrm{A}}(\theta))/(1 - p_m^{\mathrm{B}}(\theta)) \to 1$ as $\theta \to 0$, and in the higher regime of θ if $p_m^{\mathrm{A}}(\theta)/p_m^{\mathrm{B}}(\theta) \to 1$ as $\theta \to \infty$.*[2]

If the street system A has index set $\mathcal{M}_{\mathrm{A}}$ and the street system B has index set $\mathcal{M}_{\mathrm{B}}$, then the equivalence of A and B is defined only for the typical vehicles of orders $\mathcal{M}_{\mathrm{A}} \cap \mathcal{M}_{\mathrm{B}}$. If A and B are strictly equivalent, then either A or B is sufficient to capture all the geographical regions that can be characterized by them. Else, substituting one model for the other would depend on the complexity of the model and the value of ϵ, which we will discuss in detail in Section 3.4.3.

3.1.5 Further Notation

Conditioning on $o \in \mathcal{P}_2$ implies that a street passes through the origin, conditioning on $o \in \mathcal{P}_3$ implies that a street passes through the origin while another street ends at the origin, and conditioning on $o \in \mathcal{P}_4$ implies that two streets pass through the origin. We denote by $\mathcal{V}^m = (\mathcal{V} \mid o \in \mathcal{P}_m)$ the point process of vehicles with the origin

[2]For all models, the success probability of the typical vehicle $p_m(\theta) \to 1$ as $\theta \to 0$. Hence, considering ratios of success probabilities is not meaningful in this regime as they would all be equivalent. Similarly, the outage probability $1 - p_m(\theta) \to 1$ as $\theta \to \infty$, so in this regime, it does not make sense to consider the ratio of outage probabilities. To obtain non-trivial equivalence results, the quantities of interest need to go to zero.

being on at least one street. Also, let $\mathcal{V}_o^m$ denote the vehicles on the streets that pass through or end at the origin. $\mathcal{V}_!$ denotes the vehicles on the rest of the streets, *i.e.,* $\mathcal{V}_! = \mathcal{V}^m \setminus \mathcal{V}_o^m$. We index the streets based on the distances of the perpendiculars from the streets to the origin. Based on the indexing, V_k denotes the point process of vehicles on the kth street. Then $\mathcal{V}_o^m = \cup_{1\leq k\leq \lceil m/2\rceil} V_k$, and $\mathcal{V}_! = \cup_{k>\lceil m/2\rceil} V_k$. Let I_o^m and $I_!$ denote the interference from the vehicles in $\mathcal{V}_o^m$ and $\mathcal{V}_!$, respectively. $\delta \triangleq 2/\alpha$, where α is the path-loss exponent.

3.2 Properties of Vehicular Networks

Lemma 3.1. *The mean total street length per unit area in the OG and PLP is* $\tau = \mu$.

Proof. The total expected length of the lines that intersect $b(o,r)$ is given by

$$\begin{aligned}\mathbb{E}[|\mathcal{S}\cap b(o,r)|_1] &= \mu\int_0^{\pi}\int_{-r}^{r} 2\sqrt{r^2-u^2}\,\mathrm{d}u\,\mathrm{d}v(\varphi)\\ &= \mu|b(o,r)|_2. \end{aligned} \tag{3.8}$$

By Definition 1 and (3.8), we get $\tau = \mu$. □

Lemma 3.2 ([32], Eq. 9)**.** *The mean total stick length per unit area in the PSP is* $\tau = 2\mu\mathbb{E}[H]$.

Let $f_H(h)$ denote the probability density function (PDF) of the half-lengths of the sticks.

Lemma 3.3. *The half-lengths of the sticks that pass through the typical vehicle are distributed with density* $\tilde{f}_H(h) = hf_H(h)/\mathbb{E}[H]$.

Lemma 3.3 is a case of the inspection paradox [33]. The length of the stick that passes through the typical vehicle is biased by the fact that the mean number of

points on the stick is proportional to its length. As a result, the half-lengths of those sticks follow the density function $\tilde{f}_H(h)$. For example, consider a case where half the streets are of length 10^{-2} and the rest are of length 10^2, and the intensity of vehicles on each street is 1. Then the typical vehicle lies on a long street with a probability of about 99.99%, which is very different from the 50% probability of the typical street to be a long one. On the other hand, in the PLM, a stick that ends at a T-junction follows the inherent distribution $f_H(h)$ since each stick has exactly one such endpoint a.s. If all the sticks are of the same length $2h_0$, then $\tilde{f}_H(h) = f_H(h) = \delta(h - h_0)$.

In the lilypond model, the growth of a stick is determined by the locations and the orientations of the other sticks since each stick grows at a constant rate until one of its endpoints hits another stick. This simultaneous touch-and-stop growth process makes it difficult, most likely impossible, to derive the exact distribution of the half-lengths. However, a suitable approximation for the distribution of the half-lengths can be found, as stated in Lemma 3.4.

Lemma 3.4. *The half-lengths of the sticks in the PLM are approximately Rayleigh distributed with PDF* $\hat{f}_H(h) = 2bh\exp(-bh^2)$, $h \geq 0$. *It follows that* $\mathbb{E}[H] \approx \sqrt{\pi/4b}$, *where* b *is proportional to the street intensity* μ *and can be estimated from the empirical mean of the half-lengths.*

Proof. See Appendix A.1. □

Combining Lemmas 3.3 and 3.4, we note that the PDF of half-lengths of the sticks that pass through the typical vehicle in PLM can be approximated as $\tilde{f}_H(h) \approx h\hat{f}_H(h)/\mathbb{E}[H]$. Fig. 3.3a illustrates their histogram and the fitted density functions $\tilde{f}_H(h)$ and $f_H(h)$. We observe that $h\hat{f}_H(h)/\mathbb{E}[H]$ provides a good fit to the histogram, validating the approximation $\hat{f}_H(h)$.

To appreciate the differences between the PSP-PPP and PLM-PPP, we consider the case where the half-lengths in the PSP are Rayleigh distributed as in the PLM. Let

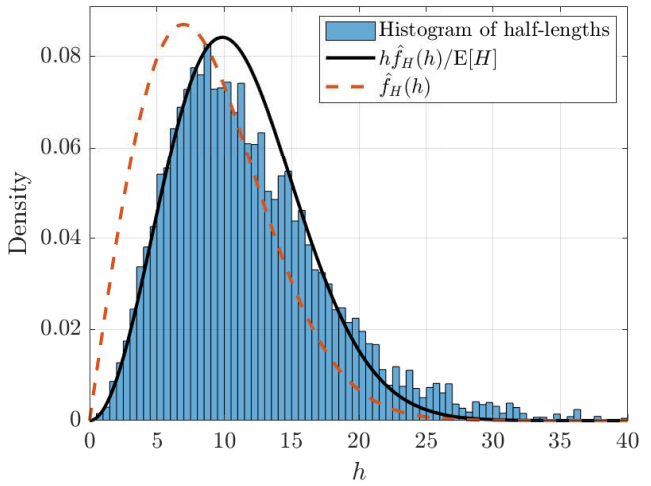

(a)

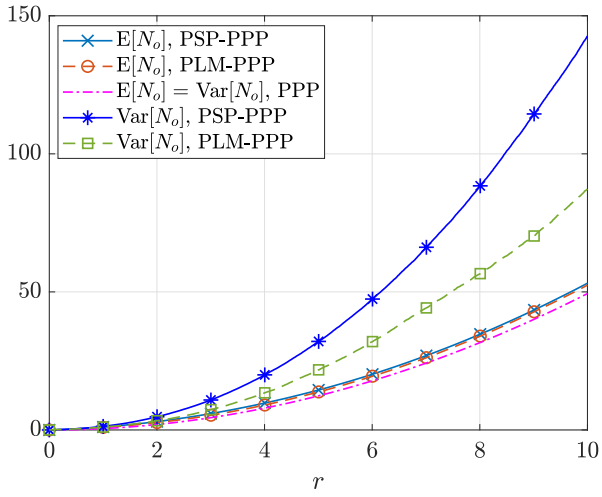

(b)

Figure 3.3: (a) Fitting $h\hat{f}_H(h)/\mathbb{E}[H]$ to the half-lengths of the streets that pass through the typical vehicle in the PLM. (b) Mean and variance of number of neighbors to the typical general vehicle in the PLM-PPP vs. PSP-PPP with $f_H(h) = \hat{f}_H(h) = 2bh\exp(-bh^2)$. $\mu = 0.01$ and $\lambda = 0.3$. The value of b corresponding to $\mu = 0.01$ is 0.0103. The intensity of 2D PPP is $2\lambda\mu\mathbb{E}[H]$, which is the 2D intensity of the PLM-PPP/PSP-PPP.

$N_o(r)$ denote the number of neighbors to the typical vehicle at o within a distance r. Fig. 3.3b compares the mean and variance of $N_o(r)$ in the PLM-PPP and PSP-PPP. The correlation among the stick lengths resulting from the touch-and-stop mechanism in the PLM-PPP leads to a smaller variance of $N_o(r)$ than in the PSP-PPP, where the stick lengths are independent. On the other hand, $\mathbb{E}[N_o]$ is the same for both the PSP-PPP and PLM-PPP when both follow the same distribution for half-lengths as their first-order statistics are the same. Also, the statistics of N_o for the PLM-PPP and PSP-PPP differ significantly from that for a 2D PPP of equivalent intensity, highlighting the differences in having the street geometry and not.

Lemma 3.5. *The nearest-neighbor distance distribution for a vehicular network with the street system characterized by Definition 3.1 can be decomposed as*

$$F_R(r) = 1 - (1 - F_{R,\mathcal{V}_o^m}(r))(1 - F_{R,\mathcal{V}_\mathrm{r}}(r)), \tag{3.9}$$

where $F_{R,\mathcal{V}_o^m}(r)$ is the probability of finding a neighbor in $\mathcal{V}_o^m$ within distance r, and $F_{R,\mathcal{V}_\mathrm{r}}(r)$ is with respect to $\mathcal{V}_\mathrm{r}$. $F_{R,\mathcal{V}_\mathrm{r}}(r)$ also denotes the contact distance distribution, the distribution of the distance from an arbitrary location to the nearest vehicle in $\mathcal{V}$.

Proof. See Appendix A.2. □

Lemma 3.6. *The nearest-neighbor distance distribution for the OG-PPP/PLP-PPP is $F_R(r) = 1 - \exp(-m\lambda r - 2\mu \int_0^r (1 - \exp(-2\lambda\sqrt{r^2 - u^2}))\mathrm{d}u)$, where $m \in \{2, 4\}$.*

Proof. See Appendix A.3. □

An alternative proof of the nearest-neighbor distance distribution for the case $m = 2$ in the PLP-PPP can be found in [28]. Lemma 3.6 presents a slightly more general result that also applies to an intersection vehicle and the OG-PPP, which can be obtained by rotating each line $L \in \Xi_L$ (Definition 3.4) constituting the PLP-PPP such that they are orthogonal to each other.

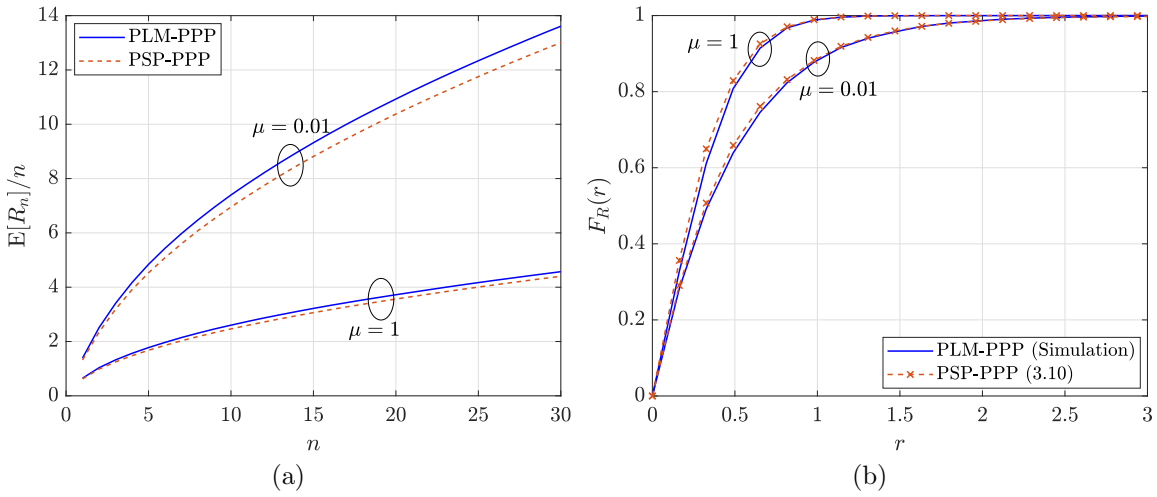

Figure 3.4: Comparison of (a) mean distance from the typical general vehicle to its n-th nearest neighbor and (b) nearest-neighbor distance distributions in the PLM-PPP and PSP-PPP given by (3.10) with $f_H(h) = \hat{f}_H(h) = 2bh\exp(-bh^2)$, where $b = 1.04$ for $\mu = 1$, and 0.0103 for $\mu = 0.01$. $\lambda = 0.3$.

Theorem 3.1. *The nearest-neighbor distance distribution for the PSP-PPP is*

$$F_R^{\mathrm{PSP-PPP}}(r) = 1 - \left[\int_0^{\infty} \frac{1}{h} \int_0^{h} \exp(-\lambda \ell(\gamma, 0, 0)) \tilde{f}_H(h) \mathrm{d}\gamma \mathrm{d}h\right]^{m/2} \times \exp\left(-\frac{\mu}{\pi} \int_0^{\infty} \int_0^{\pi} \int_0^{2\pi} \int_0^{r+h} \exp(-\lambda \ell(\gamma, \phi, \varphi)) \gamma f_H(h) \mathrm{d}\gamma \mathrm{d}\phi \mathrm{d}\varphi \mathrm{d}h\right), \tag{3.10}$$

where $\ell(\gamma, \phi, \varphi) = \ell_1(\gamma, \phi, \varphi)\mathbb{1}_{\gamma \le r} + \ell_2(\gamma, \phi, \varphi)\mathbb{1}_{\gamma > r}$. $\ell_1(\gamma, \phi, \varphi), \ell_2(\gamma, \phi, \varphi) = |\min(u_1, h) \pm \min(u_2, h)|$, *where* $u_1, u_2 = |-\gamma\cos(\phi - \varphi) \pm \sqrt{r^2 - \gamma^2 \sin^2(\phi - \varphi)}|$. $\tilde{f}_H(h) = h f_H(h)/\mathbb{E}[H]$, *and* $m \in \{2, 4\}$.

Proof. See Appendix A.4. □

Fig. 3.4a shows the normalized mean distance $\mathbb{E}[R_n]/n$ to the n-th nearest neighbor in the PLM-PPP and PSP-PPP with Rayleigh distributed half-lengths. The rate of change in $\mathbb{E}[R_n]/n$ of the PLM-PPP from that of the PSP-PPP is at most 6%

for $\mu = 0.01$, and 5% for $\mu = 1$. Fig. 3.4b compares the nearest-neighbor distance distributions for different values of μ. We see that the nearest-neighbor distance distribution in the PLM-PPP is tightly upper bounded by that in the PSP-PPP in accordance with Fig. 3.4a, which shows that the mean distance to the nearest neighbor in the PLM-PPP is tightly lower bounded by that in the PSP-PPP. We presume that the inference obtained from Fig. 3.4b extends to the n-th nearest neighbor for $n > 1$ as well.

Conjecture 3.1. *The distance from the typical general vehicle to the n-th nearest neighbor in the PLM-PPP stochastically dominates that distance in the PSP-PPP with Rayleigh distributed half-lengths.*

To facilitate the comparison of the success probabilities in the general street-based Cox models and the homogeneous PPP, we recall the success probability of the typical vehicle in a PPP. Let Φ_d denote a stationary d-dimensional PPP of intensity λ_d and c_d denote the volume of a unit d-dimensional ball. In particular, $c_1 = 2$ and $c_2 = \pi$.

Lemma 3.7 ([4], Sec. 5.2)**.** *The success probability p_{s} of the typical vehicle in Φ_d is*

$$p_{\mathrm{s}}^{\Phi_d} = \exp(-c_d \lambda_d D^d \theta^\delta \Gamma(1+\delta')\Gamma(1-\delta')), \tag{3.11}$$

where $\delta' = d/\alpha$.

Next, we analyze the success probabilities of the typical vehicle in Cox vehicular networks.

3.3 Success Probabilities

Using (3.7) and the notations in Section 3.1.5, we express the success probability p_m of the typical vehicle of order m as

$$p_m = \mathbb{P}(g > \theta D^\alpha I)$$

$$= \mathbb{E}[\exp(-\theta D^{\alpha}(I_o^m + I_!)]. \tag{3.12}$$

We can simplify (3.12) for all the Cox vehicular networks considered but the PLM-PPP as follows:

$$p_m \overset{(a)}{=} \mathbb{E}[\exp(-\theta D^{\alpha} I_o^m)]\mathbb{E}[\exp(-\theta D^{\alpha} I_!)] \tag{3.13}$$

$$\overset{(b)}{=} \mathcal{L}_{I_o^m}(s)\mathcal{L}_{I_!}(s)|_{s=\theta D^{\alpha}}, \tag{3.14}$$

where (a) is due to the independence of the PPPs on the streets, and (b) applies the definition of the Laplace transform. For the PLM-PPP, (3.13) does not hold as the length of each street is dependent on that of other streets.

Proposition 3.1. *The success probability of the typical vehicle in the OG-PPP/PLP-PPP is given by*

$$p_m = \exp\left(- m\lambda p D \theta^{\delta/2}\Gamma(1+\delta/2)\Gamma(1-\delta/2) - 2\mu \int_0^{\infty} (1 - \mathcal{L}_{I_x}(\theta D^{\alpha}))\mathrm{d}x \right), \tag{3.15}$$

where $\mathcal{L}_{I_x}(s) = \exp\big(- \lambda p s^{\delta/2} \int_{v_x}^{\infty} \frac{1}{\left(1+v^{1/\delta}\right)\sqrt{v-v_x}}\mathrm{d}v\big)$ *with* $v_x = \frac{x^2}{s^{\delta}}$, *and* $m \in \{2, 4\}$.

Proof. See Appendix A.5. □

The success probability of the typical vehicle of order 2 in the PLP-PPP is derived in [27]. The success probability (3.15) depends only on the distances of the interferers to the typical vehicle, not their orientations. In Appendix A.5, we give a general proof that shows the effect of the order of the vehicle and the irrelevance of the orientations on the success probability.

Proposition 3.2. *The Laplace transform of the interference from the vehicles on streets that pass through the typical vehicle of order* $m \in \{2, 4\}$ *in the PSP-PPP with*

half-length density function $f_H(h)$ is given by

$$\mathcal{L}_{I_o^m}^{\mathrm{PSP-PPP}}(s) = \left(\int_0^\infty \left(\frac{1}{2h} \int_{-h}^{h} \exp\left(-\lambda p s^{\delta/2} \int_{(-w-h)s^{-\delta/2}}^{(-w+h)s^{-\delta/2}} \frac{1}{1+v^{2/\delta}} \mathrm{d}v \right) \mathrm{d}w \right) \tilde{f}_H(h)\,\mathrm{d}h \right)^{m/2}, \tag{3.16}$$

where $\tilde{f}_H(h) = h f_H(h)/\mathbb{E}[H]$.

Proof. See Appendix A.6. □

Proposition 3.3. *The Laplace transform of the interference from the vehicles on all but the streets that pass through the typical vehicle in the PSP-PPP with half-length density function $f_H(h)$ is given by*

$$\mathcal{L}_{I_{\mathrm{r}}}^{\mathrm{PSP-PPP}}(s) = \exp\left(-\frac{\mu}{\pi} \int_0^\infty \int_0^\pi \int_0^{2\pi} \int_0^\infty (1 - \mathcal{L}_{I_a}(s)) \gamma f_H(h)\,\mathrm{d}\gamma\,\mathrm{d}\phi\,\mathrm{d}\varphi\,\mathrm{d}h \right), \tag{3.17}$$

where

$$\mathcal{L}_{I_a}(s) = \exp\left(-\lambda p \int_{-h}^{h} \left(1 + \left(\frac{\gamma^2 + u^2 + 2\gamma u \cos(\phi - \varphi)}{s^\delta} \right)^{1/\delta} \right)^{-1} \mathrm{d}u \right).$$

Proof. See Appendix A.7. □

Following (3.14), the success probability of the typical vehicle in the PSP-PPP is

$$p_m^{\mathrm{PSP-PPP}} = \mathcal{L}_{I_o^m}^{\mathrm{PSP-PPP}}(\theta D^\alpha) \mathcal{L}_{I_!}^{\mathrm{PSP-PPP}}(\theta D^\alpha), \tag{3.18}$$

where $\mathcal{L}_{I_o^m}^{\mathrm{PSP-PPP}}(s)$ and $\mathcal{L}_{I_!}^{\mathrm{PSP-PPP}}(s)$ are given by (3.16) and (3.17), respectively.

Proposition 3.4. *The success probabilities of the typical general vehicle (order 2)*

and the typical T-junction vehicle (order 3) in the PLM-PPP can be approximated as

$$p_2^{\mathrm{PLM-PPP}} \approx p_2^{\mathrm{PSP-PPP}} = \mathcal{L}_{I_o^2}^{\mathrm{PSP-PPP}}(\theta D^\alpha)\mathcal{L}_{I_!}^{\mathrm{PSP-PPP}}(\theta D^\alpha), \tag{3.19}$$

$$p_3^{\mathrm{PLM-PPP}} \approx p_2^{\mathrm{PSP-PPP}} \times \int_0^\infty \exp\left(-\lambda p D\theta^{\delta/2} \int_0^{\frac{2h}{D\theta^{\delta/2}}} \frac{1}{1+v^{2/\delta}}\mathrm{d}v\right)\hat{f}_H(h)\,\mathrm{d}h, \tag{3.20}$$

respectively. $\mathcal{L}_{I_o^2}^{\mathrm{PSP-PPP}}(s)$ *is given by* (3.16) *and* $\mathcal{L}_{I_!}^{\mathrm{PSP-PPP}}(s)$ *by* (3.17) *with* $f_H(h) = \hat{f}_H(h) = 2bh\exp(-bh^2)$.

Proof. See Appendix A.8. □

Fig. 3.5 compares the success probabilities of the typical general and intersection/T-junction vehicles. We omit the plot for the success probability of the typical vehicle in the OG-PPP as it is the same as that in the PLP-PPP by Proposition 3.1. We see that the success probability of the typical general vehicle is higher than that of the typical intersection/T-junction vehicle in all the Cox vehicular networks. The reason is that as two streets pass through or end at the typical vehicle at an intersection or a T-junction, the received interference is higher compared to the typical general vehicle through which only one street passes.

Remark 3.1. *Fig. 3.5c indicates that the success probability of the typical general vehicle in the PLM-PPP is tightly lower bounded by that in the PSP-PPP with Rayleigh distributed half-lengths.*

Remark 3.2. *The approximation* (3.20) *to the success probability of the typical T-junction vehicle serves as a tight lower bound (Fig. 3.5c). The integral term on the right-hand side of* (3.20) *is the Laplace transform of the interference from the vehicles on the street that has its endpoint at the origin. We can rephrase* (3.20) *as follows. The success probability of the typical T-junction vehicle in the PLM-PPP is tightly lower bounded by the success probability of the typical vehicle (with one street*

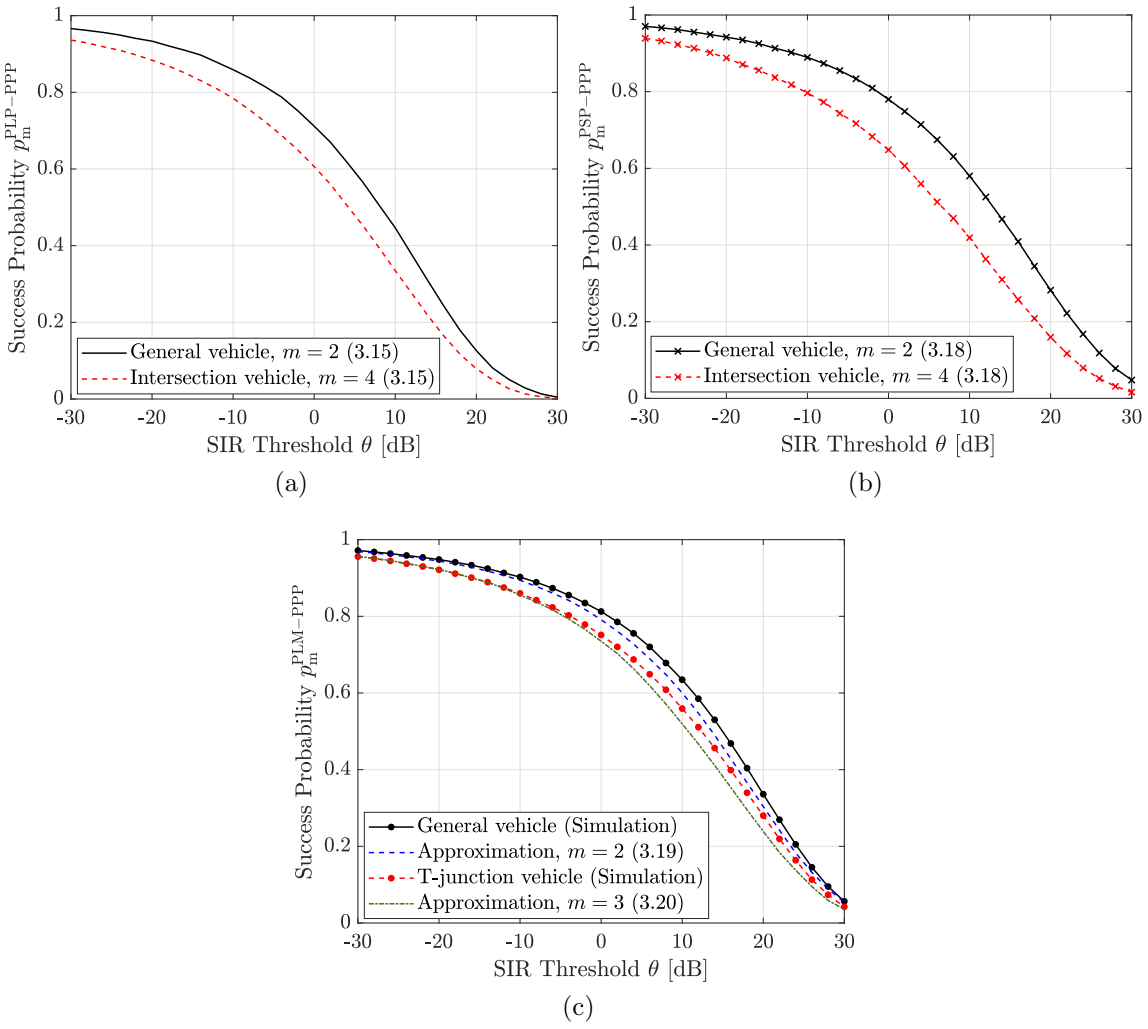

Figure 3.5: Success probabilities of the typical general and intersection/T-junction vehicles in the (a) PLP-PPP (b) PSP-PPP and (c) PLM-PPP. $\lambda p = 0.3, D = 0.25$, $\alpha = 4$, $\mu = 2$, 0.1, and 0.3 for the PLP, PSP, and PLM, respectively. $f_H^{\mathrm{PSP}}(h) = \delta(h - 10)$. The equation numbers are given in parentheses in the legends.

passing through) in the network formed by conditioning a street in the PSP-PPP (with Rayleigh distributed half-lengths) such that one of its endpoints is at the origin.

Next, we analyze the equivalence between the spatial models using their properties and the success probabilities of the typical vehicle in those models.

3.4 Equivalence of Spatial Models

To differentiate the street intensities of the models OG, PLP, PSP, and PLM, we denote them as μ_{OG}, μ_{PLP}, μ_{PSP}, and μ_{PLM}, respectively.

3.4.1 OG-PPP and PLP-PPP

Theorem 3.2. *The PLP-PPP of street intensity μ_{PLP} is strictly equivalent to the OG-PPP with street intensity $\mu_{\mathrm{OG}} = \mu_{\mathrm{PLP}}$.*

Proof. The equivalence is a direct consequence of the success probabilities of the typical vehicle in the OG-PPP and PLP-PPP given in Proposition 1. □

3.4.2 PSP-PPP and PLP-PPP

Theorem 3.3. *Let $H \triangleq cH_1$, where c is a constant and H_1 is a random variable with mean 1. The PLP is the limiting process of the PSP as $c \to \infty$ and $\mu_{\mathrm{PSP}} \to 0$ such that $2\mu_{\mathrm{PSP}}\mathbb{E}[H] = 2c\mu_{\mathrm{PSP}} = \mu_{\mathrm{PLP}}$.*

Proof. We formalize the heuristic arguments on the relation between the PLP and PSP given in [32]. From Definitions 3.4 and 3.5, we learn that the parameter spaces of line and stick are different. To compare the line process with the stick process, we first establish compatible parametrizations. Let $S'(r, \phi, q)$ denote the infinitely extended stick $S(y, \varphi, h)$, where $q = \overline{yz}$ is the distance between the midpoint of the stick $y = (u, v)$ and $z = (r\cos\phi, r\sin\phi)$, the closest point to the origin from $S'(r, \phi, q)$. Fig. 3.6 illustrates $S'(r, \phi, q)$ and $S(y, \varphi, h)$ using overlaid dashed and

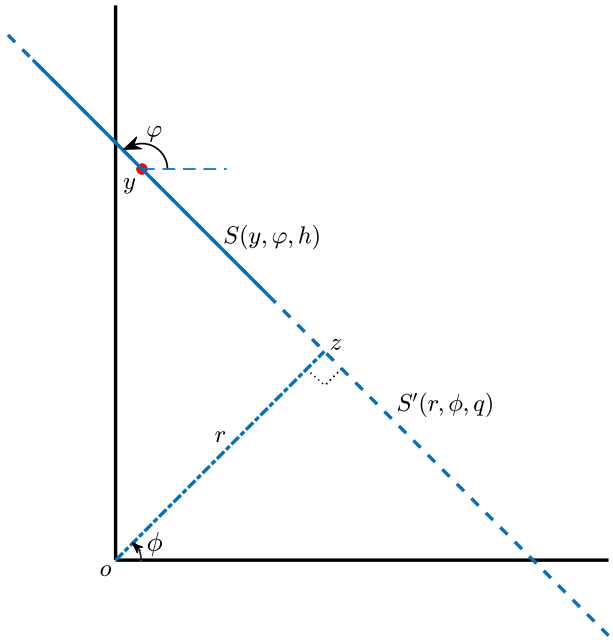

Figure 3.6: Reparametrization of the PSP. The stick $S(y, \varphi, h) \in \Xi_{\mathrm{S}}$ is extended to form a line $S'(r, \phi, q)$. The perpendicular from the extended stick is at a distance r from o and forms an angle ϕ with the $x-$axis.

solid lines, respectively. We can express $y = (u, v)$ and φ in terms of (r, ϕ) and q as $u = r\cos\phi - q\sin\phi$, $v = r\sin\phi + q\cos\phi$, and $\varphi = \phi - \pi/2$. The differential element $\mathrm{d}u\mathrm{d}v\mathrm{d}\varphi$ equals $\mathrm{d}r\mathrm{d}\phi\mathrm{d}q$, *i.e.,* the two parametrizations are equivalent.

By (3.4), the line is just the projection of the stick from the parameter space (r, ϕ, q) to (r, ϕ) when the latter is extended to infinity. However, we learn from Lemmas 3.1 and 3.2 that the properties of the PLP and PSP differ. Then, to obtain the PLP from PSP, we need to equate their statistical properties. Equating the mean total street length per unit area in the PLP and PSP given in Lemmas 3.1 and 3.2, we obtain $2\mu_{\mathrm{PSP}}\mathbb{E}[H] = \mu_{\mathrm{PLP}}$. For $\mu_{\mathrm{PSP}}\mathbb{E}[H] = c\mu_{\mathrm{PSP}}$ to remain finite, μ_{PSP} should go to zero as $c \to \infty$. □

Remark 3.3. *The PSP-PPP, and its limiting case, the PLP-PPP, are strictly equivalent. As the PLP and PSP are identically distributed as $c \to \infty$ and $\mu_{\mathrm{PSP}} \to 0$, equivalence is not restricted to PPPs on the streets but also holds for general point*

processes of vehicles.

3.4.3 PLM-PPP and PSP-PPP

We learned from Proposition 4 that the success probability of the typical general vehicle in the PLM-PPP is approximated by that in the PSP-PPP with the same half-length density function as the PLM-PPP. Furthermore, from Figs. 3.4a and 3.4b, we infer that the n-th nearest-neighbor distance distribution in the PLM-PPP is tightly upper bounded by that in the PSP-PPP. Consequently, we can deduce that the approximation to the success probability in the PLM-PPP is tight. Fig. 3.7 compares the simulated success probability of the typical general vehicle in the PLM-PPP with its lower bound. The maximum difference between the success probabilities in the PSP-PPP and PLM-PPP is $\epsilon = 0.0297$ for $\mu = 0.01$ and 0.0219 for $\mu = 1$. Though the PLM can characterize T-junctions, it is too complex to permit an exact analytical expression.

Remark 3.4. *The PLM-PPP is $\epsilon-$equivalent with $\epsilon \ll 1$ to the PSP-PPP with the same half-length distribution and street intensity as the PLM-PPP. Consequently, the PSP-PPP serves as a good substitute for the PLM-PPP.*

We see from Fig. 3.7 that the success probabilities of the typical general vehicle in the PLM-PPP and PSP-PPP with Rayleigh distributed half-lengths are even closer in the asymptotic regions of θ than in the middle regions of θ. Theorem 3.4 proves this observation formally.

Theorem 3.4. *The PLM-PPP is asymptotically equivalent in both the lower and upper regimes of θ to the PSP-PPP with the same half-length density as the PLM-PPP.*

Proof. First, we study the asymptotic behavior of the PSP-PPP as $\theta \to 0$ and ∞. Then, we compare them with that of the PLM-PPP.

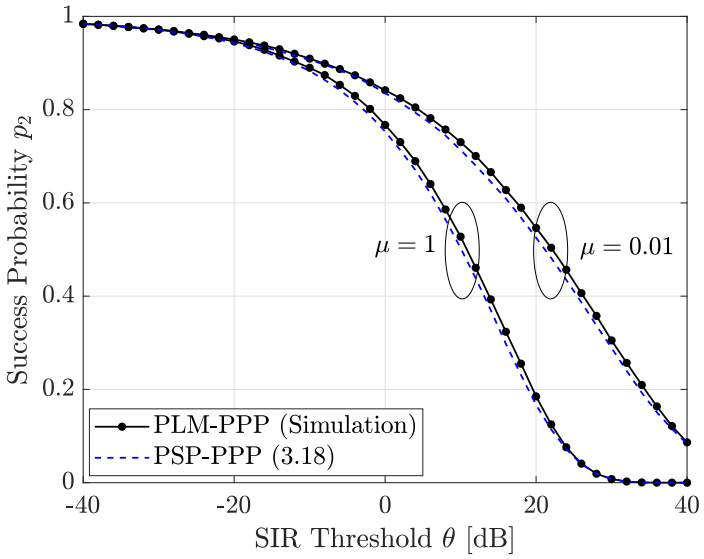

Figure 3.7: Success probability of the typical general vehicle in the PLM-PPP vs. that in the PSP-PPP-based approximation given by (19) with $f_H(h) = 2bh\exp(-bh^2)$, where $b = 1.04$ for $\mu = 1$, and 0.0103 for $\mu = 0.01$. $\lambda p = 0.3$, $D = 0.25$, and $\alpha = 4$.

Lemma 3.8. *As $\theta \to 0$, the PSP-PPP behaves like a vehicular point process formed only by the typical vehicle's streets, i.e.,*

$$1 - p_m^{\mathrm{PSP-PPP}}(\theta) = \Theta(\theta^{\delta m/4}). \tag{3.21}$$

Proof. See Appendix A.9. □

Lemma 3.9. *As $\theta \to \infty$, the success probability of the typical vehicle in the PSP-PPP tends to that in a 2D PPP, i.e.,*

$$p_m^{\mathrm{PSP-PPP}}(\theta) \sim \exp(-\pi\lambda_2 p D^2 \theta^{\delta}\Gamma(1+\delta)\Gamma(1-\delta)), \tag{3.22}$$

where $\lambda_2 = 2\mu\lambda\mathbb{E}[H]$ is the 2D intensity of the PSP-PPP.

Proof. See Appendix A.10. □

Equipped with the two lemmas, we continue with the proof of the theorem. As $\theta \to 0$, for SIR $> \theta$ to hold, it suffices not to have any interferers within a small disk

TABLE 3.1

CONDITIONS FOR EQUIVALENCE BETWEEN THE SPATIAL MODELS

Model A	Model B	Conditions for Equivalence
OG-PPP	PLP-PPP	$\mu_{\text{OG}} = \mu_{\text{PLP}}$
PLP-PPP	PSP-PPP	$\mu_{\text{PSP}} \to 0$ and $c \to \infty$ s.t. $2\mu_{\text{PSP}}\mathbb{E}[H] = 2c\mu_{\text{PSP}} = \mu_{\text{PLP}}$
PSP-PPP	PLM-PPP	$\mu_{\text{PSP}} = \mu_{\text{PLM}}$, $f_H^{\text{PSP}}(h) = f_H^{\text{PLM}}(h)$

around the typical vehicle. With high probability, the small disk intersects only the street(s) passing through the typical vehicle. Consequently, the system performance converges to that of only the typical vehicle's streets as $\theta \to 0$. The outage probability of the typical vehicle due to its streets alone is proportional to $\lambda p \theta^{\delta m/4}$ as $\theta \to 0$. On the other hand, as $\theta \to \infty$, for SIR $> \theta$, a large disk around the typical vehicle must be devoid of interferers. It follows from Lemma 3.9 that the street geometry outside a large disk does not matter as $\theta \to \infty$ since the PSP-PPP is similar to a 2D PPP at a large scale.

Lemma 3.8 extends to the PLM-PPP as the interaction between the sticks is irrelevant when $\theta \to 0$. Also, the success probability of the typical general vehicle with respect to its street alone in the PLM-PPP is the same as that in the PSP-PPP with the same half-length density as the PLM-PPP. In Appendix A.10, we reasoned that the PSP-PPP behaves like a 2D PPP as $\theta \to \infty$ through mapping all the points on the sticks to their respective midpoints. The same logic holds for the PLM-PPP as it is also formed by sticks whose midpoints form a PPP. As the PLM-PPP and PSP-PPP with the same half-length density as the PLM-PPP behave like 2D PPPs of the same intensities as $\theta \to \infty$, they are equivalent as $\theta \to \infty$. □

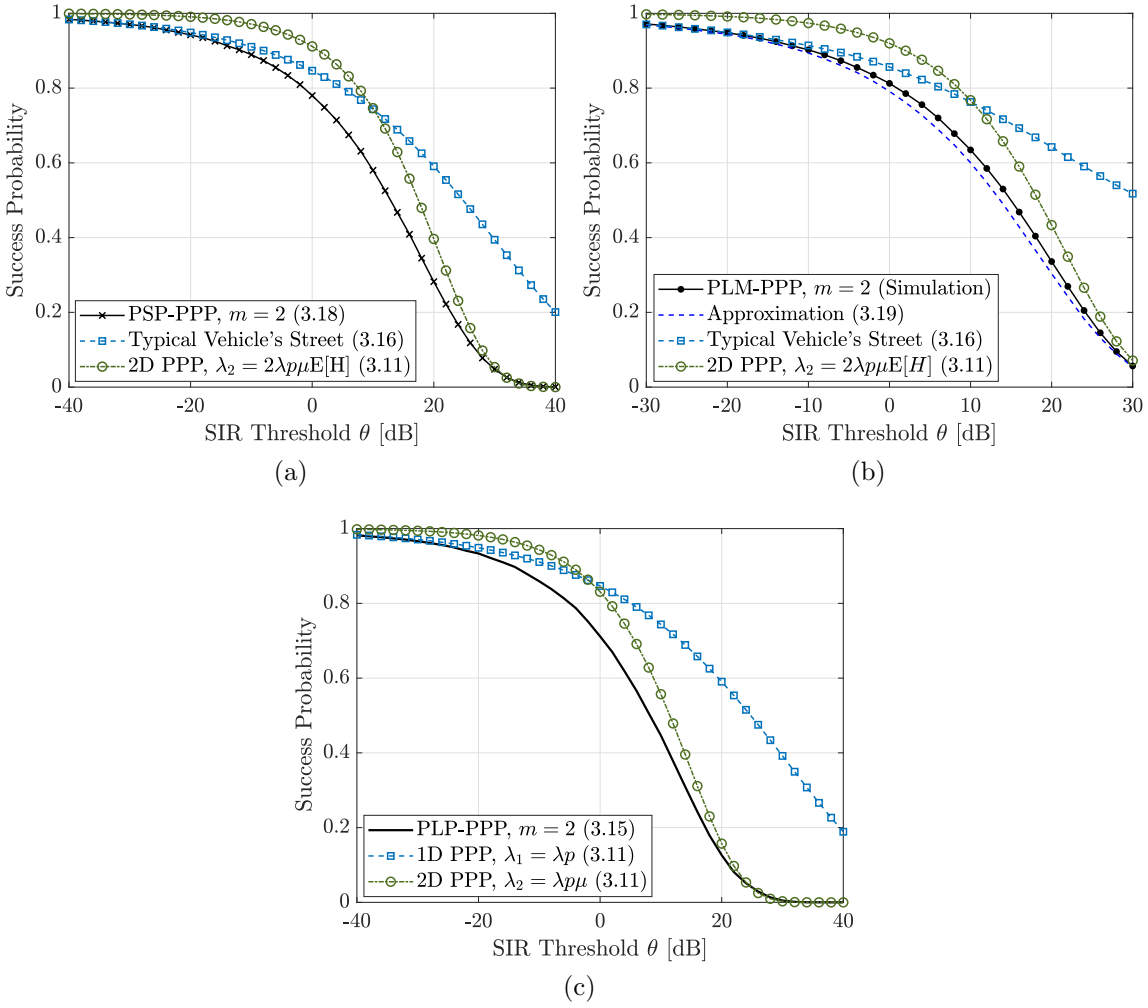

Figure 3.8: Success probability of the typical general vehicle in the (a) PSP-PPP (b) PLM-PPP (c) PLP-PPP vs. that of the typical vehicle in 1D and 2D PPPs. $\lambda p = 0.3, D = 0.25$, $\alpha = 4$, $\mu = 0.1$, 0.3, and 2 for the PSP, PLM, and PLP, respectively. $f_H^{\text{PSP}}(h) = \delta(h-10)$. The equation numbers are given in parentheses in the legends.

Fig. 3.8 compares the success probabilities of the typical general vehicle in the street-based Cox vehicular networks with that of the typical vehicle in 1D and 2D PPPs. The success probability of the typical vehicle in the PSP-PPP and PLM-PPP tends to that in the network formed only by the typical vehicle's street(s) as $\theta \to 0$ and to that of the 2D PPP as $\theta \to \infty$, as given in Theorem 3.4 and the lemmas therein. The same holds for the PLP-PPP (we defer the proofs to Chapter 4). As vehicles on each street in the PLP-PPP form a 1D PPP, the PLP-PPP behaves like a 1D PPP as $\theta \to 0$.

Until now, we have assumed that the link distance D is fixed. Next, we discuss the equivalence between the spatial models when the link distances are random. Here, the success probability is obtained by averaging the Laplace transform of the interference over the link distances.

3.4.4 Equivalence Under Random Link Distances

3.4.4.1 PLP-PPP vs. OG-PPP

The OG-PPP is just a rotational variant of the PLP-PPP. Both of them have the same statistical properties such as the mean total street length per unit area (Lemma 3.1), distribution of the distance to the nearest neighbor (Lemma 3.6), and the Laplace transform of the interference (Proposition 3.1). Hence, the OG-PPP and PLP-PPP are strictly equivalent even if the link distances are random.

3.4.4.2 PSP-PPP vs. PLP-PPP

The PLP is the limiting process of the PSP as the lengths of the sticks extend to infinity and street intensity tends to zero (Theorem 3.3). By the inherent nature of the PSP, it is equivalent to the PLP irrespective of the mode of communication.

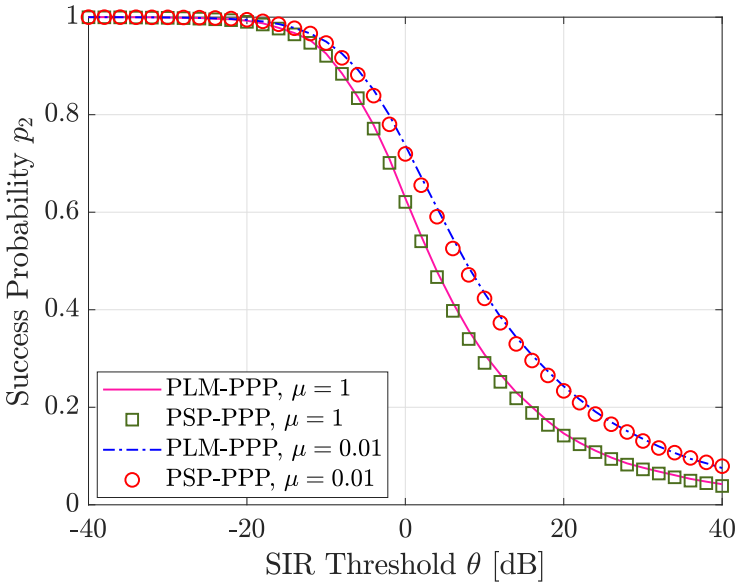

Figure 3.9: Success probabilities of the typical general vehicle that receives a message from its nearest neighbor. $\lambda p = 0.5$ and $\alpha = 4$. $f_H(h) = \hat{f}_H(h) = 2bh\exp(-bh^2)$, where $b = 1.04$ for $\mu = 1$, and 0.0103 for $\mu = 0.01$.

3.4.4.3 PLM-PPP vs. PSP-PPP

We deduced from Figs. 3.4a and 3.4b that the n-th nearest-neighbor (or interferer) distance distribution in the PLM-PPP is tightly upper bounded by that in the PSP-PPP with Rayleigh distributed half-lengths. It follows that irrespective of the distribution of the distance to the intended transmitter, the PLM-PPP and PSP-PPP with Rayleigh distributed half-lengths are $\epsilon-$equivalent. Fig. 3.9 validates the above inference for the case where the typical general vehicle receives a message from its nearest neighbor (transmitter) through simulations.

Remark 3.5. *The notion of equivalence enables us to consider only a representative set of spatial models to obtain insights on the effect of the network parameters, thereby reducing the computational costs and time associated with large-scale experiments and system-level simulations. The success probabilities of the typical vehicle in the OG-PPP, PLP-PPP, and PLM-PPP can be obtained from that in the PSP-PPP by a suitable mapping between the parameters as summarized in Table 3.1.*

3.5 Conclusions

We developed a Coxian framework for the modeling and analysis of vehicular networks. The spatial models in this framework can characterize different street geometries involving intersections and T-junctions, and street lengths that can be independent or dependent on each other. Streets of infinite lengths and different orientations forming intersections can be characterized by PLPs and their rotational variants. PSPs and PLMs can model streets of varying finite lengths forming intersections and T-junctions, respectively. We evaluated the reliability of a vehicle-to-vehicle link in the Cox vehicular networks when the receiving vehicle is at an intersection, a T-junction, or a general location, and its transmitter is at a certain fixed distance. Our approach to defining the street system as a union of points of different orders facilitates general analytical results for different types of typical vehicles. The expressions for the reliability can be used to investigate the interplay among the network parameters such as data rate, street intensity, vehicle density, and the type of vehicle.

The concept of equivalence demonstrates that one does not need different spatial models to analyze the reliability of a vehicle-to-vehicle link in different geographical regions. The models considered in the Coxian framework are equivalent in terms of reliability. This implies that the expression for the reliability of the typical vehicle in the PSP-PPP is sufficient to evaluate that in the OG-PPP, PLP-PPP, and PLM-PPP by appropriately mapping the system parameters. Also, the vehicular networks behave like PPPs only in the asymptotic regimes of the reliability or data rate. Hence, the street geometry is relevant to understand vehicular network behavior.

An interesting future extension would be to understand how two or more models developed in the Coxian framework can be superimposed to represent an intricate geographic region with intersections and T-junctions, and streets and highways. Also, one may look for tractable models that characterize curved streets and examine whether they are equivalent to the line/stick-based vehicular networks.

CHAPTER 4

TRANSDIMENSIONAL MODELS FOR VEHICULAR NETWORKS

Although the PPPs are tractable, coupling them with PLPs/PSPs turns them into Cox models that lead to complex analytical expressions for the success probability (see Propositions 3.1–3.4 and [23, 24, 25, 26, 27, 29]). Nevertheless, vehicle locations cannot be simply modeled as random points as in a 2D PPP neglecting the street geometry [21]. The random locations of points in a PPP defy the certainty of vehicles to be located on a line/stick. In this chapter, we explore the middle route between the complicated Cox vehicular network models and the oversimplified 2D PPP and introduce a model that provides a good trade-off between accuracy *and* tractability.

4.1 The Transdimensional Poisson Point Process

We propose a transdimensional model that includes the vehicles on the street(s) passing through the typical vehicle of order m at the origin and models the remaining vehicles on the plane as a 2D PPP neglecting the geometry of the other streets. By such superposition, we account for the geometry of the street(s) passing through the receiver, and, at the same time, we obviate the need to incorporate the geometry of the remaining streets. The formal definition follows.

Definition 4.1. *Let* $\Psi_k = \{(t_1, 0), (t_2, 0), \dots\}$ *where* $\{t_i\}$, $i \in \mathbb{N}$, *is a 1D PPP of intensity* λ *on* $\mathcal{R}_k \subseteq \mathbb{R}$, $1 \leq k \leq m/2$, *and* $m \in \{2, 4\}$. *Let* $\Psi_o^m = \bigcup_{k=1}^{m/2} \Psi_k$ *denote the point process on* $m/2$ *streets that pass through the typical vehicle of order* m. *The transdimensional Poisson point process (TPPP) with respect to the typical*

vehicle of order m is the superposition of Ψ_o^m *and a 2D PPP* Φ_2 *of intensity* λ_2*, i.e.,* $\mathcal{T} \triangleq \Psi_o^m \cup \Phi_2$.

Ψ_o^m is equivalent in distribution to $\mathcal{V}_o^m$ as the 1D PPPs on $m/2$ streets are independent, and their orientations are i.i.d. $\mathcal{R}_k$ is an infinite or a finite interval that contains the origin. $\mathcal{R}_k = \mathbb{R}$ if the street is a line, and $\mathcal{R}_k \subset \mathbb{R}$ if the street is a stick. By the superposition property of the PPP, Ψ_o^m—the union of 1D PPPs of intensity λ on $m/2$ lines passing through the typical vehicle of order m—is equivalent to a 1D PPP of intensity $m\lambda/2$. By Lemma 3.2, $\lambda_2 = \lambda\mu$. Fig. 4.1a shows a realization of the TPPP corresponding to the PLP-PPP.

The superposition property does not extend to the PSP-PPP even if the sticks are of the same finite length. The reason is that the origin can be located at a distance $w \in (0, h_y)$ from the midpoint y of the stick. The lengths of the sticks on both sides of the origin need not be the same. In other words, the interference measured at the origin with respect to the two streets may differ. The streets passing through the origin form a Cox process as they are stochastic with respect to the length of the stick as well as their starting or ending points. Figs. 4.1b and 4.1c show the snapshots of the TPPP with respect to the typical general and intersection vehicles in the PSP-PPP, where the half-length of a stick follows the Rayleigh distribution. For the sake of visualization, we show the streets to be orthogonal in Fig. 4.1c rather than being on top of each other as given in Definition 4.1. We have $\lambda_2 = 2\lambda\mu\mathbb{E}[H]$ by Lemma 3.2.

The TPPP $\mathcal{T}$ is non-stationary as the neighborhood seen by a point in Ψ_o^m is different from that in Φ_2 as at least one street passes through the typical vehicle.

We have so far focused on the success probability as the performance metric, which represents the average performance of the vehicles. Hereafter, we broaden our focus to a more refined metric, the SIR meta distribution, whose special case is the success probability.

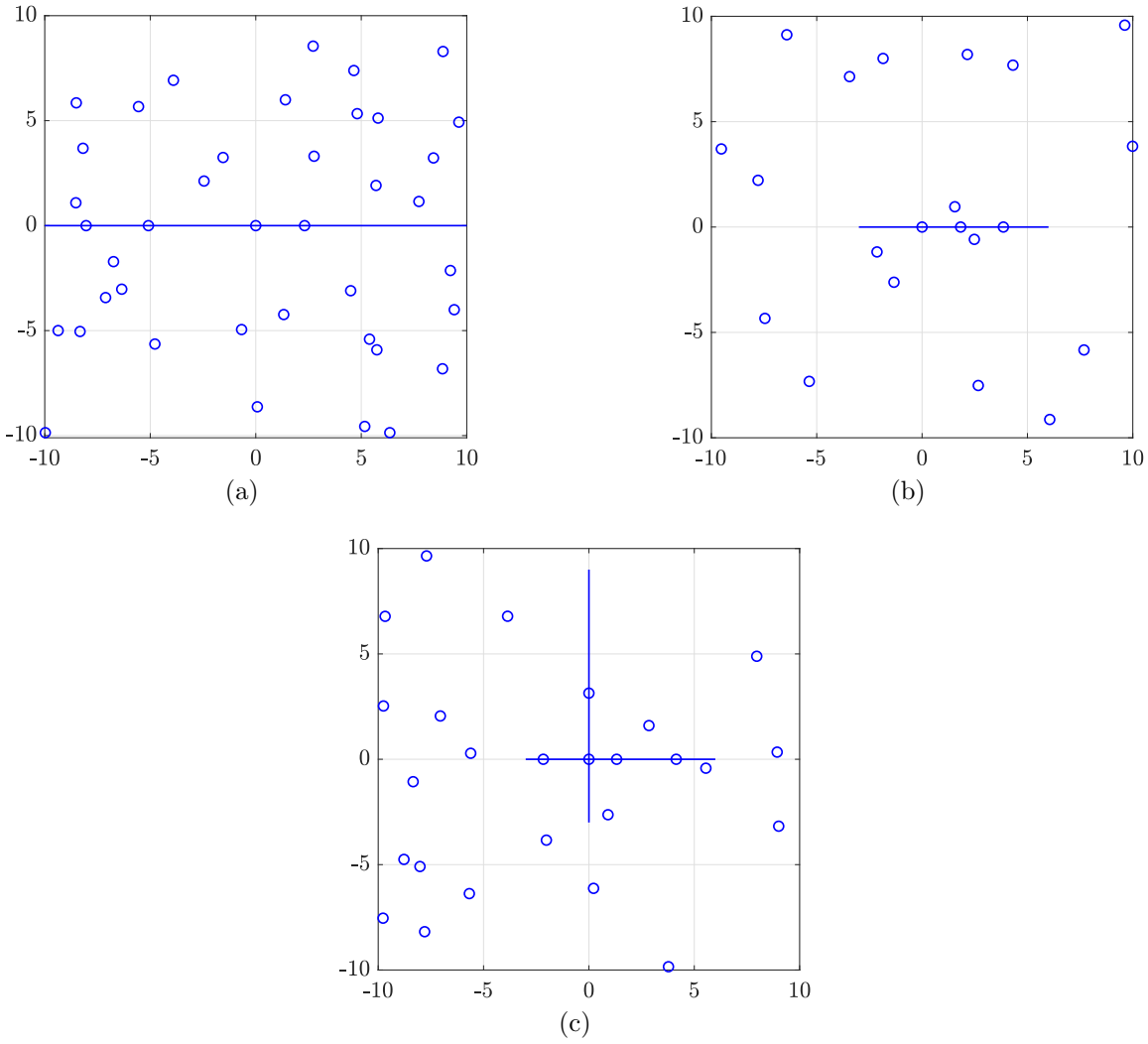

Figure 4.1: Snapshot of the TPPP with respect to the typical vehicle in the PLP-PPP is shown in (a), where $m\lambda/2 = \lambda_2 = 0.1$. Snapshots of the TPPP with respect to the typical general and intersection vehicles in the PSP-PPP are shown in (b) and (c), respectively, where $\lambda = 0.3$, $\mu = 0.01$, $f_H(h) = 2ch\exp(-ch^2)$ with $c = 0.01$, and $\lambda_2 = 2\lambda\mu\mathbb{E}[H]$. Line/stick denotes a street and 'o' denotes a vehicle.

4.2 SIR Meta Distribution

The SIR MD naturally includes a reliability constraint on the individual transmitter-receiver links [34, 35, 36]. It answers questions like *what fraction of the links support a target data rate of* 10 *Kbps with a probability of at least* 0.99*?*, whereas the success probability answers questions like *what fraction of the links support a target data rate of* 10 *Kbps?*, focusing on the average performance without reliability constraint.

We illustrate the need to look beyond the average using Fig. 4.2. It depicts the histogram of the link success probabilities of the vehicles in two different scenarios with the intensity of the active vehicles λp being constant. The success probability is the mean of the link success probabilities. We observe that though the mean success probability is the same, the distributions of the link success probabilities differ. The mean does not provide any information on the performance of the vehicles with bad link success probabilities. As vehicle safety is a serious concern, it is significant to understand the reliability of each vehicle-to-vehicle link.

4.2.1 Related Work

The SIR MD was first introduced in [34] and was evaluated for Poisson bipolar and cellular networks. Further, it was extended to carry out a fine-grained analysis of the base station cooperation, power control, and device-to-device (D2D) underlays in cellular networks. Apart from the SIR, the MD can also be defined for the data rate, energy harvested, etc. (see [37] and references therein).

In terms of vehicular networks, the SIR MD was analyzed for linear motorways [38] and intersections [39]. The intersection is formed by two finite road segments with vehicles forming a PPP on each segment. It is shown that the MD is bimodal, *i.e.,* the individual link success probabilities are either low or high, not concentrated near their average. In the linear motorway model, the inter-vehicle distances follow a shifted exponential distribution, *i.e.,* the vehicles are separated by a constant plus a

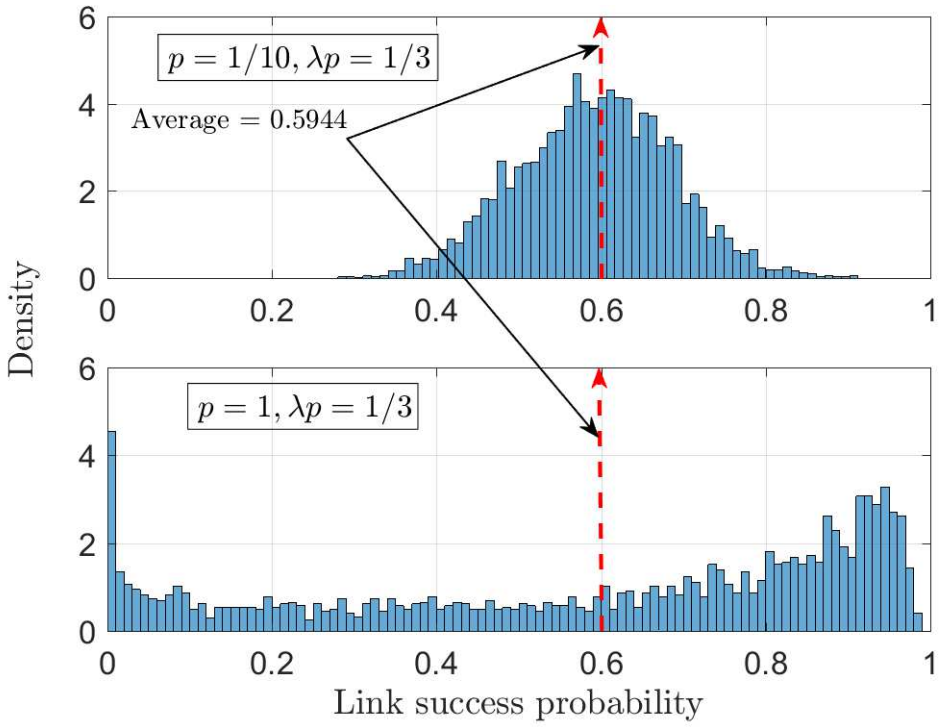

Figure 4.2: The histogram of the empirical probability density function of the link success probability for transmit probabilities $p = 1/10$ and $p = 1$. Both cases have the same mean success probability of 0.5944, but we see a different distribution of link success probabilities for different values of λ and p. For $p = 1/10$, the link success probabilities mostly lie between 0.4 and 0.8 (concentrated around their mean), while for $p = 1$, they are spread much more widely. Taken from [1].

distance modeled by the exponential distribution.

Furthermore, using the SIR MD, we can find the maximum density of concurrently active links that satisfy a certain reliability constraint, referred to as the spatial outage capacity (SOC) [1]. The SOC captures the trade-off between the density of active links and the fraction of the reliable links. Also, we can find insights on how to adapt the transmission parameters at a given vehicle density to avoid network congestion. When the channel load increases beyond a certain threshold, the number of packet collisions sharply increases, and the channel is said to be congested. The common methods to combat congestion include controlling the transmit i) rate, ii) power, and iii) data rate, and their combinations [40]. In this chapter, we show how to handle congestion using the SIR MD by exploring the trade-off between the transmit rate and the fraction of reliable links.

4.2.2 Formulation

The success probability on the link between the vehicle at the origin of order m and its transmitter is

$$P_m(\theta) = \mathbb{P}(\mathsf{SIR} > \theta \mid \mathcal{V}), \tag{4.1}$$

where θ is the SIR threshold that parametrizes the data rate. Conditioning on $\mathcal{V}$ in (4.1) implies that we average only over the fading and the transmitter point process (determined by slotted ALOHA). Due to the conditioning, we also refer to the link success probability as conditional success probability.

The meta distribution of the SIR is given by [34, 35]

$$\bar{F}_{P_m}(\theta, x) = \mathbb{P}(P_m(\theta) > x), \quad x \in [0, 1], \tag{4.2}$$

where x is the reliability threshold. By the Gil-Pelaez theorem, the SIR meta distri-

bution can be expressed as

$$\bar{F}_{P_m}(\theta, x) = \frac{1}{2} + \frac{1}{\pi} \int_0^\infty \frac{\Im(e^{-jt \log x} M_{jt,m})}{t} \mathrm{d}t, \tag{4.3}$$

where

$$M_{b,m}(\theta) = \mathbb{E}[P_m(\theta)^b], \;\; b \in \mathbb{C}. \tag{4.4}$$

The average of the conditional success probabilities is the success probability p_m, *i.e.,*

$$p_m = \mathbb{E}[P_m(\theta)] = \mathbb{P}(\mathsf{SIR} > \theta). \tag{4.5}$$

Since $p_m = M_{1,m}(\theta)$, the terms 'first moment' and 'success probability' can and will be used interchangeably.

Now, we are ready to analyze the SIR meta distributions for the PLP-PPP, PSP-PPP, and their respective TPPPs, and discuss the logic behind using the TPPP for vehicular network analysis. To this end, we derive the moments (4.4) required to calculate the SIR meta distribution (4.3) for the PLP-PPP and the corresponding TPPP; then, we perform a comparative analysis of the moments of different orders in the PLP-PPP and TPPP followed by that of their respective SIR meta distributions.

4.3 The Transdimensional Approach to the PLP-PPP

4.3.1 Derivation of Moments

Theorem 4.1. *The b-th moment of the conditional success probability* $P_m^{\mathrm{PLP-PPP}}(\theta)$ *of the typical vehicle of order* $m \in \{2, 4\}$ *in the PLP-PPP is given by*

$$M_{b,m}^{\mathrm{PLP-PPP}} = \exp(-m\lambda D \theta^{\delta/2} \Gamma(1+\delta/2)\Gamma(1-\delta/2)\mathfrak{D}_b(p, \delta/2) - 2\mu \textstyle\int_0^\infty (1 - G_b(t))\mathrm{d}t), \tag{4.6}$$

where $G_b(t) = \exp\left(-\lambda\delta \int_{t^{2/\delta}}^{\infty} \left[1-\left(1-\frac{ps}{v+s}\right)^b\right] \frac{v^{\delta-1}}{\sqrt{v^\delta - t^2}} \mathrm{d}v\right)$, $s = \theta D^\alpha$, $\mathfrak{D}_b(p, \delta/2) = pb\,{}_2F_1(1-b, 1-\delta/2; 2; p)$, *and* $\delta = 2/\alpha$,.

Proof. See Appendix B.1. □

Corollary 4.1. *The first moment* $M_{1,m}^{\mathrm{PLP-PPP}}$ *or, equivalently, the success probability* $p_m^{\mathrm{PLP-PPP}}$ *is*

$$M_{1,m}^{\mathrm{PLP-PPP}} = \exp(-m\lambda p D\theta^{\delta/2}\Gamma(1+\delta/2)\Gamma(1-\delta/2) - 2\mu \textstyle\int_0^\infty (1 - \mathcal{L}_{I_t}(\theta D^\alpha))\mathrm{d}t), \tag{4.7}$$

where $\mathcal{L}_{I_t}(s) = \exp\left(-\lambda p s^{\delta/2} \int_{u_t}^{\infty} \frac{1}{\left(1+u^{1/\delta}\right)\sqrt{u-u_t}} \mathrm{d}u\right)$ *with* $u_t = t^2 s^{-\delta}$.

Proof. It directly follows from (4.6) by noting that $\mathfrak{D}_1(p, \delta/2) = p$ and the change of variable $u = v^\delta$ in $G_b(t)$ with $b = 1$. □

See the proof of Proposition 3.1 and [27] for alternative proofs.

Corollary 4.2. *For a given transmitter density* $\lambda p = C$, *as* $p \to 0$, *we have*

$$\lim_{\substack{p\to 0 \\ \lambda p = C}} P_m^{\mathrm{PLP-PPP}} = M_{1,m}^{\mathrm{PLP-PPP}}$$

in mean square (and probability and distribution).

Proof. See Appendix B.2. □

The conditional success probabilities converge to their average only when $p \to 0$. Generally, the average gives very little information on the individual links.

Theorem 4.2. *The b-th moment of* $P_m^{\mathrm{TPPP}}(\theta)$ *of the typical vehicle in the TPPP is*

$$M_{b,m}^{\mathrm{TPPP}} = \exp(-m\lambda D\theta^{\delta/2}\Gamma(1+\delta/2)\Gamma(1-\delta/2)\mathfrak{D}_b(p, \delta/2)$$

$$- \lambda\mu\pi D^2\theta^{\delta}\Gamma(1+\delta)\Gamma(1-\delta)\mathfrak{D}_b(p,\delta)), \tag{4.8}$$

where $\delta = 2/\alpha$ *and* $\mathfrak{D}_b(p,q) = pb\,{}_2F_1(1-b,1-q;2;p)$.

Proof. In a d-dimensional PPP Φ_d of intensity λ_d, the b-th moment of the conditional success probability for a link distance D is [34, Eqn. (4)]

$$M_b^{\Phi_d} = \exp(-\lambda_d c_d D^d \theta^{\delta'}\Gamma(1+\delta')\Gamma(1-\delta')\mathfrak{D}_b(p,\delta')), \tag{4.9}$$

where $\delta' = d/\alpha$. By the independence of the point processes Ψ_o^m and $\Phi_2 \subset \mathcal{T}$, $M_{b,m}^{\text{TPPP}}$ is the product of the moments of the conditional success probabilities in Ψ_o^m and Φ_2 given by (4.9) with $\lambda_1 = (m/2)\lambda$ and $\lambda_2 = \lambda\mu$. □

The success probability p_m^{TPPP} of the typical vehicle is the first moment $M_{1,m}^{\text{TPPP}}$. It is obtained by setting $b = 1$ in (4.8), *i.e.,*

$$M_{1,m}^{\text{TPPP}} = \exp(-m\lambda p D\theta^{\delta/2}\Gamma(1+\delta/2)\Gamma(1-\delta/2) - \lambda p\mu\pi D^2\theta^{\delta}\Gamma(1+\delta)\Gamma(1-\delta)). \tag{4.10}$$

The second term in the exponential in (4.6) has two nested integrals over infinite ranges, while that in (4.8) has none. The numerical evaluation of (4.6), in particular when used in (4.3), is tedious since it involves three layers of complex-valued integrals. Note that it takes about 100,000 times longer to numerically evaluate the first moment for the PLP-PPP (4.7) than that for the TPPP (4.10). To demonstrate that the TPPP is an accurate yet simple model, we compare the SIR MDs of the PLP-PPP and the corresponding TPPP, starting with the first moment.

4.3.2 First-Order Moment Analysis for the PLP-PPP

The moments of the conditional success probability for the PLP-PPP (4.6) do not have closed-form expressions. To gain insights into $M_{1,m}^{\mathrm{PLP-PPP}}$ or $p_m^{\mathrm{PLP-PPP}}$, we begin with the asymptotic analysis with respect to θ.

Theorem 4.3. *The success probability of the typical vehicle tends to that in a 1D PPP as $\theta \to 0$, i.e.,*

$$1 - p_m^{\mathrm{PLP-PPP}}(\theta) \sim m\lambda p D \theta^{\delta/2} \Gamma(1+\delta/2)\Gamma(1-\delta/2), \ \ \theta \to 0. \tag{4.11}$$

Intuitively, as $\theta \to 0$, for SIR $> \theta$ to hold, it suffices not to have any interferers within a small disk around the typical vehicle. With high probability, the small disk intersects only the street(s) passing through the typical vehicle. Consequently, as $\theta \to 0$, the success probability of the typical vehicle in the PLP-PPP converges to that in the network formed only by the typical vehicle's streets.

Proof. See Appendix B.3. □

Theorem 4.4. *The success probability of the typical vehicle tends to that in a 2D PPP as $\theta \to \infty$, i.e.,*

$$p_m^{\mathrm{PLP-PPP}}(\theta) \sim \exp(-\pi\lambda p \mu D^2 \theta^{\delta} \Gamma(1+\delta)\Gamma(1-\delta)), \ \ \theta \to \infty. \tag{4.12}$$

Proof. See Appendix B.4. □

Here the intuition is that as $\theta \to \infty$, for SIR $> \theta$, a large disk around the typical vehicle must be devoid of interferers. The fact that $p_m^{\mathrm{PLP-PPP}}$ tends to the success probability of the typical vehicle in a 2D PPP as $\theta \to \infty$ signifies that the geometry of the vehicle locations outside the large disk does not matter. This is further corroborated by the nature of the pair correlation function of the PLP-PPP

given by [41, Ch. 8]

$$g^{\mathrm{PLP-PPP}}(r) = 1 + \frac{1}{\mu r}. \tag{4.13}$$

It tends to 1 as $r \to \infty$ implying that the locations of the vehicles separated by larger distances are independent as in a PPP [4].

Fig. 4.3 compares the success probability in the PLP-PPP to that in the 1D and 2D PPPs. We observe from Fig. 4.3 that the success probability of the typical vehicle is upper bounded by the minimum of the success probabilities of the typical vehicle in 1D and 2D PPPs. This implies that either a 1D PPP or a 2D PPP alone is insufficient to characterize the vehicular network. We also see that the success probabilities of the typical vehicle in the PLP-PPP tend to that in the 1D and 2D PPPs in the asymptotic regimes as established in Theorems 4.3 and 4.4. This hints at the possibility of using a simpler, purely PPP-based model that has the properties of both the 1D and 2D PPPs for vehicular network analysis. In the next subsection, we show that the TPPP model indeed results in a highly accurate approximation of the PLP-PPP.

4.3.3 Comparison of First-Order Moments

We remark that the TPPP, by its inherent nature, behaves like a 1D PPP as $\theta \to 0$ and a 2D PPP as $\theta \to \infty$. By Theorems 4.3 and 4.4, the PLP-PPP exhibit the same behavior as the TPPP in the asymptotic regimes of θ. Here, we analyze the non-asymptotic behavior of $M_{1,m}^{\mathrm{PLP-PPP}}$ and $M_{1,m}^{\mathrm{TPPP}}$.

Theorem 4.5. *The nearest-neighbor distance in the PLP-PPP is stochastically dominated by the distance from the typical vehicle at the origin in the TPPP to its nearest neighbor.*

Proof. Using $e^{-x} \geq 1 - x$, we can bound the nearest-neighbor distance distribution

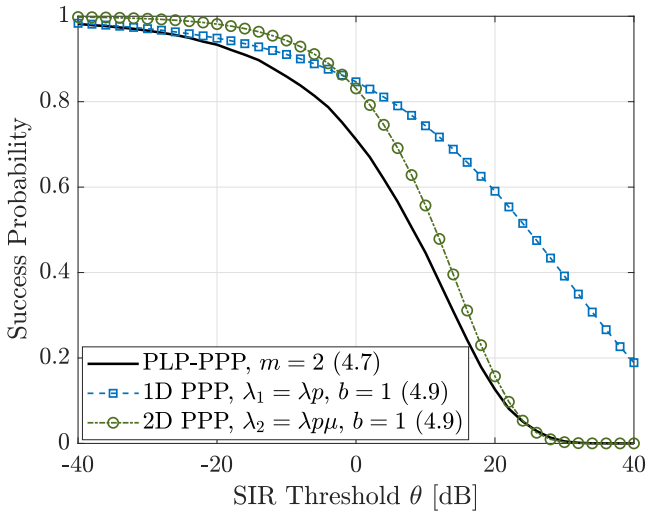

(a)

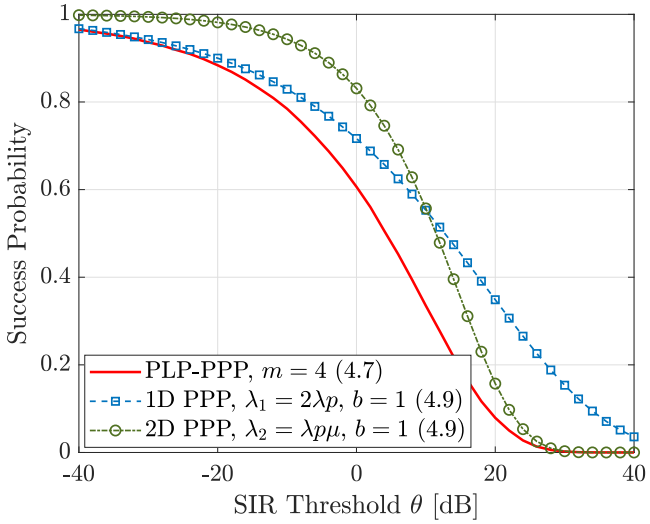

(b)

Figure 4.3: Comparison of success probabilities of the (a) typical general vehicle and (b) typical intersection vehicle in the PLP-PPP to that of the typical vehicle in 1D and 2D PPPs. $\mu = 2$, $\lambda = 1$, $p = 0.3$, $D = 0.25$, and $\alpha = 4$. The equation numbers are given in the parentheses in the legends.

in the PLP-PPP given in Lemma 3.6 as

$$F_R^{\text{PLP}-\text{PPP}}(r) \leq 1 - \exp(-\lambda m r - 4\pi\mu\lambda \int_0^r \sqrt{r^2 - u^2}\,\mathrm{d}u)$$
$$= 1 - \exp(-\lambda m r - \lambda\mu\pi r^2). \tag{4.14}$$

The nearest-neighbor distance distribution in a d-dimensional PPP Φ_d is given by

$$F_R^{\Phi_d}(r) = 1 - \exp(-c_d \lambda_d r^d), \tag{4.15}$$

where $c_1 = 2$ and $c_2 = \pi$. By Definition 4.1, Ψ_o^m is a union of m 1D PPPs. Comparing (4.14) and (4.15), we observe that $F_R^{\text{PLP}-\text{PPP}}(r) \leq F_R^{\Psi_o^m \cup \Phi_2}(r) \equiv F_R^{\text{TPPP}}(r)$ with $\lambda_1 = (m/2)\lambda$ and $\lambda_2 = \lambda\mu$. □

Conjecture 4.1. *The distance from the typical vehicle at the origin to the n-th nearest neighbor in the TPPP stochastically dominates that in the PLP-PPP for all $n \in \mathbb{N}$.*

An important consequence of Conjecture 4.1 is that the success probability of the typical vehicle at the origin in the PLP-PPP is lower bounded by that in the TPPP. Here, we give a heuristic argument for Conjecture 4.1. The 2D density of the vehicles in the TPPP is the same as that in the PLP-PPP. Then the comparison of the distances to the n-th nearest neighbor r_n can be based only on the vehicle placement with respect to the typical vehicle.

Fig. 4.4 compares the simulated values of $\mathbb{E}[r_n^2]/n$ in the PLP-PPP and TPPP. We observe that the mean squared distance from the typical general vehicle to the n-th nearest neighbor is higher for the PLP-PPP than the TPPP. The case of $n = 1$ follows from Theorem 4.5. We presume that this observation can be extended to higher values of n. Since the TPPP includes points at random independent locations compared to the PLP-PPP with points only concentrated on the lines, the probability

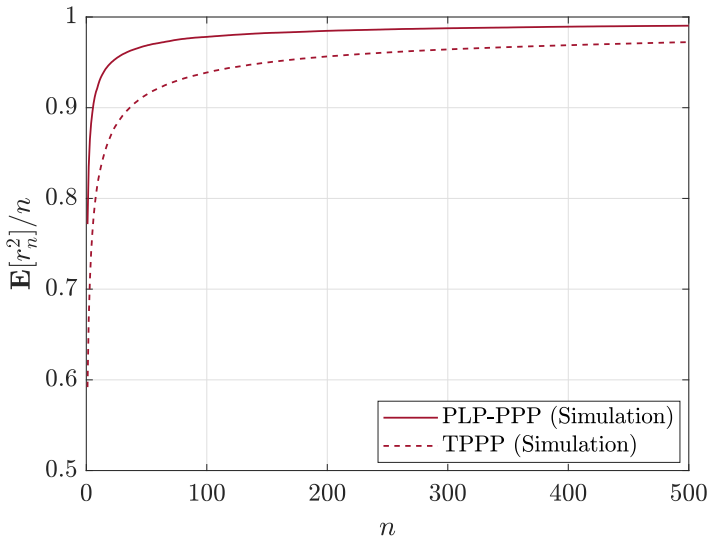

Figure 4.4: Comparison of normalized mean squared distances to the n-th nearest neighbor from the typical general vehicle at the origin in the PLP-PPP and TPPP. $\lambda = \mu = 1$.

that the n-th nearest neighbor is at a distance r_n is higher for the TPPP. It follows that the average distance to the n-th nearest interferer from the origin is higher for the PLP-PPP, which in turn, leads to a higher success probability than for the TPPP.

Fig. 4.5 plots the difference in the success probabilities of the typical general vehicle in the PLP-PPP and TPPP. Letting $x = \lambda p$ and $y = D^2\theta^\delta$, the integrated difference $\int_0^\infty \int_0^\infty (p_2^{\mathrm{PLP-PPP}}(x,y) - p_2^{\mathrm{TPPP}}(x,y))\mathrm{d}x\mathrm{d}y$ is maximized at $\mu = 0.204$, which is the value we choose to plot the difference in Fig. 4.5. The maximum difference between the success probabilities of the PLP-PPP and TPPP is about -14 dB (0.0404). Therefore, the success probability in the TPPP is a tight lower bound to that in the PLP-PPP. Note that the inferences obtained from Figs. 4.4 and 4.5 also apply to the typical intersection vehicle as the characterization of the streets that pass through the typical vehicle is the same in both the PLP-PPP and TPPP.

Fig. 4.6 compares the outage probabilities of the typical general vehicle in the PLP-PPP and TPPP to that of the typical vehicle in a 1D PPP. We observe that the TPPP better approximates the PLP-PPP for small θ than just a 1D PPP. As

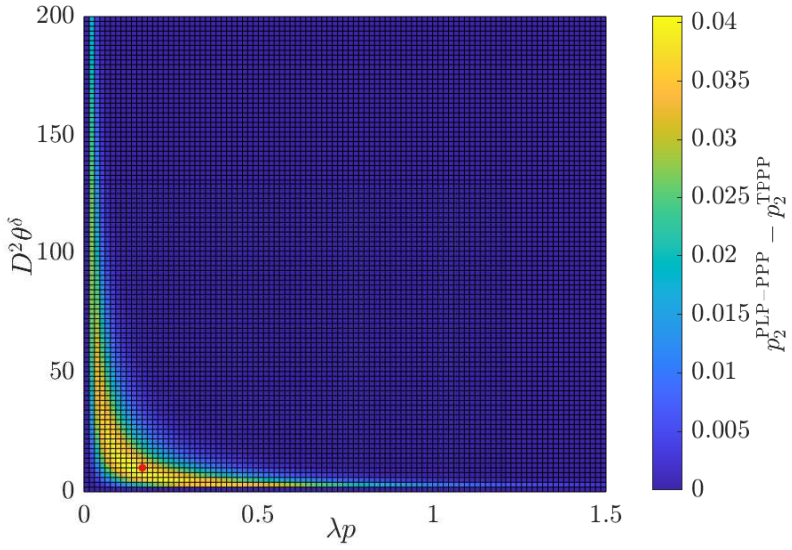

Figure 4.5: Difference between the success probabilities of the typical general vehicle in the PLP-PPP (4.7) and TPPP (4.10) as a function of λp and $D^2\theta^\delta$. $\mu = 0.204$, $\delta = 2/\alpha$, and $\alpha = 4$. The maximum difference of 0.0404 corresponding to the pair $(0.12, 10.1)$ is highlighted using a red filled circle.

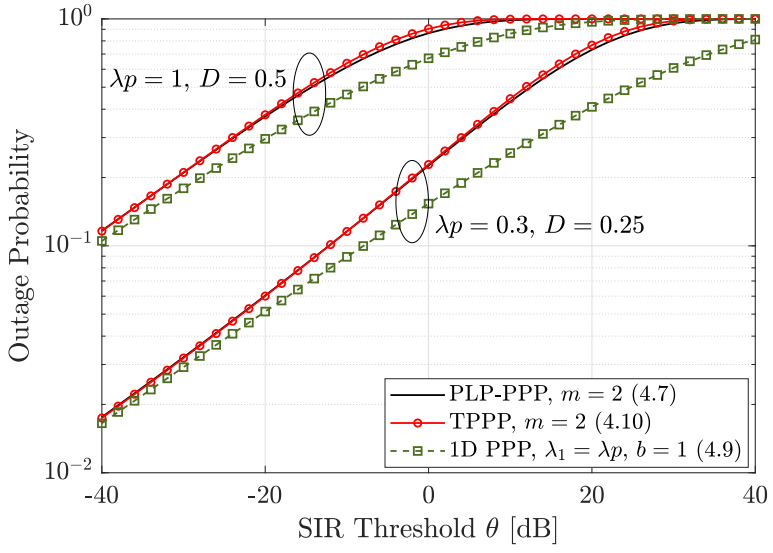

Figure 4.6: Outage probabilities of the typical general vehicle in the PLP-PPP, TPPP, and that of the typical vehicle in a 1D PPP. $\mu = 1$ and $\alpha = 4$. The equation numbers corresponding to the success probability are given in the parentheses in the legend.

$\theta \to 0$, for SIR $> \theta$, there should not be any interferers in a small disk $b(o, r)$ of some radius r centered at the origin. The pair correlation function for the PLP-PPP (4.13) diverges as $r \to 0$, which indicates there definitely exists at least one line with vehicles of intensity λ intersecting $b(o, r)$. For infinitesimally small θ, only the typical street intersects $b(o, r)$. However, for non-vanishing values of θ, there may be more than one line intersecting $b(o, r)$, and the 1D PPP is not sufficient to capture the effect of the streets other than the typical street intersecting $b(o, r)$.

Remark 4.1. *The success probability of the typical vehicle in the PLP-PPP can be tightly approximated by that in the TPPP. In particular, the approximations are asymptotically exact at the upper and lower tails of the success probability.*

Next, we compare the moments of order $b > 1$ in the PLP-PPP and TPPP followed by their respective SIR meta distributions.

4.3.4 Comparison of Higher-Order Moments and SIR Meta Distributions

Fig. 4.7 compares the moments of P_m in the PLP-PPP, TPPP, 1D PPP, and 2D PPP. We observe that the moments in the PLP-PPP are lower bounded by that in the TPPP. Through Conjecture 4.1, we heuristically showed that the success probability of the typical vehicle in the PLP-PPP is lower bounded by that in the TPPP. The argument based on the stochastic dominance of the nearest-neighbor distance in the TPPP to the PLP-PPP in Conjecture 4.1 extends to the moments of order $b > 1$ as well. Also, we observe that the difference between the moments in the PLP-PPP and 2D PPP decreases with SIR threshold as in the case for $M_1(\theta)$ established in Theorem 4.4.

Fig. 4.8 plots the SIR meta distributions for the PLP-PPP, TPPP, 1D PPP, and 2D PPP. For an SIR threshold θ of 0 dB, 80% of the links are at least 60% reliable, whereas only 20% of the links are at least 95% reliable. To make 80% of the links at

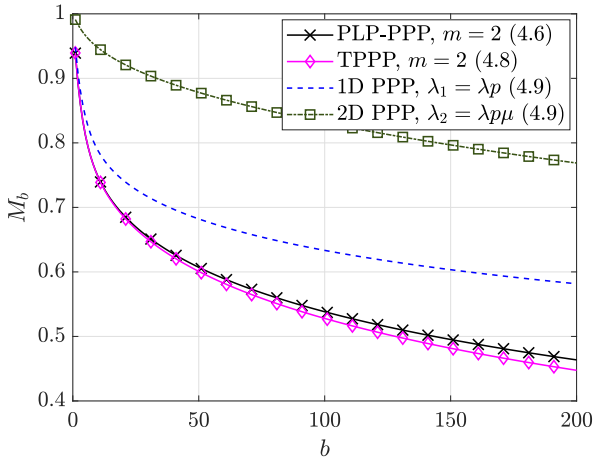

(a) $\theta = -20$ dB

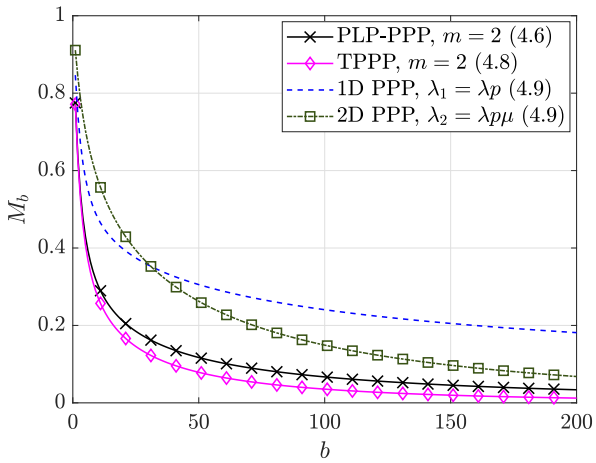

(b) $\theta = 0$ dB

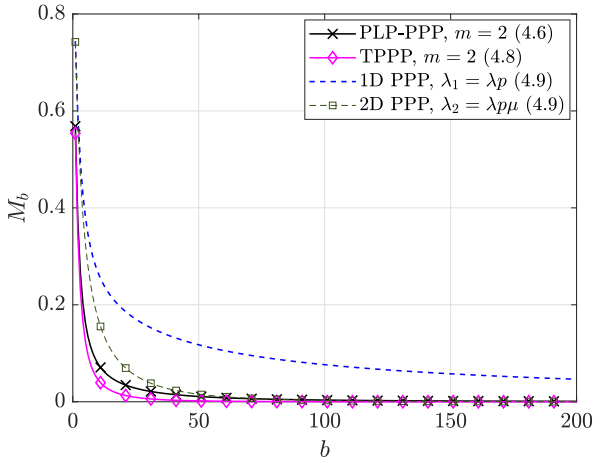

(c) $\theta = 10$ dB

Figure 4.7: Moments of the conditional success probabilities for different SIR thresholds. $\mu = 1$, $\lambda = 1$, $p = 0.3$, $D = 0.25$, and $\alpha = 4$. The equation numbers of the moments M_b are given in the parentheses in the legends.

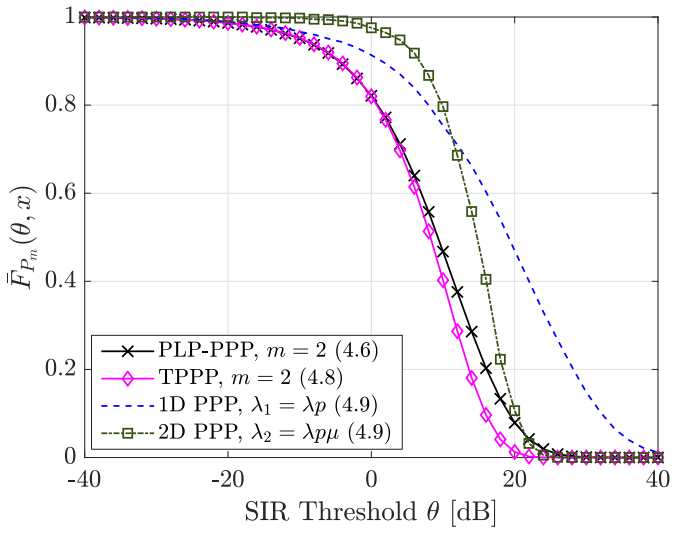

(a) $x = 0.6$

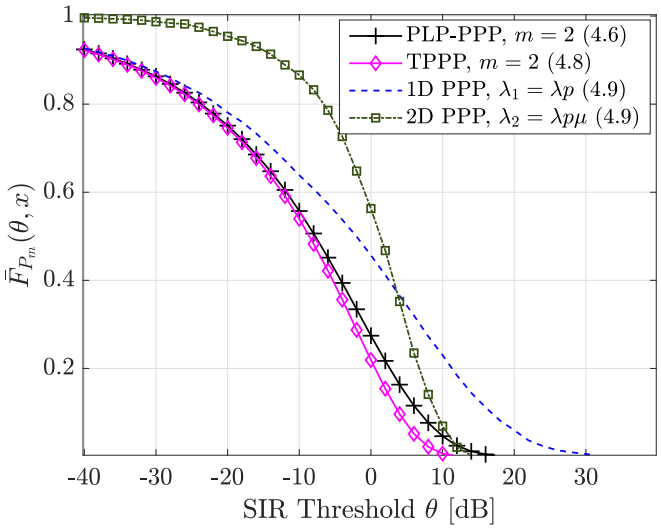

(b) $x = 0.95$

Figure 4.8: SIR meta distributions for different reliabilities. $\mu = 1$, $\lambda = 1$, $p = 0.3$, and $D = 0.25$. The equation numbers of the moments required to evaluate $\bar{F}_{P_m}(\theta, x)$ are given in the parentheses in the legends.

least 95% reliable, we need to reduce θ to -24 dB. Using the SIR MD, we can obtain the trade-offs between data rate (parametrized by θ) and reliability. Also, we can find how to change the transmit probability p to maintain a certain value of the MD, which we will discuss in detail in Section 4.5. In terms of comparison with the TPPP, we observe that the SIR MDs for the TPPP and PLP-PPP are asymptotically exact with the gap being slightly larger in the middle ranges of θ than observed between their success probabilities (Fig. 4.5). As the exact expression (4.3) also involves the moments of order $b > 1$, the differences between the moments $M_{b,m}^{\mathrm{PLP-PPP}}$ and $M_{b,m}^{\mathrm{TPPP}}$ combined produces a slightly larger gap than for the success probability (first moment). The PLP-PPP behaves like a 1D PPP as $\theta \to 0$ and 2D PPP as $\theta \to \infty$ as given in Theorems 4.3 and 4.4.

4.3.5 Presence of Shadowing

Now, let us assume that the channels are also subject to shadowing in addition to Rayleigh fading in the PLP-PPP and TPPP. Using (3.7), the SIR expression including shadowing can be written as

$$\mathsf{SIR} = \frac{g\nu D^{-\alpha}}{\sum_{z\in\chi} g_z \nu_z \|z\|^{-\alpha} B_z}, \tag{4.16}$$

where ν, ν_z are i.i.d. shadowing random variables with mean 1 and variance σ^2. $\chi = \mathcal{V}$ in the PLP-PPP, while $\chi = \mathcal{T}$ in the TPPP.

Theorem 4.6. *Fix $\lambda' > 0$ and let the density of vehicles on each street be $\lambda = \lambda'/\mathbb{E}[\nu^\delta]$. Then, as $\sigma \to \infty$,*

$$\bar{F}_{P_m}^{\mathrm{PLP-PPP}}(\theta, x) \sim \bar{F}_{P_m}^{\mathrm{TPPP}}(\theta, x), \quad \theta \in \mathbb{R}^+,\ x \in [0,1].$$

Proof. The PLP-PPP and TPPP differ only in the distribution of the vehicles that do

not lie on the typical vehicle's streets. Hence we need to show that the interference distributions from the rest of the vehicles that form the point processes $\mathcal{V}^!$ in the PLP-PPP and Φ_2 in the TPPP are identical as $\sigma \to \infty$. To this end, we focus on the propagation loss processes $\Upsilon_\chi \triangleq \{\|z\|^\alpha/\nu_z : z \in \chi\}$ for $\chi = \Phi_2$ and $\chi = \mathcal{V}^!$. By [42, Lemma 1], Υ_{Φ_2} is a PPP on $\mathbb{R}^+$ with intensity function $\lambda(r) = \lambda'\mu\pi\delta r^{\delta-1}$. By [43, Theorem 7], $\Upsilon_{\mathcal{V}^!}$ converges in distribution to a PPP with the same intensity function as $\sigma \to \infty$. □

The scaling of the density by $\mathbb{E}[\nu^\delta]$ in Theorem 4.6 is necessary since without it, the intensity function of the one-dimensional point processes Υ_χ would go to 0 or approach ∞ as σ increases. While the convergence result would still hold, it would be trivial since in both models, there would either be no interference or infinite interference.

A simple approximation to the SIR MD is obtained by just using the first two moments of the conditional success probability. As it varies between 0 and 1, the beta distribution characterized by the first two moments is a natural choice. It is shown that the beta distribution can tightly approximate the SIR meta distribution in Poisson bipolar and cellular networks [34]. In the next subsection, we explore whether the beta approximation works for vehicular networks.

4.3.6 Beta Approximation of the SIR Meta Distribution

The probability density function (pdf) of a beta distributed random variable X with parameters α and β is given by

$$f_X(x) = \frac{x^{\alpha-1}(1-x)^{\beta-1}}{B(\alpha,\beta)}, \tag{4.17}$$

where $B(a,b) = \frac{\Gamma(a)\Gamma(b)}{\Gamma(a+b)}$. The first and second order moments of X are

$$\mathbb{E}[X] = \frac{\alpha}{\alpha+\beta}, \text{ and } \mathbb{E}[X^2] = \frac{\alpha+1}{\alpha+\beta+1}\mathbb{E}[X], \tag{4.18}$$

respectively. We obtain α and β by equating $\mathbb{E}[X] = M_{1,m}(\theta)$ and $\mathbb{E}[X^2] = M_{2,m}(\theta)$. The complementary cumulative distribution function of X is the beta approximation of the SIR meta distribution, *i.e.,*

$$\bar{F}_{P_m}(x) \approx 1 - I_x(\alpha,\beta), \tag{4.19}$$

where $I_x(\alpha,\beta)$ is the regularized incomplete beta function.

Fig. 4.9 shows a different cross-section of the SIR MD of the typical general vehicle in the PLP-PPP and compares it to that in the TPPP and the beta approximations for the PLP-PPP and TPPP. The SIR MD for the PLP-PPP tightly approximates that for the TPPP in the asymptotic regimes of θ as in Fig. 4.8, and in that of x. At $x = 1-p$, which is 0.7 in the considered network setting, there is a transition in the meta distribution curves, particularly noticeable at lower SIR thresholds. The reason is that as $\theta \to 0$, there should not be any interferers in a small disk around the typical vehicle. If the nearest interferer is absent with probability $1-p$, then there exists a non-zero fraction of links that can satisfy a reliability of $1-p$. We can neglect the case of two or more interferers present within that small distance to the typical vehicle, as the probability of such an event vanishes asymptotically. We observe that the beta approximation is tight at higher SIR thresholds, whereas at lower SIR thresholds, the first two moments that define the beta approximation are not sufficient to tightly characterize the transition at $x = 1-p$ in both the PLP-PPP (Fig. 4.9a) and TPPP (Fig. 4.9b). Instead, the beta approximation smoothes out the meta distribution. Furthermore, we can doubly approximate the SIR MD for the PLP-PPP by the beta approximation of the SIR MD for the TPPP (Fig. 4.9b),

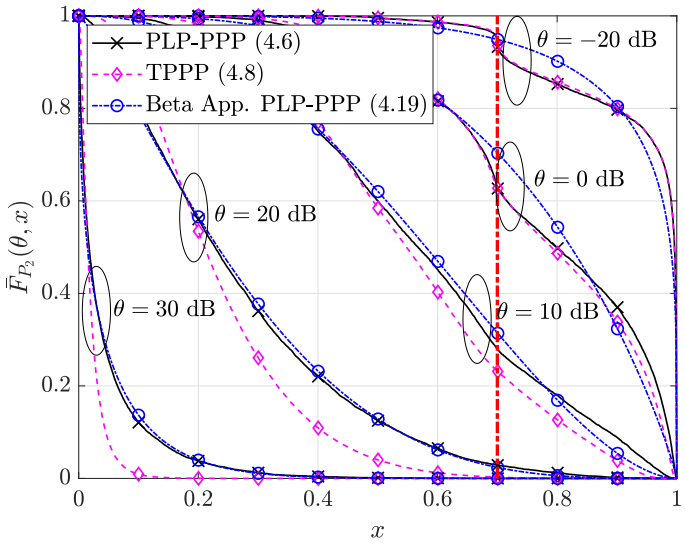

(a)

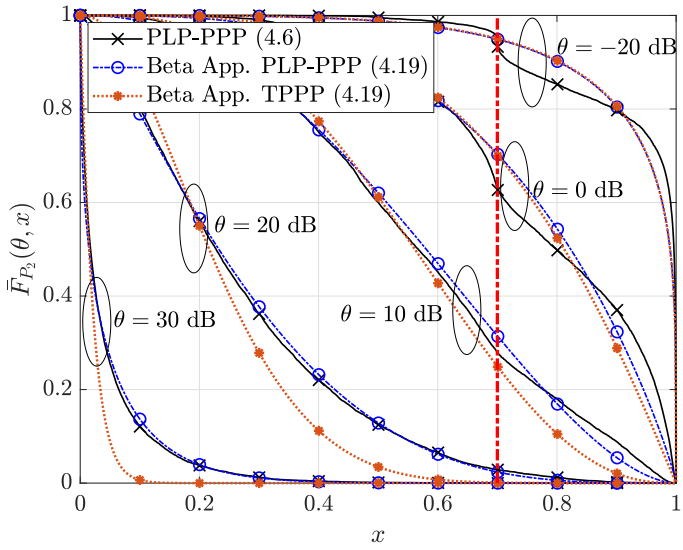

(b)

Figure 4.9: SIR meta distributions for the PLP-PPP, TPPP and their beta approximations. $\mu = 1$, $\lambda = 1$, $p = 0.3$, $\alpha = 4$, and $D = 0.25$. The transition at $x = 1 - p$ is highlighted by the dashed line. The equation numbers in the parentheses in the legends either refer to the moments or expression of $\bar{F}_{P_2}(\theta, x)$.

which is tight in the asymptotic regimes of θ and x.

Remark 4.2.

1. *The maximum difference between the success probabilities $M_{1,m}^{\mathrm{PLP-PPP}}$ and $M_{1,m}^{\mathrm{TPPP}}$ is about -14 dB over the entire parameter space (Fig. 4.5).*
2. *Fig. 4.9a suggests that there exists some $\hat{\theta}$ such that the SIR MD for the PLP-PPP tends to its beta approximation for $\theta > \hat{\theta}$ and to that for the TPPP for $\theta \leq \hat{\theta}$, $\forall x$. Hence, it is not always necessary to evaluate all the $b-th$ ($b \in \mathbb{N}$) moments of the conditional success probability to evaluate the SIR MD.*
3. *The beta approximation of the SIR MD for the TPPP is fairly accurate $\forall \theta$ and $\forall x$ and becomes increasingly tight as $\theta \to 0$ or ∞ and $x \to 0$ or 1 (Fig. 4.9b).*
4. *The accuracy of the TPPP further improves under shadowing. The SIR MD for the TPPP approaches that for the PLP-PPP as the variance of the shadowing increases. This implies that the worst-case TPPP approximation is the case of no shadowing.*

4.4 The Transdimensional Approach to the PSP-PPP

First, we analyze the first moment of the conditional success probability, and then the SIR MDs for the PSP-PPP and corresponding TPPP as in Section 4.3.

4.4.1 First-Order Moments: PSP-PPP vs. TPPP

By (B.2), the moment $M_{b,m}$ can be expressed as $M_{b,m} = M_{b,m}^{o} M_{b,m}^{!}$, where $M_{b,m}^{o}$ considers only the interference from the vehicles on the typical vehicle's streets, and $M_{b,m}^{!}$ takes into account the interference from the vehicles on the rest of the streets.

The success probability $p_m^{\mathrm{PSP-PPP}}$, or the first moment of the conditional success probability $M_{1,m}^{\mathrm{PSP-PPP}} = M_{1,m}^{o} M_{1,m}^{!}$ is given by (3.18). It tends to that in a point process formed only on the typical vehicle's streets as $\theta \to 0$ and a 2D PPP as $\theta \to \infty$ as established in Lemmas 3.8 and 3.9. Next, we derive the first moment for the transdimensional model of the PSP-PPP formed by the superposition of the point process on the typical vehicle's streets and a 2D PPP.

Lemma 4.1. *The success probability of the typical vehicle of order $m \in \{2, 4\}$ at the origin in the TPPP corresponding to the PSP-PPP is given by*

$$p_m^{\text{TPPP}} = M_{1,m}^o(\theta D^\alpha) \exp(-2\lambda p \mu \pi \mathbb{E}[H] D^2 \theta^\delta \Gamma(1+\delta)\Gamma(1-\delta)), \tag{4.20}$$

where $M_{1,m}^o(\theta D^\alpha)$ is given by (3.16)*, and $\delta = 2/\alpha$.*

Proof. The point processes Ψ_o^m and Φ_2 forming the TPPP are independent. It follows that the success probability of the typical vehicle at the origin in the TPPP corresponding to the PSP-PPP is the product of $M_{1,m}^o(\theta D^\alpha)$ given by (3.16) and the success probability of the typical vehicle in Φ_2 given by (4.9) with $b = 1$. The intensity of active transmitters in Φ_2 is $2\lambda p \mu \mathbb{E}[H]$ by Lemma 3.2. □

Fig. 4.10 compares the success probabilities of the typical vehicle in the PSP-PPP and the corresponding TPPP for different values of λ and μ. We observe that the success probability of the typical vehicle in the TPPP tightly lower bounds that in the PSP-PPP. The reason is that the probability of finding the n-th nearest neighbor within a distance r is higher in the TPPP than in the PSP-PPP as the vehicles are randomly placed on the plane without clustering to the streets. We presume that Conjecture 4.1 that focuses on the stochastic dominance of the n-th nearest neighbor holds for the PSP-PPP as well. The case of $n = 1$ can be proved similarly to Theorem 4.5 using (3.10) and (4.15).

4.4.2 SIR Meta Distribution: PSP-PPP vs. TPPP

We observe from (3.18) that the first moment of the conditional success probability for the PSP-PPP involves multiple nested integrals. The moments of order $b > 1$ are even more complicated and hence omitted. We analyze the SIR meta distributions for the PSP-PPP through simulations. Fig. 4.11 compares the SIR meta distributions for the PSP-PPP, the TPPP, and the beta approximation. The behavior is the same

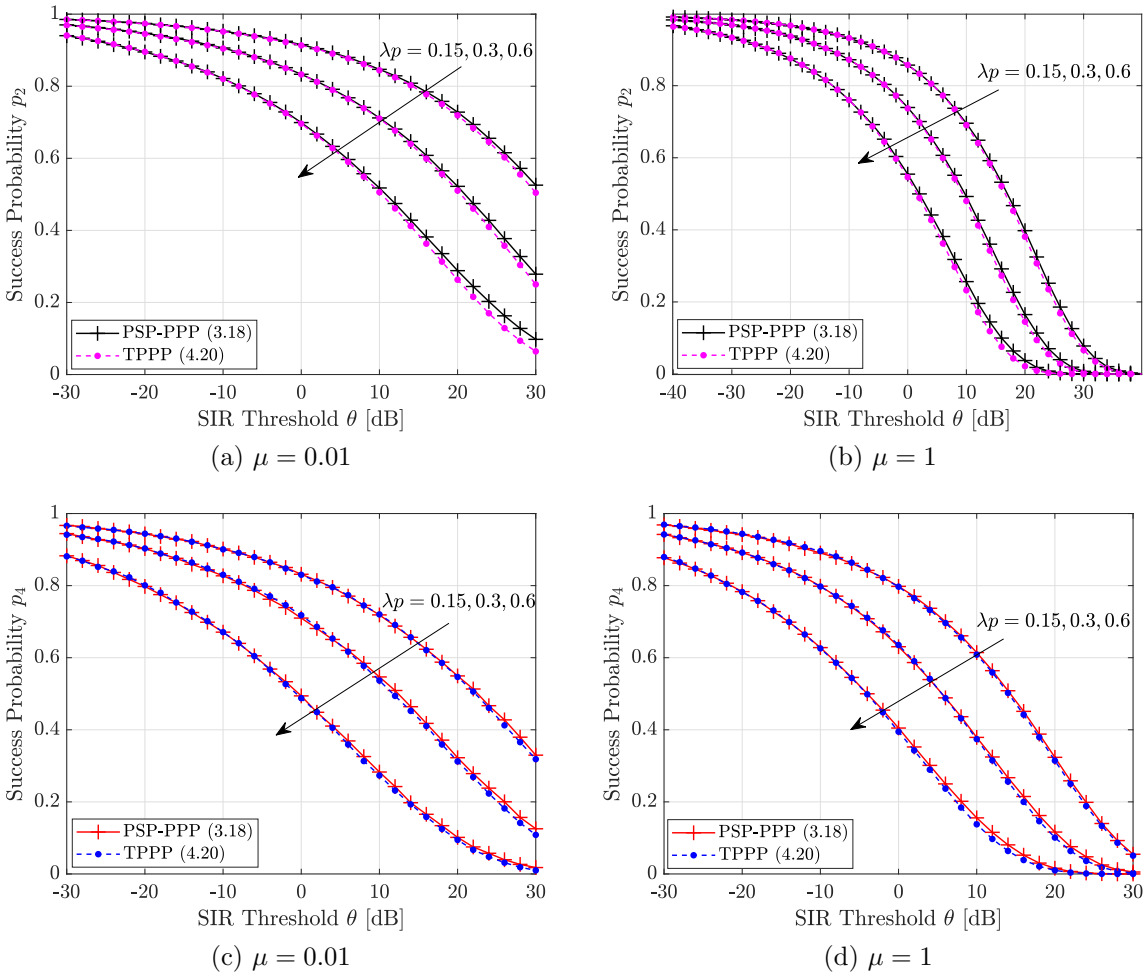

Figure 4.10: Success probabilities of the typical general ((a) and (b)) and intersection ((c) and (d)) vehicles in the PSP-PPP (3.18) and the corresponding TPPP (4.20). $f_H(h) = 2ch\exp(-ch^2)$ with $c = \mu$, $D = 0.25$, and $\alpha = 4$.

as observed in Fig. 4.9 for the PLP-PPP, and thus Remark 2 also holds for the PSP-PPP.

Remark 4.3. *The success probability expression of the PSP-PPP* (3.18) *involving multiple integrals can be approximated by a much simpler expression* (4.20) *obtained by its transdimensional model. In the case of the SIR meta distribution, the transdimensional model well approximates the PSP-PPP, especially, in the asymptotic regimes of* θ *and* x *(Fig. 4.11).*

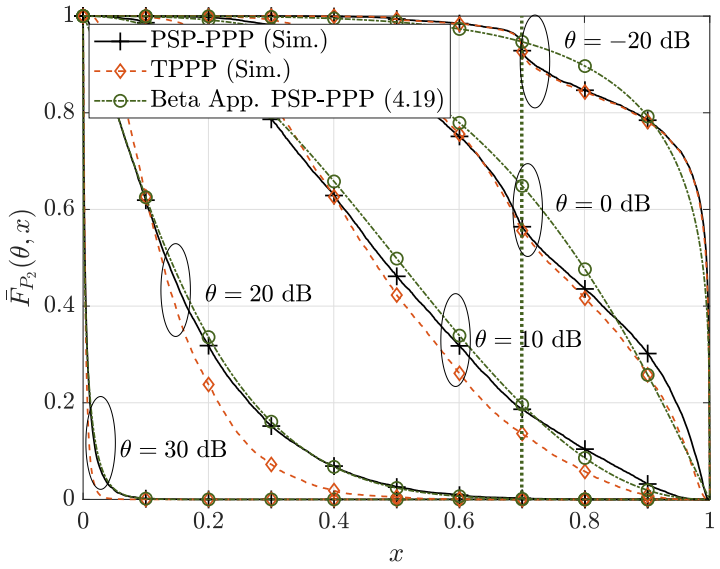

Figure 4.11: Comparison of exact SIR meta distribution for the PSP-PPP and its approximations. $f_H(h) = 2ch\exp(-ch^2)$ with $c = 1$, $\mu = 1$, $\lambda = 1$, $p = 0.3$, $\alpha = 4$, and $D = 0.25$. The transition at $x = 1 - p$ is highlighted by the dotted line. The beta approximation to $\bar{F}_{P_2}(\theta, x)$ is given by (4.19).

4.5 Application to Congestion Control

We have established that the TPPP is sufficient to analyze the complicated PLP-PPP and PSP-PPP. Particularly, the beta approximation of the SIR MD for the TPPP provides tight approximations to the SIR MD for the PLP-PPP and PSP-PPP in the asymptotic regimes of x and θ. In this section, we introduce the transmit rate control in the PLP-PPP using the beta approximation of the SIR MD of the TPPP. The insights presented in this section also hold for the PSP-PPP. First, we begin with success probability-based congestion control to demonstrate the need for SIR MD-based congestion control.

4.5.1 Success Probability-Based Congestion Control

Fig. 4.12a plots the pairs $(1/\lambda, p)$ that satisfy the target success probability of the typical general vehicle $p_2(\lambda, p) = q$ for different values of q. It is convenient to plot $1/\lambda$ vs. p rather than λ vs. p to illustrate the difference between success probability-based

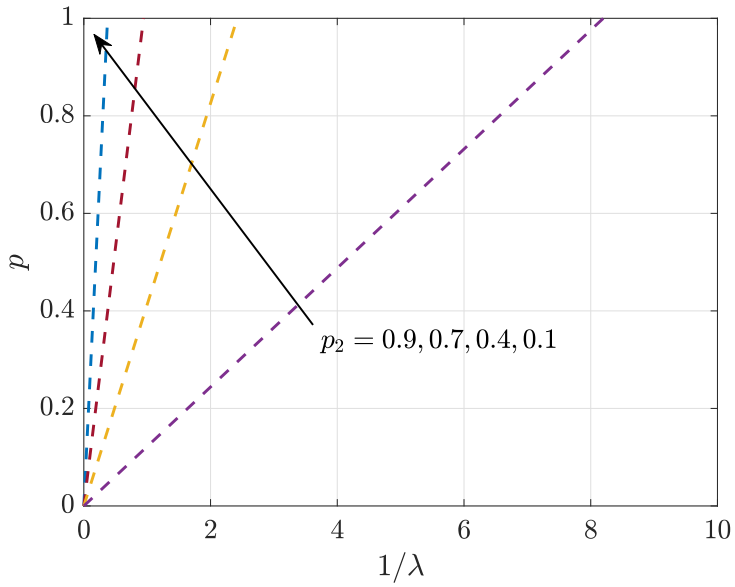

(a)

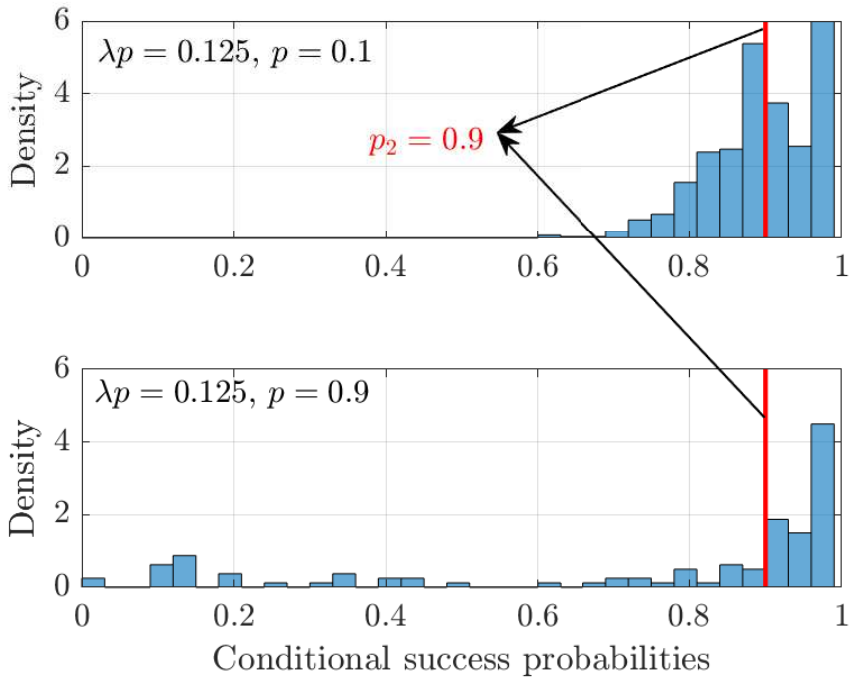

(b)

Figure 4.12: (a) Pairs of $(1/\lambda, p)$ such that $p_2(\lambda, p) = q$ for $q = 0.1, 0.5, 0.8, 0.9$ in the TPPP. $\theta = 0$ dB, $D = 0.25$, $\mu = 1$, and $\alpha = 4$. The equation numbers of p_2 are given in the parentheses in the legends. (b) Histograms of conditional link success probabilities for different combinations of $(1/\lambda, p)$ that yield $p_2 = 0.9$ in (a).

and beta approximation-based congestion control methods. It follows from (4.10) that p is a linear function of $1/\lambda$, and each line follows an equation of the form $\lambda p = C$, where C is a constant. For a given target p_2, as λ scales by a, p is scaled by $1/a$. Further, we observe that for the same λ, we have to more aggressively reduce p at higher target p_2 than in the lower target values.

Fig. 4.12b shows the histograms of conditional success probabilities for different combinations of $(1/\lambda, p)$ picked from the line corresponding to $p_2 = 0.9$ in Fig. 4.12a. We see that for a given λp, the conditional success probabilities exhibit higher variance for $p = 0.9$ than for $p = 0.1$. This implies that the fraction of links that are reliable with a probability of at least x varies for different $(1/\lambda, p)$ even though they yield the same success probability. Therefore, to maintain certain link-level reliability, we need to use the SIR MD for congestion control.

4.5.2 Beta Approximation-Based Congestion Control

To make the dependence of the MD on λ and p explicit, we are adding these two parameters as arguments to the MD as $\bar{F}_{P_2}(\theta, x, \lambda, p)$. Fig. 4.13 plots the pairs $(1/\lambda, p)$ such that $\bar{F}_{P_2}(1, x, \lambda, p) = q$ for different values of q and x. We observe that the $(1/\lambda, p)$ contours transition from concave to linear to convex as we increase x for all values of $\bar{F}_{P_2}$. For example, as $\lambda \to \infty$ $(1/\lambda \to 0)$, we can more aggressively vary p at lower values of x than at higher values of x. The converse is observed as $\lambda \to 0$ $(1/\lambda \to \infty)$. This implies that we have to change p differently with respect to the reliability constraint rather than simply changing p such that $\lambda p = C$ as in the success probability-based congestion control. In other words, to maintain a certain target fraction of reliable links, λp, and, in turn, the success probability, cannot be kept constant.

Fig. 4.14 presents a different cross-section of Fig. 4.13 that helps us compare the success probability-based and beta approximation-based congestion control schemes.

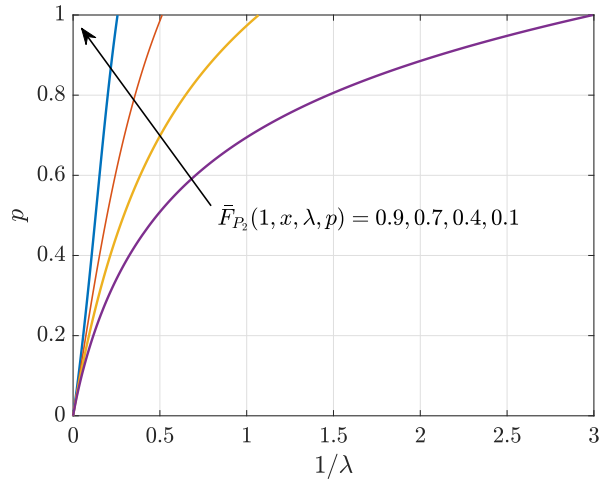

(a) $x = 0.1$

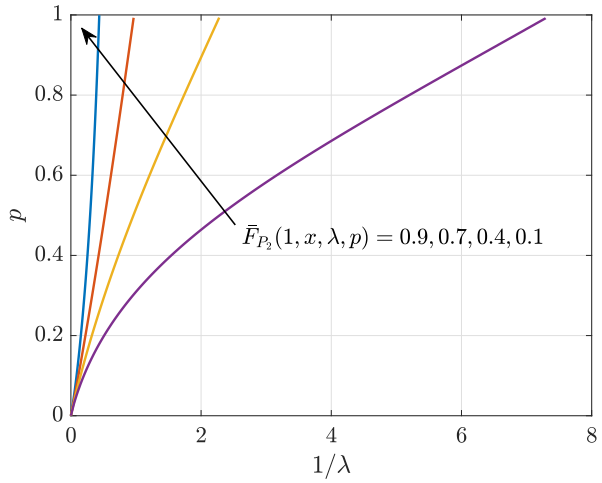

(b) $x = 0.5$

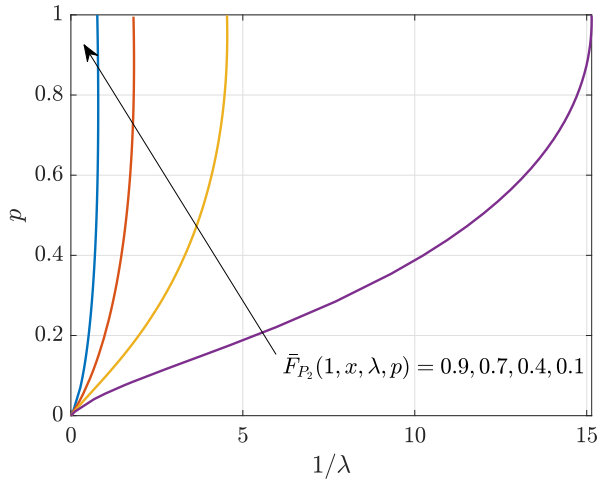

(c) $x = 0.9$

Figure 4.13: Pairs $(1/\lambda, p)$ such that $\bar{F}_{P_2}(1, x, \lambda, p) = q$ for $q = 0.1, 0.4, 0.7$, and 0.9. $D = 0.25$, $\mu = 1$, and $\alpha = 4$.

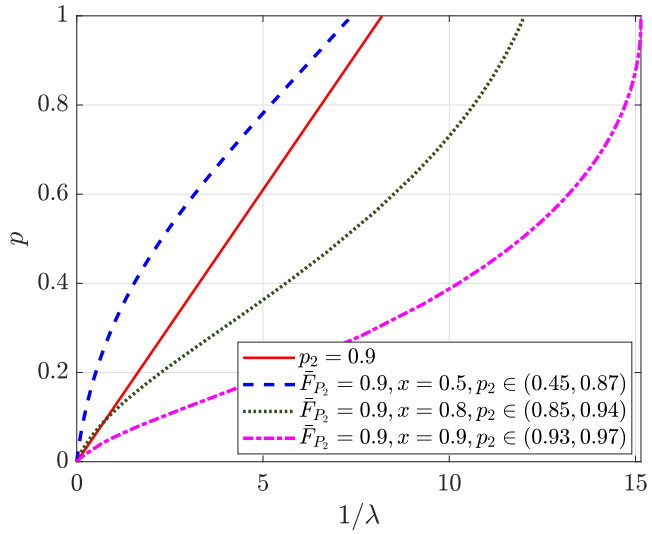

Figure 4.14: Pairs of $(1/\lambda, p)$ that satisfy the target performance given in the legends. The range of p_2 listed for each combination $(\bar{F}_{P_2}, x)$ is obtained by finding the success probabilities for different values of $(1/\lambda, p)$ sampled along the contour that satisfies $\bar{F}_{P_2}(1, x, \lambda, p) = 0.9$ for a given x. $D = 0.25$, $\mu = 1$, and $\alpha = 4$.

We observe that the transmit probability p that achieves $p_2 = 0.9$ (solid line) is higher than the p that guarantees 90% of links to be at least 80% reliable (dotted curve), especially, at lower λ. To guarantee a minimum of 80% reliability, we shall vary p based on the dotted curve rather than the solid line that yields $p_2 = 0.9$. This would lower the success probability to as low as 0.85, implying that we can sacrifice the success probability p_2 to maintain a certain reliability at each link. Therefore, the success probability is not an adequate measure of congestion when the conditional success probabilities exhibit significant variance, *i.e.,* when vehicles form a non-regular point process. In contrast, if vehicles form a lattice, the conditional success probabilities are concentrated around the success probability, because the distances to the interferers are the same at each receiver.

Next, we see whether the inference obtained for congestion control using the beta approximation-based scheme holds for the PLP-PPP. In Fig. 4.15, we plot the exact SIR MDs for the PLP-PPP for different values of λ, with the corresponding p values chosen according to the beta approximation-based congestion control

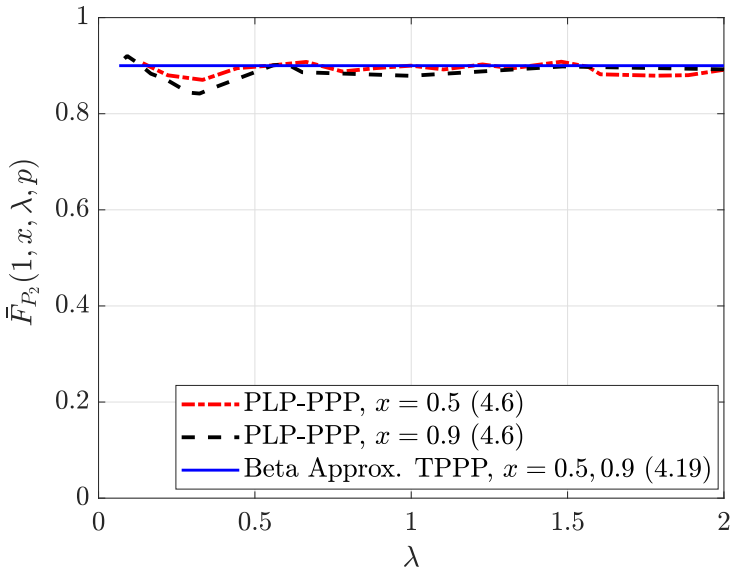

Figure 4.15: Comparison of exact SIR MD for the PLP-PPP and beta-approximated SIR MD for the TPPP. For each λ, p is chosen according to the beta approximation-based congestion control scheme such that the SIR MD for the TPPP equals 0.9. $\mu = 1$, $D = 0.25$, and $\alpha = 4$. The equation numbers in the parentheses in the legends either refer to the moments or expression of $\bar{F}_{P_2}$.

scheme. These (λ, p) pairs yield an SIR MD of 0.9 for the TPPP for $x = 0.5$ and 0.9 (Figs. 4.13b and 4.13c). We observe in Fig. 4.15 that the SIR MDs for the PLP-PPP are highly concentrated around 0.9 with small deviations. This validates that the beta approximation of the SIR MD for the TPPP is sufficient for congestion control. In fact, using the exact SIR MD of the PLP-PPP for congestion control would be prohibitively complicated due to the infinitely many moments involved and their unwieldy expression (4.6).

In the next section, we explore whether the transdimensional model can be extended to non-Poisson point processes.

4.6 Extension to Non-Poisson Point Processes

We assume that the vehicles form a Matérn hard-core process (MHCP) of type II [4, Sec. 3.5]. The reason we choose MHCP is that it is shown to provide good

approximations to the system-level simulations in [6]. MHCP of type II can be obtained by starting with independent 1D PPPs of intensity λ on each streets and then apply dependent thinning to impose the minimum hard-core distance r_{M} between the points. Associate with each point x a mark $t(x)$ uniformly distributed on $(0, 1)$. Flag for removal the points that have a neighbor within r_{M} that has a smaller mark. The MHCP-based vehicular network is given by

$$\Psi^m = \{x \in \mathcal{V}^m : t(x) < t(y) \quad \text{for all} \quad y \in \mathcal{V}^m \cap (b(x, r_{\mathrm{M}}) \setminus \{x\})\}, \tag{4.21}$$

where $\mathcal{V}^m$ is the point process of vehicles with vehicles on each street forming 1D PPPs.

A d-dimensional MHCP of intensity λ' is obtained by starting with a d-dimensional PPP of intensity λ_d and applying dependent thinning such that the points are at a minimum distance of r_{M} from each other. The intensity λ' can be written in terms of λ_d as [4, Sec. 3.5]

$$\lambda' = \frac{1 - \exp(-\lambda_d c_d r_{\mathrm{M}}^d)}{c_d r_{\mathrm{M}}^d}. \tag{4.22}$$

Note that $c_1 = 2$ and $c_2 = \pi$.

Fig. 4.16 illustrates realizations of the vehicular networks formed by MHCP on the PLP (PLP-MHCP) and on the PSP (PSP-MHCP).

Following Definition 4.1, the transdimensional non-Poisson point process (TNPP) $\mathcal{T}'$ is given by $\Psi_m^o \cup \mathcal{P}$, where Ψ_m^o denotes the point process of vehicles on the streets passing through the typical vehicle of order m that follow the hard-core constraint. $\mathcal{P}$ is a 2D MHCP generated from a 2D PPP whose intensity equals the 2D intensity of $\mathcal{V}^m$. The intensity of the 2D MHCP can be evaluated using (4.22). Note that the hard-core constraint applies to Ψ_o^m and $\mathcal{P}$ individually, not jointly except around the typical vehicle.

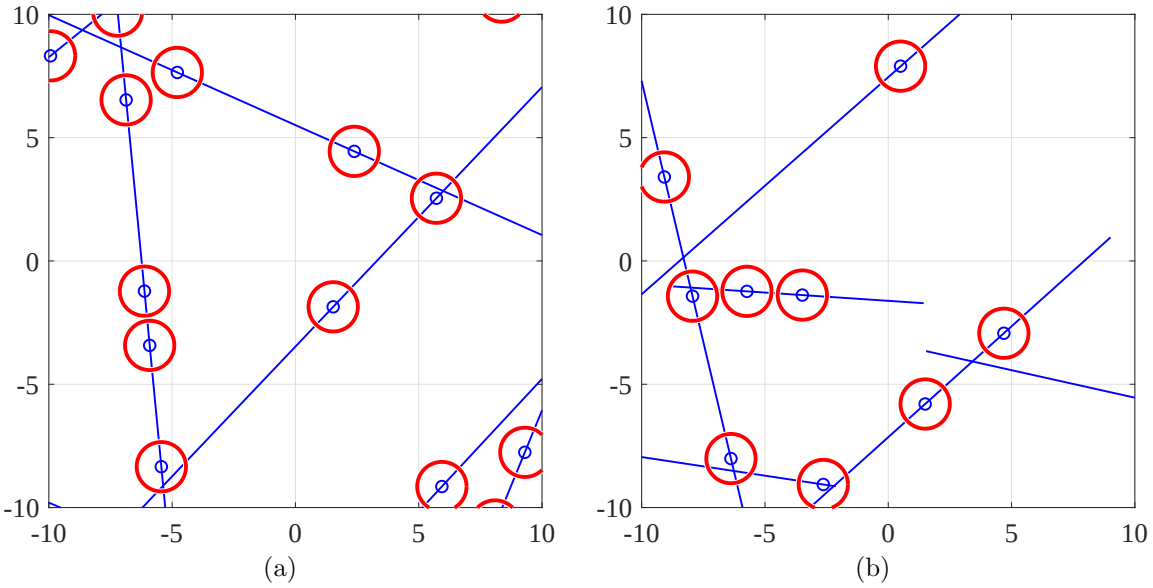

Figure 4.16: Realizations of the (a) PLP-MHCP with $\mu = \lambda = 0.3$ (b) PSP-MHCP with $\mu = 0.01$, and $\lambda = 0.1$. $r_{\mathrm{M}} = 2$. Lines/sticks represent streets, and 'o' represent vehicles. The disks around the vehicles are of radius $r_{\mathrm{M}}/2$.

4.6.1 The Transdimensional Approach to the PLP-MHCP

The transdimensional process TNPP corresponding to the PLP-MHCP is shown in Fig. 4.17. The orientation of the street passing through the typical general vehicle does not matter as the distances from the interferers on that street to the origin remains the same if the street is rotated around the origin. Without loss of generality, we assume that the orientation of the street passing through the typical general vehicle is zero. The orientations of the streets passing through the typical intersection vehicle are uniformly distributed on $[0, \pi)$.

Another transdimensional model of interest is where $\mathcal{P}$ is a 2D PPP with the intensity of PLP-MHCP. For the ease of notation, we refer to the TNPP with $\mathcal{P}$ forming a 2D MHCP as TNPP-I, and $\mathcal{P}$ forming a 2D PPP as TNPP-II.

Fig. 4.18 compares the success probabilities of the typical general vehicle in the PLP-MHCP, TNPP, and TNPP-II. We observe that the success probability of the typical vehicle in the TNPP is a lower bound to that in the PLP-MHCP. The bound

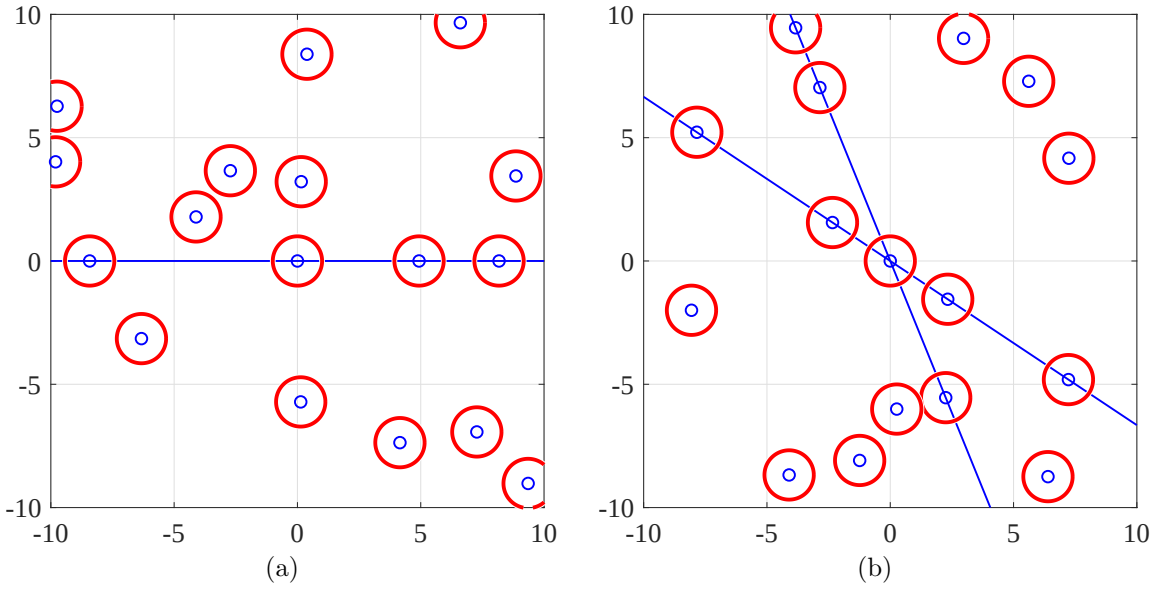

Figure 4.17: Snapshots of the TNPP with respect to the a) typical general vehicle and b) typical intersection vehicle in the PLP-MHCP. $\lambda = \mu = 0.3$, and $r_{\mathrm{M}} = 2$. The estimated 2D intensity is $\lambda_2 = 0.035$. Lines represent streets, and 'o' represent vehicles. The disks around the vehicles are of radius $r_{\mathrm{M}}/2$.

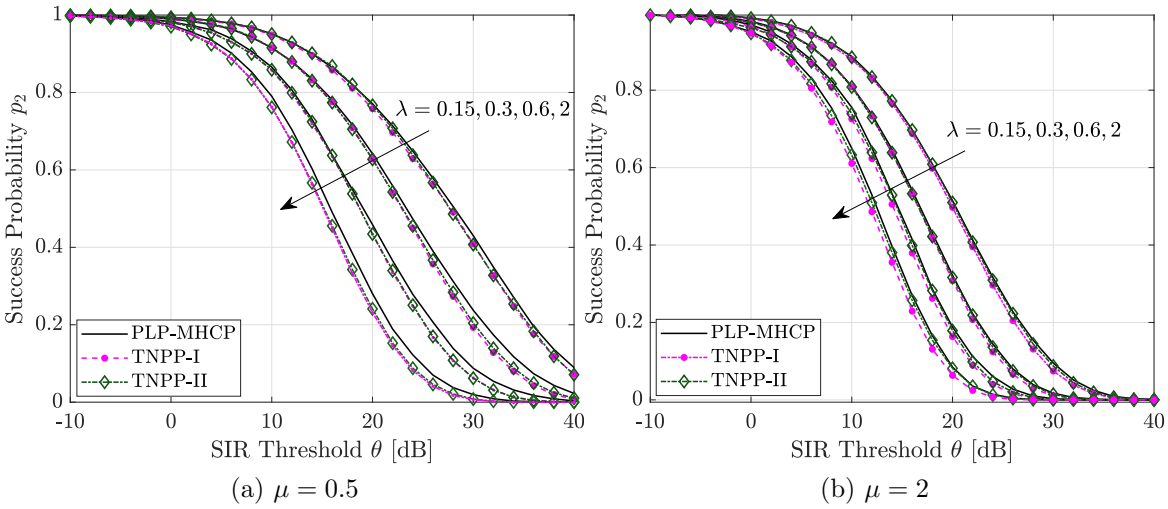

Figure 4.18: Comparison of success probabilities of the typical general vehicle in the PLP-MHCP, and the corresponding TNPP-I and TNPP-II. $r_{\mathrm{M}} = 0.5$. The estimated 2D intensities of the PLP-MHCP for $\mu = 0.5$, and $\lambda = 0.15, 0.3, 0.6$, and 2 are $0.067, 0.117$, 0.193, and 0.324, respectively. When $\mu = 2$, $\lambda_2 = 0.248, 0.42, 0.632$, and 0.872.

gets tighter with increasing μ and/or decreasing λ. The success probability of the typical vehicle in the model TNPP-II is comparable to that in the TNPP and PLP-MHCP.

4.6.2 The Transdimensional Approach to the PSP-MHCP

Fig. 4.19 shows the realizations of the TNPP-I with respect to the PSP-MHCP. Fig. 4.20 shows that the success probabilities of the typical vehicle in the PSP-MHCP can be well-approximated by that in the stick-based TNPP-I and TNPP-II.

The inferences obtained for the typical general vehicle extend to the typical intersection vehicle as Ψ_m^o is the same in the PLP-MHCP/PSP-MHCP and their transdimensional models. We conjecture that the SIR MDs for the TNPP will serve as a good approximation to that for the MHCP-based vehicular networks as in the case of the TPPP.

Remark 4.4. *The transdimensional point processes are alternative models to the more complicated vehicular networks whether the lengths of the streets are infinite or varying finitely, and the point process of vehicles on the streets is Poisson or hard-core. They provide insights into the network behavior as well as the more complicated vehicular networks and with better tractability.*

4.7 Conclusions

We introduced a simple transdimensional approach to analyze complicated vehicular network models such as the PLP-PPP or PSP-PPP, where the streets are characterized by the PLP or PSP and vehicles on each street form a 1D PPP. The TPPP accounts for only the geometry of the vehicle locations on the street(s) passing through the typical vehicle and models the rest of the vehicles as random points on the 2D plane ignoring their street geometry. Such a transdimensional approach leads

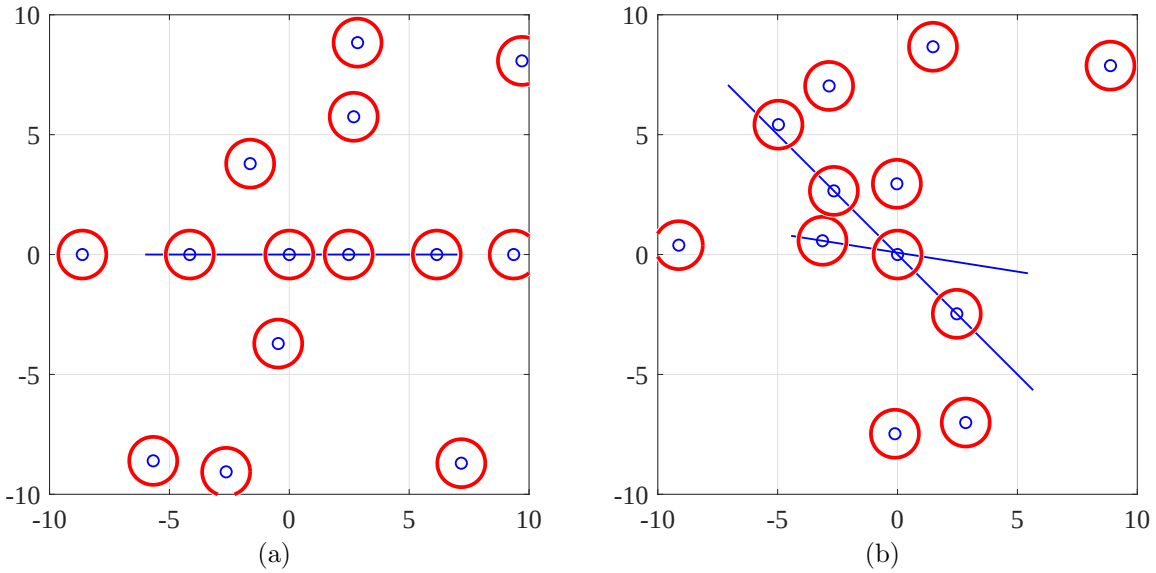

Figure 4.19: Snapshots of the PSP-MHCP with respect to the a) typical general vehicle and b) typical intersection vehicle at the origin. $\mu = 0.01$, $\lambda = 0.1$ and $r_{\mathrm{M}} = 2$. $f_H(h) = 2bh\exp(-bh^2)$ with $b = 0.0103$. The estimated 2D intensity is $\lambda_2 = 0.013$. Sticks represent streets, and 'o' represent vehicles. The disks around the vehicles are of radius $r_{\mathrm{M}}/2$.

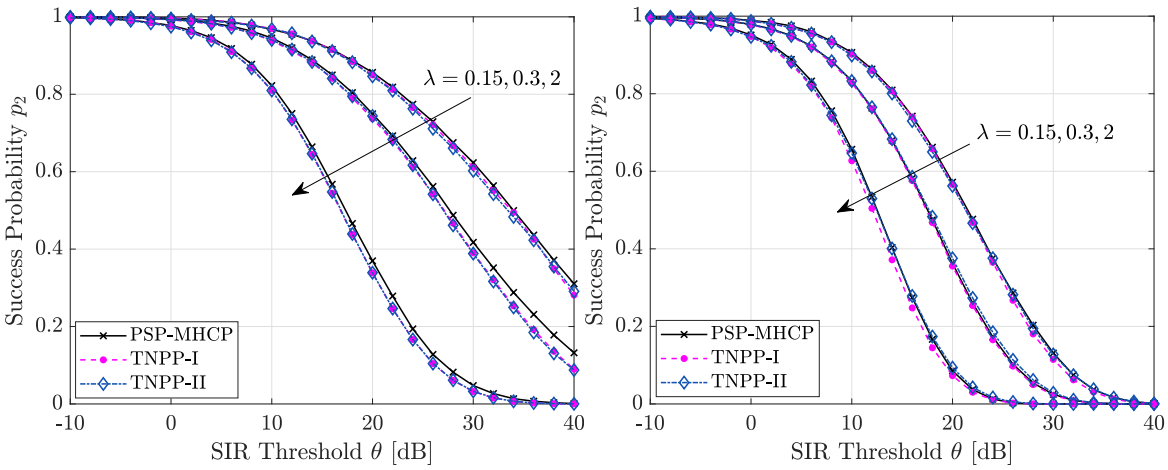

Figure 4.20: Comparison of success probabilities of the typical general vehicle in the PSP-MHCP, and the corresponding TNPP-I and TNPP-II. $f_H(h) = 2bh\exp(-bh^2)$. The values of b corresponding to $\mu = 1$ and 0.01 are 1.08 and 0.0103, respectively. $r_{\mathrm{M}} = 0.5$. The estimated 2D intensities of the PSP-MHCP for $\mu = 0.01$, and $\lambda = 0.15, 0.3$, and 2 are $0.023, 0.044$, and 0.133, respectively. When $\mu = 1$, $\lambda_2 = 0.218, 0.375$, and 0.893.

to a much simpler and more tractable analysis of the PLP-PPP and PSP-PPP with good accuracy. We showed that under no shadowing, the SIR meta distribution for the TPPP well approximates that for the PLP-PPP and PSP-PPP, and particularly, the approximations are tight in the asymptotic regimes of data rate and reliability. We proved that the SIR meta distribution for the TPPP becomes exact as the variance of the shadowing increases. Hence, it is not essential to account for the geometry of every single street for vehicular network analysis. From the perspective of network simulation, the TPPP model enables us to focus on simpler simulation setups, thus saving computational costs and time.

We conjecture that the TPPP is sufficient even if the streets are curved segments or circles, etc., rather than lines as in the PLP or sticks as in the PSP. The reason is that any PPP-based vehicular network interloops both the properties of both 1D and 2D PPPs, which indeed is the fundamental principle behind the construction of the TPPP.

We also showed that the transdimensional approach extends to the non-Poisson point processes as well, where the vehicles that pass through the typical vehicle's streets form a non-Poisson point process on the streets and the rest of the vehicles form a 2D non-Poisson point process.

Further, the SIR meta distribution enables network congestion control while ensuring fairness among the links, by guiding the choice of the transmit rate such that each transmitter-receiver link is reliable with a probability of at least x. We showed that the success probability or packet reception rate, a measure of the average reliability of the links, is inadequate to understand and alleviate congestion in a network with irregular vehicle spacing since it cannot guarantee that a certain fraction of links achieves the required reliability.

CHAPTER 5

DETERMINANTAL POINT PROCESSES FOR VEHICULAR NETWORKS: MODELING, ANALYSIS, AND SYSTEM-LEVEL SIMULATIONS

Vehicles broadcast their messages over the shared wireless medium. If two vehicles located within the communication range of each other transmit simultaneously, then the receivers located between these two vehicles may fail to receive any of those messages since one will interfere with the other. This can be avoided if each vehicle senses the wireless medium to check if it is idle before transmitting its messages. Such sense-and-transmit mechanism cause repulsion among the concurrently transmitting vehicles. In the vehicular standards such as DSRC and LTE-/NR-V2X, a sense-and-transmit mechanism is implemented using CSMA/CA in DSRC [44], CAT-n LBT, $n \in 2, 3, 4$, in LTE-V2X, and Type-1, 2A, 2B channel access schemes in NR-V2X [45]. Type-2A and Type-2B channel access schemes are similar to CAT-2 LBT, and Type-1 channel access scheme and CSMA/CA are similar to CAT-4 LBT, where CAT-n refers to n-th category. The rest of the acronyms are defined on page xv. For the ease of notation, we refer to the above-mentioned schemes as LBT, the abbreviation of *listen before talk*, in the rest of the chapter.

To facilitate the mathematical analysis of LBT, we need a point process that exhibits its repulsion property. We recall that a widely used point process to model the locations of transmitting vehicles is the PPP due to its analytical tractability. The PPP is shown to provide a lower bound to real-world vehicular networks on a widely used performance metric—success probability [6]. In the PPP, the numbers of points in any two disjoint regions are independent. This implies that two vehicles

that are selected to transmit can be within the communication range of each other, thus defying the nature of LBT.

There are other point processes that can capture the inherent repulsive nature of the LBT mechanism. For instance, it is shown in [6] that the MHCP is a good choice to model transmitter locations. The vehicles form a PPP, and transmitters are selected such that they are at least a distance r_{M} apart from each other, thus creating repulsion. An alternative hard-core model is to place vehicles with their headway distances following a shifted exponential distribution [38], *i.e.,* to separate vehicles by a constant plus a distance modeled by the exponential distribution. The exact analyses of the hard-core models are difficult; approximation techniques such as modeling far-field interferers by a PPP or approximating the interference distribution [46] are generally required to obtain good bounds on the performance metrics of interest.

In practice, two vehicles located closely may not listen to each other due to channel impairments and thus can transmit simultaneously. Another possible situation is both finding the channel idle at the same time. Hence, there may not be a strict minimal distance between the transmitters, resulting in them forming a *soft-core* process rather than its extreme variant, the hard-core process. Hence, we need a point process that exhibits soft and adaptable repulsiveness yet remains tractable.

In this chapter, we show that the (discrete) determinantal point processes (DPPs) are excellent candidates to model the concurrent transmitters due to their soft repulsion property in a broadcast communication scenario. To this end, first, we formulate the binned meta distribution of the signal-to-interference-plus-noise ratio (SINR), which answers questions such as *what fraction of the links with distances in the range of* 100-200 *meters can satisfy a target data rate of* 10 *Kbps with a probability of at least* 0.99*?* The binned MD is a nuanced version of the MD discussed in Chapter 4. The former provides insights into the effective broadcast communication range while

the latter focuses on the maximum achievable broadcast distance. Then, we derive the analytical expression for the binned SINR MD in the DPPs and show that it matches the system-level simulations performed in the network simulator ns-3 [47].

5.1 Related Work

Determinantal Point Processes The DPPs are point processes that model repulsion among the points. They have been used in random matrix theory since the 1960s and were referred to as fermion point processes as they were used to model the statistical distribution of fermions in thermal equilibrium. Borodin [48] introduced the term 'determinantal' in 2000 which has become a standard now. The DPPs are defined by the n-th order product densities in the continuous space that are expressed as the determinants of a kernel. They have appealing mathematical properties such as analytical expressions for n-th order moments, Laplace functional, and closure under the reduced Palm distribution; and they lend to easier simulation and inference compared to the Gibbs processes, another class of point processes that model repulsion [49]. In [50, 51], it is shown that the repulsion between the base station locations can be captured well using the continuous DPPs with Gaussian and Cauchy kernels. The analytical expressions for the statistical measures such as empty space function, Laplace functional, etc. involve integrals over the support of the n-th order product density functions [51].

The DPPs can be made even more tractable by defining them on discrete spaces. Limiting the DPPs to discrete spaces reduces the mathematical derivations involving integrals to simpler linear algebraic expressions. In [52], the authors showed how the discrete DPPs can be applied to machine learning problems that involve selecting subsets of images, news stories, etc., balancing the quality and diversity. Given a ground set of items, the DPP is modeled such that the best set of items are picked. The use of discrete DPPs for wireless networks was first considered in [53]. Coined

as determinantal thinning in the spirit of stochastic geometry, a subset of points is selected from a ground set of points that form a PPP. The authors fitted DPPs with different kernels to the MHCP and triangle point process by learning the parameters through maximum likelihood estimation. Later, in [54], they derived the probability that the typical node receives a message successfully from its transmitter at a certain distance in a generic DPP model with some kernel K. A DPP-based wireless framework that determines the subset of active links which maximizes the network sum-throughput is analyzed in [55]. We work with discrete DPPs in the rest of the chapter, and we simply refer to them as DPPs.

ns-3 vs. Stochastic Geometry In [6], the authors have shown that the MHCP provides good approximations for the success probability to that in the ns-3 simulations under different traffic densities. The marks associated with the points in the MHCP are determined based on the backoff mechanism in CSMA/CA. The marks along with the hard-core distance r_{M} determine the set of concurrent transmitters. It is also shown that the PPP provides lower bounds to the ns-3 simulations. To compensate for the over-estimation of the interference in the PPP-modeled CSMA/CA-based wireless networks, the authors in [56] propose to transform the SINR threshold to include sensing overhead and the channel access probability resulting from the backoff scheme.

See the Chapters 2-4 for the works on SINR MD and the alternative stochastic geometry models for vehicular networks. Before we delve into the DPP-based vehicular network modeling, we will discuss the analogies between ns-3 and stochastic geometry.

5.2 ns-3 and Stochastic Geometry

ns-3 is a discrete-event network simulator (ns) with '3' referring to the 3rd version [47]. It includes models for packet data networks which can be used either as

standalone models for system-level simulations, or users can incorporate their requirements into the ns-3 models to create their experiments. ns-3 includes a suite of IEEE 802.11 models that attempt to provide accurate MAC and physical (PHY) layer implementations as per the standards. IEEE 802.11p provides MAC and PHY support for vehicular communications. We use the proprietary DSRC module built upon IEEE 802.11p in ns-3 by Toyota Motor North America [57] for system-level simulations. One can alternatively use an open-source ns-3-based simulator 'ms-van3t' to study DSRC [58]. Tools from stochastic geometry (SG) complement system-level simulations by mimicking their complex behavior and yield interpretable analytical expressions. Below, we address the key similarities and differences in ns-3 and SG-based vehicular network models we consider in this chapter. They apply in general to other SG models in the literature as well.

Network Stack As the name suggests, ns-3 provides functionalities to equip each node (vehicle) with a network protocol stack. It is a hierarchy of software layers, starting from the application layer where packets are generated to the physical layer where they are sent over a channel. The MAC layer decides whether generated packets will be sent to the PHY layer for transmission or not. In the SG models, we model the locations of vehicles that generate packets using some point process and then select the vehicles for transmission based on the MAC scheme in ns-3. The layers in between the application and MAC layer are not accounted for in the SG models.

Packet-level Decoding Each vehicle operates in a half-duplex state, *i.e.,* it either transmits or receives. ns-3 performs packet-level decoding by default. Let $T = T_1 + T_2$, where T_1 and T_2 denote the numbers of slots required to transmit the preamble and data, respectively.

If a vehicle detects a signal with its energy exceeding the preamble detection threshold, it starts receiving the packet. Let us denote the packet as E. If the

SINR measured at the end of T_1-th slot exceeds the preamble decoding threshold, it continues receiving the packet E, else drops E. In case of interference from another vehicle, say at the M-th slot ($M > T_1$), SINR is measured for E and the interfering packet F at the end of M-th slot. If the SINR of E exceeds the data decoding threshold θ, its reception is continued and F is dropped. Otherwise, E is dropped and packet reception is switched to F if its SINR exceeds θ. If an interferer transmits in the M-th slot with $M < T_1$, the preamble decoding threshold is used to choose between the packets. We found that the proportion of packets lost due to interference in the M-th ($M < T_1$) slot are negligible when T_1 is much smaller than T_2. A packet is considered to be received successfully if the SINR measured at the end of T_2-th slot exceeds θ. In the SG models, SINR is evaluated for all the concurrently transmitted packets and a transmission is considered a success if its SINR exceeds θ. The SINR evaluation is simplified without accounting for preamble decoding. Note that at most $1/k$ packets can attain the SINR threshold $\theta > k$ [59].

Memory vs. Memoryless Consider a scenario where each vehicle broadcasts a message periodically. This implies that no vehicle transmits its messages consecutively in ns-3. We model the transmissions in the SG models as memoryless, *i.e.,* the intervals between transmissions may take any value, but the average number of transmissions matches that in ns-3. It is common to model the packet arrivals using a statistical distribution that leads to analysis.

SG models differ from ns-3 in the interference calculation as well, as explained by the following example. Consider two vehicles A, B and C. Assume that A and B start transmitting at the beginning of the first and $T/2$-th slot. B acts as an interferer to A and vice versa. If C starts transmitting at the $(T+1)$-th slot, it is interfered by B and vice versa. In the SG models, a slot is generally modeled as the transmission duration of the entire packet. The interfering vehicles vary independently among the packet durations, unlike C accounting for the interference from B in ns-3. Such memoryless

nature of the SG models might lead to the interference being over-estimated.

The motivation behind using the SG models is that they can provide crisper insights into the network behavior than system-level simulations. Due to the differences cited above, it is possible that the results obtained in ns-3 do not match exactly that in the SG models. It is shown that the SINR MDs, and, in turn, success probability, for any general stationary point processes can be obtained by horizontally shifting the respective curves for the PPPs in cellular networks [60]. This implies it might be possible to shift the SINR MD curves in the SG models horizontally to match those in ns-3. By doing so, we are not modeling all the complexities in the network yet obtaining an analytical expression that can be shifted to match that in ns-3. Alternatively, one can tune the parameters of the SG model to account for the differences. The goal is to see whether the parameters of the SG model can effectively characterize the simulations in ns-3, especially, whether the slope of the SINR MD curves obtained in ns-3 matches that in the SG-models. Once we have such a model, we can use it to analyze critical concerns such as congestion control, spatial outage capacity [1], etc.

5.3 Baseline Network Models and Determinantal Point Processes

We assume that vehicles form a 1D PPP Φ of intensity λ on $\mathcal{R} \subseteq \mathbb{R}$. Transmitting vehicles broadcast their messages over a single channel. We model the channel fading as Rayleigh and path loss using log-distance propagation loss model. For a transmitted power of P_{t}, the power P_{r} received at distance D is

$$P_{\mathrm{r}} = g\mathrm{PL}_0 P_{\mathrm{t}} D^{-\alpha}, \tag{5.1}$$

where PL_0 is the path-loss constant and α is the path-loss exponent. g is the channel power gain due to fading, which follows exponential distribution with mean 1.

The point process of transmitters $\mathcal{X}$ is determined by a thinning of Φ, which is the process of removing certain points independent or dependent on each other. We start with recalling how we obtain the baseline network models—PPPs and MHCPs—by thinning Φ, followed by the construction of the DPPs from the PPPs. $\mathcal{R} = \mathbb{R}$ in the case of baseline models, and $\mathcal{R} \subset \mathbb{R}$ in the DPP.

5.3.1 Poisson Point Processes

Let p denote the probability that a point is retained independently. The retained points (transmitters) form a 1D PPP of intensity λp. This model characterizes the ALOHA MAC scheme.

5.3.2 Matérn Hard-Core Processes

Here, points are dependently thinned such that there is at least a distance r_{M} between the points. There are two types of MHCPs—Type-I and Type-II. In Type-I, all the points that have a neighbor within distance r_{M} are removed. Type-II achieves denser packing than Type-I. Each point has a mark that is uniformly distributed between 0 and 1. All the points that have a neighbor with a smaller mark within distance r_{M} are removed in Type-II. We focus on MHCPs of Type-II in this chapter. The intensity of the transmitter process λ' is given by [4, Ch. 3]

$$\lambda' = \frac{1 - \exp(-2\lambda r_{\mathrm{M}})}{2r_{\mathrm{M}}}. \tag{5.2}$$

5.3.3 Determinantal Point Processes

Let $\phi = \{y_1, y_2, \ldots, y_N\}$ denote a finite realization of Φ defined on $\mathcal{R} \subset \mathbb{R}$. Here, $\mathcal{X}$ refers to a discrete point process defined on ϕ, *i.e.,* $\mathcal{X} \subseteq \phi$.

Definition 5.1. *(Determinantally Thinned Poisson Point Process)* $\mathcal{X}$ *is called a determinantal point process (DPP) if there exists a* $N \times N$ *positive semi-definite*

matrix K parametrized by the elements of ϕ such that

$$\rho(Y) = \mathbb{P}(Y \subseteq \mathcal{X} \mid \Phi = \phi) = \det(K_Y(\phi)), \quad Y \subseteq \phi. \tag{5.3}$$

It is denoted as $\mathcal{X} \sim DPP(K)$.

K is referred to as the kernel. K_Y denotes the submatrix of K parameterized by the elements in Y. By convention, $\det(K_\varnothing) = 1$. $\rho(Y)$ is referred to as the inclusion probability as it the probability of Y being included in the realizations of $\mathcal{X}$. The points of ϕ are thinned based on K. Each point is retained with probability K_{ii}, $1 \leq i \leq N$. K_{ij} denotes the element of matrix K parameterized by the i-th and j-th elements of ϕ.

Remark 5.1. *The DPP enables us to model vehicles with different transmit probabilities. It can be interpreted as a spatially adaptive ALOHA. If $K_{ij} = 0 \ \forall i \neq j$ and $K_{ii} = p \ \forall i$, the DPP reduces to the ALOHA model on a finite space.*

Definition 5.1 determines the class of DPPs. In general, it is easier to define the joint probability distributions than inclusion probabilities. This led to the formation of a slightly less general class of DPPs, referred to as the *L-ensembles*. The formal definition follows.

Definition 5.2 ([61]). *(L-ensemble) Let L denote a $N \times N$ positive semi-definite matrix parameterized by the elements of ϕ. A point process $\mathcal{X}$ is called the L-ensemble if it is defined by the probabilities of the realizations*

$$\mathbb{P}(\mathcal{X} = Y \mid \Phi = \phi) \propto \det(L_Y(\phi)), \quad Y \subseteq \phi. \tag{5.4}$$

An L-ensemble is a DPP with kernel $K = L(I + L)^{-1}$.

The normalization factor in (5.4) is $\sum_{Y \subseteq \mathcal{V}} \det(L_Y) = \det(I + L)$ [52, Th. 2.1], where I is an identity matrix. We adopt $\det(L_\varnothing) = 1$. An L-ensemble is a DPP,

however the converse may not be true. A DPP with marginal kernel K is an L-ensemble iff all the eigenvalues of K are positive and less than 1 ($0 \preceq K \prec I$) since $L = K(I-K)^{-1}$, *i.e.,* K is positive semi-definite, which is denoted as $K \succeq 0$, and $I - K$ is positive definite, which is denoted as $I \succ K$. The advantages in using the L-ensembles are i) $0 \preceq L \preceq I$ is not required as the probabilities of observing a realization (5.4) are defined proportionally, whereas, $0 \preceq K \preceq I$ must hold as (5.3) calculates the probability of the inclusion of Y; ii) the L-ensembles provide an easier structure for optimization, which is useful in fitting the data to DPPs as we will see later. Next, we provide a toy example to illustrate the L-ensemble DPP.

Let $\phi = \{0, 1, 3\}$. Consider $L_{ij} = \exp(-|y_i - y_j|)$, $i, j \in \{1, 2, 3\}$. Then we have

$$L = \begin{bmatrix} 1 & 0.3679 & 0.0498 \\ 0.3679 & 1 & 0.1353 \\ 0.0498 & 0.1353 & 1 \end{bmatrix}.$$

The realization probabilities can be calculated using (5.4) as follows:

$$\mathbb{P}(\varnothing) = \mathbb{P}(\{0\}) = \mathbb{P}(\{1\}) = \mathbb{P}(\{3\}) = \frac{1}{\det(I+L)} = 0.13$$

$$\mathbb{P}(\{0,1\}) = \frac{1}{\det(I+L)} \begin{vmatrix} 1 & 0.3679 \\ 0.3679 & 1 \end{vmatrix} = 0.1124$$

$$\mathbb{P}(\{0,3\}) = \frac{1}{\det(I+L)} \begin{vmatrix} 1 & 0.0498 \\ 0.0498 & 1 \end{vmatrix} = 0.1297$$

$$\mathbb{P}(\{1,3\}) = \frac{1}{\det(I+L)} \begin{vmatrix} 1 & 0.1353 \\ 0.1353 & 1 \end{vmatrix} = 0.1276$$

$$\mathbb{P}(\{0,1,3\}) = \frac{\det(L)}{\det(I+L)} = 0.1103.$$

In the case of two points being selected, the probability of selecting $\{0, 3\}$ is higher

than selecting $\{0,1\}$ or $\{1,3\}$, thus giving more priority to the points that are far apart favoring repulsion. From the realization probabilities above, we can obtain the inclusion probabilities as $\rho(\{0\}) = 0.4824$, $\rho(\{1\}) = 0.4803$, $\rho(\{3\}) = 0.4976$, $\rho(\{0,1\}) = 0.2227$, $\rho(\{0,3\}) = 0.24$, $\rho(\{1,3\}) = 0.2379$, and $\rho(\{0,1,3\}) = 0.1103$. The probability of each point being selected in a realization is different, which depicts the spatially adaptive nature of the DPP. One can alternatively calculate the inclusion probabilities using the relation $K = L(I+L)^{-1}$ (by Definition 5.2) and (5.3).

The use of the PPPs and MHCPs is well established in the previous chapters. To gain a better understanding of the DPPs, we provide below a few properties of the DPP that aid in the SINR MD evaluation followed by the insights into the construction of L matrix.

5.4 Properties and Construction of DPPs

Let $\varepsilon_1, \varepsilon_2, \ldots, \varepsilon_N$ denote the eigenvalues of L. By Definition 5.4, the eigenvalues of K can be expressed as $\frac{\varepsilon_i}{1+\varepsilon_i}$, $1 \leq i \leq N$. The algorithm to sample from DPP(K) uses the eigendecomposition of the matrix K. The number of points in each sample is determined by the eigenvalues and the locations of points are determined by the eigenvectors [52, Th. 2.3].

5.4.1 Properties

Lemma 5.1 ([62])**.** *(Cardinality) The mean number of points in $\mathcal{X}$ is $\sum_{i=1}^{N} \frac{\varepsilon_i}{1+\varepsilon_i}$.*

Proof. The proof of Lemma 5.2 is given in Appendix C.2 for completeness. □

We can interpret Lemma 5.1 in terms of Bernoulli random variables d_u as follows: There are N trials in total. An u-th trial is a success ($B_i = 1$) with probability $\frac{\varepsilon_i}{1+\varepsilon_i}$. Then $|\mathcal{X}|$ is equivalent in distribution to $\sum_{i=1}^{N} B_i$.

Lemma 5.2 ([61]). *(Closed under Reduced Palm Conditioning) Let* $\mathcal{X}^{!i} \triangleq \mathcal{X} \setminus \{y_i\}$, $y_i \in \mathcal{X}$. *Conditioning on* $y_i \in \mathcal{X}$, *if* $\mathcal{X} \sim$ *DPP*(K), *then* $\mathcal{X}^{!i}$ *is also a DPP with a modified kernel* $K^{!i}$ *whose elements are given by*

$$K^{!i}_{jk} = K_{jk} - K_{ji}K_{ii}^{-1}K_{ik}, \quad j,k \neq i. \tag{5.5}$$

Proof. The proof is provided in Appendix C.2 for the convenience of the reader. □

Lemma 5.3 ([63, Th. 2.4]). *(Laplace Functional) For any non-negative function* h *on* $\mathbb{R}$, *the Laplace functional* $\mathcal{L}_{\mathcal{X}}(h)$ *of* $\mathcal{X} \sim$ *DPP*$(K(\phi))$ *is*

$$\mathcal{L}_{\mathcal{X}}(h) = \mathbb{E}\bigg[\exp\bigg(-\sum_{i=1}^{N} h(y_i)\mathbb{1}_{y_i \in \mathcal{X}}\bigg)\bigg] = \det(I - K^h(\phi)), \tag{5.6}$$

where the elements of $K^h(\phi)$ *are given by*

$$K^h_{ij} = \sqrt{1 - e^{-h(y_i)}}K_{ij}\sqrt{1 - e^{-h(y_j)}}. \tag{5.7}$$

With respect to Φ, *we have*

$$\mathcal{L}_{\mathcal{X}}(h) = \mathbb{E}\bigg[\mathbb{E}\bigg[\exp\bigg(-\sum_{i=1}^{N} h(y_i)\mathbb{1}_{y_i \in \mathcal{X}}\bigg) \mid \Phi = \phi\bigg]\bigg] = \mathbb{E}[\det(I - K^h(\Phi))]. \tag{5.8}$$

See [53, App. A] for an alternate proof of Lemma 5.3. Note that the calculation of the Laplace functional does not require the simulation of $\mathcal{X}$, just Φ is sufficient.

5.4.2 Construction of L-Matrix

The L-matrix determines how the points of ϕ are thinned. We can represent L in its decomposed form as

$$L_{ij} = q_i \Upsilon_i^T \Upsilon_j q_j = q_i S_{ij} q_j, \tag{5.9}$$

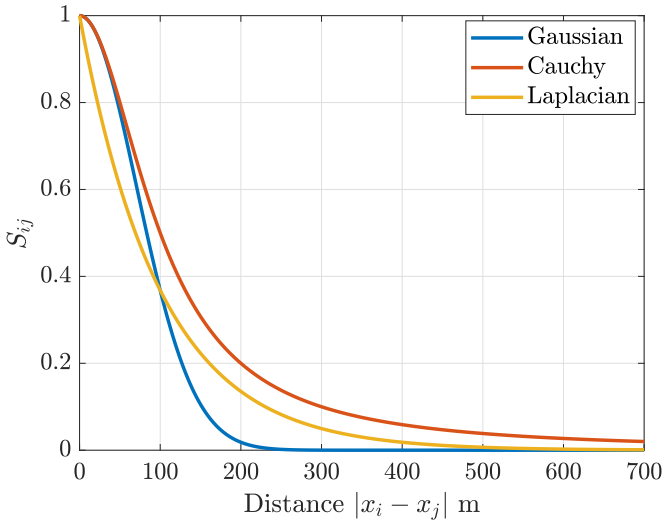

Figure 5.1: Comparison of different similarity kernels. $\sigma = 100$.

where q is called the quality factor and S is referred to as the similarity matrix. Such decomposition makes sure that L remains positive semidefinite while fitting the observed data to the DPP. The quality factor q_i is an intrinsic measure of the point y_i. The smaller the distance between the points y_i and y_j, the higher is their similarity value S_{ij}. There are multiple ways of modeling quality factors and similarity matrices. Below, we provide a few of them in the context of vehicular (or wireless) networks.

5.4.2.1 Quality Factor

We model the quality factor using logistic regression. Let

$$q_i = \exp\left(\upsilon_0 + \sum_{k=1}^{M} \upsilon_k f_{i,k}\right), \quad M \leq N. \tag{5.10}$$

If $f_{i,k} = 0 \ \forall k > 0$, all points have the same quality factor. Alternatively, we can set $f_{i,k} = d_{i,k}$, where $d_{i,k}$ is the distance to the k-th nearest neighbor of the point y_i. In this case, for $\upsilon_k \neq 0$, the quality of the point is decided by how far it is from its neighbors. The similarity matrix is a function of pairwise distances, while the quality factor can be formulated to model the relation between a point and its M neighbors.

5.4.2.2 Similarity Matrix

A few choices to model S include the Gaussian, Cauchy, and Laplacian/double exponential kernel functions. They are given by

$$\text{(a) Gaussian: } S_{ij} = \exp(-\|y_i - y_j\|^2/\sigma^2), \tag{5.11}$$

$$\text{(b) Cauchy: } S_{ij} = 1/(1 + \|y_i - y_j\|^2/\sigma^2), \tag{5.12}$$

$$\text{(c) Laplacian: } S_{ij} = \exp(-\|y_i - y_j\|/\sigma), \tag{5.13}$$

where σ is the scale parameter. As the distance $\|y_i - y_j\|$ increases, S_{ij} decreases, and, in turn, L_{ij} decreases by (5.9). Thus, the probability of selecting points that are far apart, increases by (5.4), as lower off-diagonal values yield a higher value of the determinant. Fig. 5.1 illustrates the above kernels. With the Gaussian kernel, the points that are at distances more than 230 m apart have higher chances of being selected as they have smaller S_{ij} than the points that are closer than 230 m. Nevertheless, any two points that are at a non-zero distance can get selected with some non-zero probability, resulting in a soft-core point process. The longer-tailed Cauchy and Laplacian kernels can further restrict how the points are chosen.

Next, we define our performance metric, the binned SINR MD, and analyze it for the baseline models and DPPs.

5.5 Binned Meta Distribution of the SINR

We condition a vehicle (receiver) to be at the origin. On averaging over the realizations of Φ, the vehicle becomes the typical vehicle. In broadcast communication, there may exist multiple transmitters at different distances who broadcast their messages either concurrently or otherwise. Instead of analyzing the performance metric of interest for different distances, we can group the distances into bins and analyze the network behavior over each distance bin.

Denote by c_u and d_u the endpoints of the u-th bin, $\mathcal{B}_u$, $u \in \mathbb{N}$. $\mathcal{X} \cap \mathcal{B}_u$ denotes the point process of transmitters whose distances to the typical vehicle at the origin fall in the u-th bin. Below, we first provide the preliminaries required to define the binned SINR MD, followed by its formulation.

5.5.1 Signal-to-Interference-plus-Noise Ratio

The SINR at the origin with respect to a transmitter y can be expressed using (5.1) as

$$\mathsf{SINR}_y = \frac{g\mathrm{PL}_0 P_\mathrm{t}\|y\|^{-\alpha}}{\sum_{z\in\mathcal{X}\setminus\{y\}} g_z \mathrm{PL}_0 P_\mathrm{t}\|z\|^{-\alpha} + W}, \tag{5.14}$$

where $I = \sum_{z\in\mathcal{X}\setminus\{y\}} g_z \mathrm{PL}_0 P_\mathrm{t}\|z\|^{-\alpha}$ is the total interference power at the origin, and W is the noise power.

5.5.2 Conditional Success Probability

Using (4.1), we write the conditional success probability on the link between some transmitter y and the origin as

$$P_\mathrm{s}^y(\theta) = \mathbb{P}(\mathsf{SINR}_y > \theta \mid \Phi), \quad \theta > 0, \tag{5.15}$$

where θ is the SINR threshold that parametrizes the data rate. (5.15) is obtained by averaging only over the fading and transmitter point process $\mathcal{X}$ (MAC scheme) conditioned on Φ. Now, we are ready to define the performance metric, the binned meta distribution of the SINR.

5.5.3 Formulation of the Binned Meta Distribution of the SINR

The meta distribution of the SINR for the u-th bin, $\mathcal{B}_u$, $\bar{F}_{P_{\mathrm{s},u}}(\theta, x)$, is defined as

$$\bar{F}_{P_{\mathrm{s},u}}(\theta, x) \triangleq \mathbb{P}(P_\mathrm{s}^y(\theta) > x, y \in \mathcal{X} \cap \mathcal{B}_u), \quad x \in [0,1], \quad u \in \mathbb{N}. \tag{5.16}$$

The binned SINR MD (5.16) gives the fraction of the links, whose distances to the typical vehicle fall in the u-th bin can achieve the data rate θ with a reliability of at least x. It provides insights into the distance range over which we can achieve certain target reliability, in turn, the effective distance range for broadcast communication. The binned success probability, a special case of the binned SINR MD, is a commonly used metric in vehicular network simulations/experiments [57]. It is formally defined as follows.

The success probability for $\mathcal{B}_u$, $p_{\mathrm{s},u}$ is given by

$$p_{\mathrm{s},u}(\theta) = \mathbb{P}[\mathsf{SINR}_y > \theta, y \in \mathcal{X} \cap \mathcal{B}_u] = \mathbb{E}_{\mathcal{X}\cap\mathcal{B}_u}[P_{\mathrm{s}}^y(\theta)], \quad u \in \mathbb{N}. \tag{5.17}$$

It is obtained by averaging the conditional success probability of the links whose distances fall in the u-th bin over Φ.

5.6 Key Results

Using (5.14), we can write the conditional success probability (5.15) as

$$\begin{aligned} P_{\mathrm{s}}^y(\theta) &= \mathbb{P}\left(g > \frac{\theta\|y\|^\alpha}{\mathrm{PL}_0\mathrm{P}_{\mathrm{t}}}(I+W) \mid \Phi\right) \\ &= \mathbb{E}\left[\exp\left(-\frac{\theta\|y\|^\alpha}{\mathrm{PL}_0\mathrm{P}_{\mathrm{t}}}I\right)\right] \underbrace{\exp\left(-\frac{\theta\|y\|^\alpha}{\mathrm{PL}_0\mathrm{P}_{\mathrm{t}}}W\right)}_{W'} \\ &= \mathbb{E}\left[\prod_{z\in\mathcal{X}\setminus\{y\}} \exp(-\theta\|y\|^\alpha g_z \|z\|^{-\alpha})\right] W' \\ &\overset{(a)}{=} \mathbb{E}\left[\prod_{z\in\mathcal{X}\setminus\{y\}} \frac{1}{1+\theta\|y\|^\alpha\|z\|^{-\alpha}}\right] W', \end{aligned} \tag{5.18}$$

where (a) averages over the fading.

Proposition 5.1. *The conditional success probability on the link between the trans-*

mitter $y_i \in \mathcal{X} \subseteq \phi$ and the origin in the DPP is $\det(I - \mathcal{K}^i(\phi))W'$*, where*

$$\mathcal{K}^i_{jk} = (K_{jk} - K_{ji}K_{ii}^{-1}K_{ik}) \prod_{l=j,k} \left(1 + \frac{\|y_l\|^\alpha}{\theta\|y_i\|^\alpha}\right)^{-1/2}, \quad j,k \neq i. \tag{5.19}$$

Proof. For the DPP with $\phi = \{y_1, y_2, \ldots, y_N\}$, we can rewrite (5.18) in terms of y_i, $1 \leq i \leq N$, as

$$\begin{aligned} P_{\mathrm{s}}^{y_i}(\theta) &= \mathbb{E}\bigg[\prod_{z\in\mathcal{X}\setminus\{y_i\}} \frac{1}{1+\theta\|y_i\|^\alpha\|z\|^{-\alpha})}\bigg]W' \\ &= \mathbb{E}\left[\prod_{1\leq j\leq N}^{j\neq i} \frac{1}{1+\theta\|y_i\|^\alpha\|y_j\|^{-\alpha}\mathbb{1}_{y_j\in\mathcal{X}}}\right]W' \\ &= \mathbb{E}\bigg[\exp\bigg(-\sum_{1\leq j\leq N}^{j\neq i}\log\bigg(1+\theta\|y_i\|^\alpha\|y_j\|^{-\alpha}\mathbb{1}_{y_j\in\mathcal{X}}\bigg)\bigg)\bigg]W'. \end{aligned} \tag{5.20}$$

The expectation in (5.20) is with respect to the reduced palm conditioned point process $\mathcal{X}^{!i} = \mathcal{X} \setminus \{y_i\}$. Comparing (5.20) with Lemma 5.3, we observe that $h(y_i) = \log(1 + \theta\|y_i\|^\alpha\|y_j\|^{-\alpha})$. Therefore, the resulting kernel is the kernel K modified by $\mathcal{X}^{!i}$ and $h(y_i)$. Using the Lemmas 5.2 and 5.3, we can express (5.20) as $\det(I - \mathcal{K}^i(\phi))$ with the elements of $\mathcal{K}^i$ given by (5.19). □

Remark 5.2. *The conditional success probability* (5.19) *in the DPP applies to* Φ *being any finite point process on* $\mathbb{R}^d$ *as it involves just calculating the determinant over a discrete set of points.*

Proposition 5.2. *The SINR MD for the u-th bin in the PPP is given by*

$$\bar{F}_{P_{\mathrm{s},u}}(\theta, x) = \frac{1}{d_u - c_u}\int_{c_u}^{d_u} \bar{F}_{P_{\mathrm{s}}^y}(\theta, x)\mathrm{d}y, \tag{5.21}$$

where

$$\bar{F}_{P_{\mathrm{s}}^y}(\theta, x) = \mathbb{P}(P_{\mathrm{s}}^y(\theta) > x) = \frac{1}{2} + \frac{1}{\pi}\int_0^\infty \frac{\Im(e^{-jt\log x}M_{jt}^y)}{t}\mathrm{d}t, \tag{5.22}$$

and

$$M_b^y(\theta) = \mathbb{E}[P_{\mathrm{s}}^y(\theta)^b] = \exp(-2\lambda\|y\|\theta^{\delta'}\Gamma(1+\delta')\Gamma(1-\delta')\mathfrak{D}_b(p,\delta')), \quad b \in \mathbb{C}, \quad (5.23)$$

with $\delta' = 1/\alpha$ *and* $\mathfrak{D}_b(p,\delta') = pb\,{}_2F_1(1-b, 1-\delta'; 2; p)$.

Proof. By Slivnyak's theorem [4, Ch. 8], conditioning a transmitter at y is the same as adding a transmitter at y in the PPP. To obtain the SINR MD with respect to the u-th bin, $\mathcal{B}_u$, we can add transmitters at multiple locations uniformly distributed between the endpoints c_u and d_u of $\mathcal{B}_u$ consecutively, and average the respective SINR MDs. Adding a transmitter at y implies that the link between y and the origin is active over the realizations of Φ. Then, we can rewrite the SINR MD (5.16) with respect to the u-th bin, $\mathcal{B}_u$, as

$$\begin{aligned}\bar{F}_{P_{\mathrm{s},u}}(\theta, x) &= \mathbb{P}(P_{\mathrm{s}}^y(\theta) > x, y \in \mathcal{X} \cap \mathcal{B}_u) \\ &= \int_{c_u}^{d_u} \mathbb{P}(P_{\mathrm{s}}^y(\theta) > x)\mathbb{P}(y \in \mathcal{X} \cap \mathcal{B}_u)\mathrm{d}y. \end{aligned} \quad (5.24)$$

As points in $\mathcal{B}_u$ are uniformly distributed, $\mathbb{P}(y \in \mathcal{X} \cap \mathcal{B}_u) = \frac{1}{d_u - c_u}$. Then

$$\bar{F}_{P_{\mathrm{s},u}}(\theta, x) = \frac{1}{d_u - c_u}\int_{c_u}^{d_u} \mathbb{P}(P_{\mathrm{s}}^y(\theta) > x)\mathrm{d}y = \frac{1}{d_u - c_u}\int_{c_u}^{d_u} \bar{F}_{P_{\mathrm{s}}^y}(\theta, x)\mathrm{d}y,$$

where $\bar{F}_{P_{\mathrm{s}}^y}(\theta, x)$ follows from the Gil-Pelaez theorem and is given by (5.22), and $M_b^y(\theta)$, the b-th moment of the conditional success probability (5.23), follows from (4.9).

□

Corollary 5.1. *The success probability with respect to the u-th bin,* $\mathcal{B}_u$*, in the PPP is*

$$P_{\mathrm{s},u}(\theta) = \mathbb{E}_{\mathcal{X}\cap\mathcal{B}_u}[P_{\mathrm{s}}^y(\theta)] = \frac{1}{d_u - c_u}\int_{c_u}^{d_u} M_1^y(\theta)\mathrm{d}y, \quad (5.25)$$

where $M_1^y(\theta)$ *is given by* (5.23) *with* $b = 1$.

Proof. The proof follows from the proof of Proposition 5.2 except that the distribution over the conditional success probability is replaced by the expectation in (5.24), which is given by the first moment M_1^y as shown in (5.25). □

The conditional success probability (5.18) with respect to the MHCP cannot be further simplified but for the approximation using the PPP. Here, we numerically evaluate the binned SINR MD for the MHCP. Alternatively, one can fit a DPP to the MHCP and use Proposition 5.1 to evaluate the binned SINR MD.

Remark 5.3. *To evaluate the binned SINR MD for the PPP, one can directly use the analytical expression* (5.16) *without the need to simulate the PPP. In the case of the MHCPs, no exact analysis is possible. Starting from the PPPs, we generate different realizations of the MHCPs and average over them to obtain the exact results.*

The DPPs are the middle route between the PPPs and MHCPs. To evaluate the conditional success probability (5.19)*, we just need to simulate the PPPs, not the transmitters forming the DPPs. The DPPs enable faster simulations by exploiting the analytical result, the determinant of a kernel matrix.*

5.7 Results and Discussion

We consider the vehicles (cars) to be Poisson distributed on $\mathbb{R}$ with $\lambda = 1/8, 1/16,$ and $1/32$ per meter. Equivalently, in the case of the DPP, we assume $N = 500, 250,$ and 50 vehicles Poisson distributed on a street of length 4000 m in ns-3. $N = 500$ cars refer to the high-intensity traffic case as each car is about 5 m on average, and the gap to the front/back vehicle totals an average of 3 m, implying that the road is fully packed. $N = 250$ refers to the medium-intensity traffic scenario, and $N = 50$ refers to the low-intensity traffic scenario. Each vehicle generates a basic safety message (BSM) every $\tau = 100$ ms. The BSM contains information on the vehicle's speed,

position, brake status, orientation, etc. Table 5.1 lists the other system parameters in ns-3. The parameters AIFSN and contention window size listed in Table 5.1 are specific to CSMA/CA used in DSRC. See [57] for further details on the CSMA/CA parameters. The vehicles are assumed to remain static. It does not matter as a message of size 414 bytes requires only about 550 μs to get transmitted with a data rate of 6 Mbps and vehicles do not move a significant distance in such a short duration.

We recall that the MAC layer that determines which vehicles should transmit is modeled by the transmitter point process. We need to choose the parameters of the L-matrix in the DPP such that the distribution of the selected concurrent transmitters matches that in ns-3.

5.7.1 ns-3 vs. DPP

Let ψ_t denote the set of concurrent transmitters observed in ns-3 for the PPP realizations ϕ_t at time instants $t \in \{1, 2, \ldots, T\}$. We would like to fit a DPP to the observed data that maximizes the chances of observing $\mathcal{X}$ given Φ. Mathematically, using (5.4), the maximum likelihood optimization problem can be expressed as

$$\begin{aligned} \max_{\boldsymbol{\upsilon},\sigma} \mathbb{L} &= \max_{\boldsymbol{\upsilon},\sigma} \log\left(\prod_{t=1}^{T} P(\mathcal{X} = \chi_t \mid \Phi = \phi_t)\right) \\ &= \max_{\boldsymbol{\upsilon},\sigma} \sum_{t=1}^{T} \log\left(\frac{\det(L_{\chi_t}(\phi_t))}{\det(I + L(\phi_t))}\right), \end{aligned} \tag{5.26}$$

where $\mathbb{L}$ is the log-likelihood, and $\boldsymbol{\upsilon} = (\upsilon_0, \ldots, \upsilon_n)$ and σ are the parameters of q and S given in (5.9), respectively. Note that the log-likelihood (5.26) is non-convex and hence there exist multiple local minima.

TABLE 5.1

SIMULATION PARAMETERS

Parameter	Value
BSM Size	414 bytes
Bandwidth	10 MHz
Data Rate	6 Mbps
Slot Duration	13 μs
SINR Threshold	8 dB
Carrier Sensing Threshold	-82 dBm
Preamble Detection Threshold	-94 dBm
Preamble Decoding Threshold	8 dB
Path-Loss Exponent α	2
Path-Loss Constant PL_0	-46.677 dB
Transmit Power P_t	10 dBm
Arbitrary Inter-Frame Spacing (AIFSN)	2
Contention Window Size	$2^k - 1$, $k \in [4, 10]$

5.7.1.1 Distance to the n-th Nearest Transmitter

Let R_n denote the distance to the n-th nearest transmitter from the typical vehicle. Fig. 5.2a shows the distribution $F_{R_n}(r)$ of the distance to the n-th nearest transmitter. We observe that the DPP provides a good fit to ns-3 even at higher values of n. Fig. 5.2b depicts that the mean number of transmitters within a distance r of the typical vehicle in the DPP match that in ns-3 well.

5.7.1.2 Binned SINR MD

Fig. 5.2c plots the binned SINR MD for different distance bins. The DPP does not provide a good fit to ns-3 despite the good statistical fit with respect to the n-th nearest-transmitter distance (Fig. 5.2a) for the reasons stated in Section 5.2. Nevertheless, we can tune the DPP parameters such that its SINR MD tightly matches that in ns-3 as shown in Fig. 5.3 for different traffic intensities.

5.7.2 ns-3 vs. Baseline Models

For the chosen simulation parameters given in Table 5.1, in the no fading case, at a distance of 735 m, the signal strength falls below the preamble detection threshold of -94 dBm. In ns-3, we have considered the length of the street as 4000 ($\gg 735$) m, implying that the finite model in ns-3 is sufficiently long to be compared against the theoretical stationary PPP model considered on $\mathbb{R}$. Fig. 5.4 compares the binned SINR MD and success probability for the PPP and ns-3. The transmit probability in the PPP, $p = T_p/\tau$, where $T_p = 414 \cdot 8/(6 \cdot 10^6)$ is the time taken to transmit a packet of size 414 bytes. We observe that the PPP approximates ns-3 better with decreasing N. Fig. 5.5 plots the binned SINR MD for the MHCP and ns-3. The MHCP is fitted to ns-3 by trial and error. We observe that the binned SINR MD, in turn, the binned success probability, for the MHCP nicely approximates that for ns-3. From Figs. 5.3 and 5.5, we conclude that the DPP provides a more accurate fit

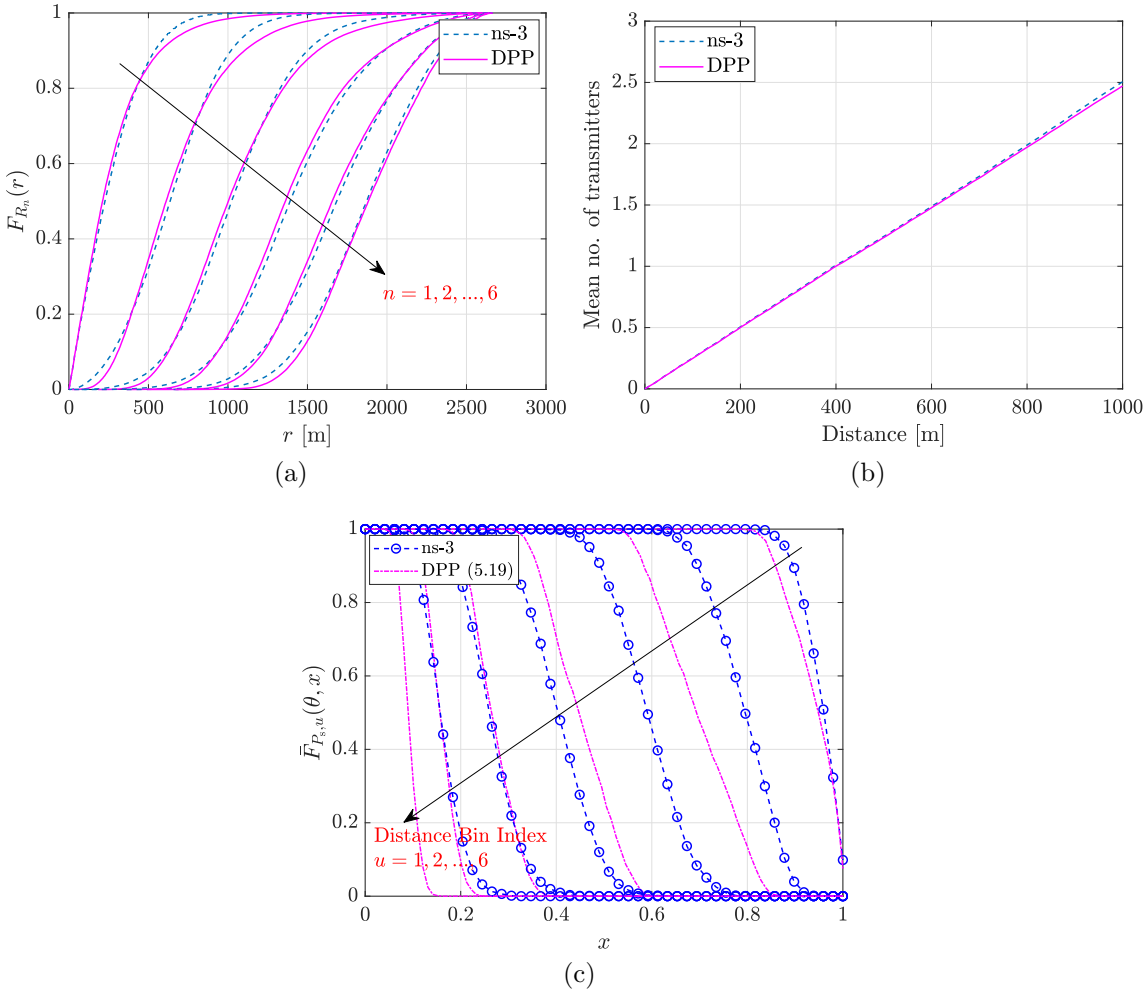

Figure 5.2: (a) n-th nearest-transmitter distance distributions (b) Mean number of transmitters within distance r of the typical vehicle (c) Comparison of the SINR MDs for ns-3 and DPP for different bin indices. S is Gaussian. $\sigma^* = 200$ and $\boldsymbol{\upsilon}^* = [-1.5543, 0.0011]$. They are obtained by optimizing (5.26). The distance bin is of length 50 m. The conditional success probability required to evaluate the binned SINR MD/success probability for the DPP is given by (5.19).

than the MHCP to ns-3 with an advantage of mathematical analysis.

In Chapters 2 and 3, to model a 2D vehicular network, we considered street geometry and placed vehicles on the streets. In the simplified transdimensional model proposed in Chapter 4, we accounted for the streets passing through the typical vehicle and approximated the rest of the vehicular point process using a 2D PPP. The PPP does not exhibit repulsion, thus it is necessary to include the street geometry to create some repulsion between the transmitting vehicle locations. However, that is not the case with the DPP. The impending question here is whether street geometry is important if 2D DPPs are used to model vehicular networks, which we will analyze in the next section.

5.8 2D DPPs for Vehicular Networks

Consider a PLP-PPP $\mathcal{V}$ on $\mathcal{R} \subset \mathbb{R}^2$ with street intensity μ and the vehicles on each street forming a 1D PPP of intensity λ (Definition 3.4). The transmitter point process $\mathcal{X}$ is determined by thinning $\mathcal{V}$ based on a kernel K. It is referred to as the PLP-DPP (DPP on a PLP).

Fig. 5.6 compares the binned SINR MD and success probability for the PLP-DPP and 2D DPP, which is obtained by thinning a 2D PPP of intensity $\lambda\mu$, the 2D intensity of the PLP-PPP (Lemma 3.1). We observe that a 2D DPP provides a tight approximation to the PLP-DPP for all bin indices. The reason is that the transmitters are selected purely based on the distances between them and hence the geometry of the streets does not matter.

Remark 5.4. *The DPP with a kernel K can accurately model the transmitter point process in d-dimensional vehicular networks. It is more accurate than the PPP and more tractable than the MHCP. There exists a trade-off between using the PPP and DPP for modeling the transmitter point process. The PPP-based vehicular network lends to analytical expressions for the binned SINR MD while the DPP lends to ex-*

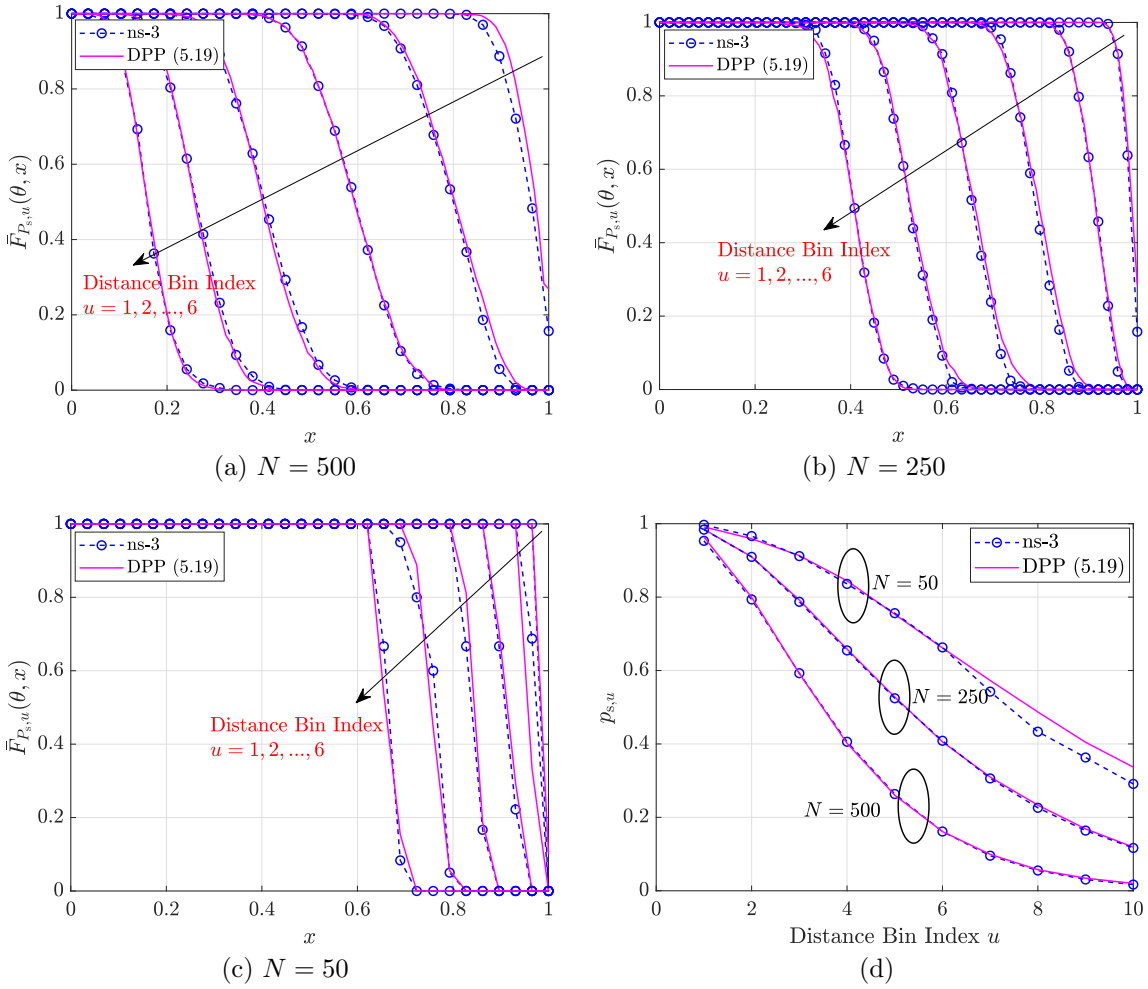

(a) $N = 500$ (b) $N = 250$ (c) $N = 50$ (d)

Figure 5.3: ns-3 vs. DPP. Figs. (a)-(c) show the binned SINR MD and (d) shows the binned success probability for different N and bin indices. S is Gaussian. The DPP parameters that match the SINR MD in ns-3 for (a) $N = 500$ are $\nu = -0.8501$ and $\sigma = 395$, (b) $N = 250$ are $\nu = -1.1945$ and $\sigma = 415$, and (c) $N = 50$ are $\nu = 280$ and $\sigma = -1.4263$. The distance bin is of length 50 m. The unit of intensity λ is per meter. The conditional success probability required to evaluate the binned SINR MD/success probability for the DPP is given by (5.19).

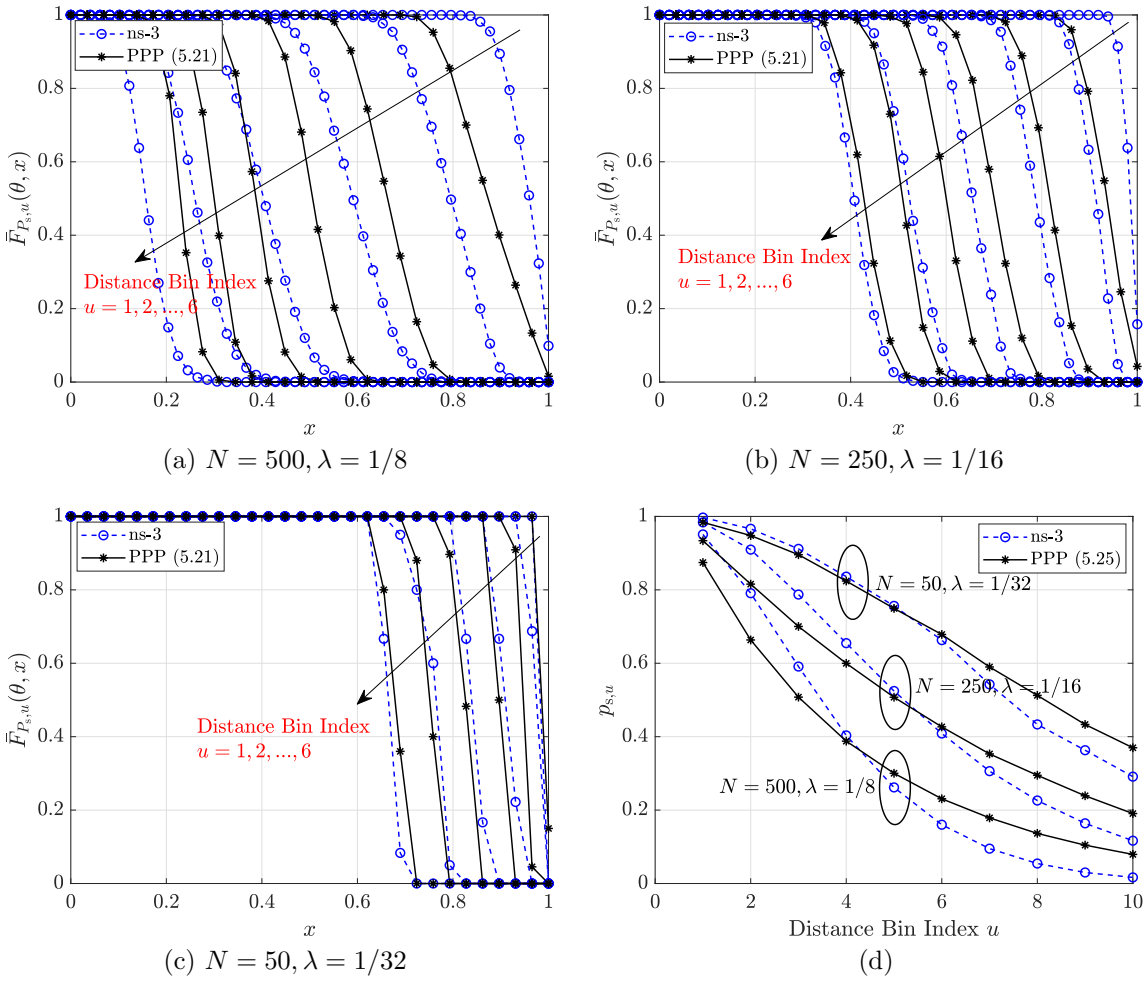

Figure 5.4: ns-3 vs. PPP. Figs. (a)-(c) show the binned SINR MD and (d) shows the binned success probability for different traffic intensities and bin indices. The transmit probability is $p = 0.0055$. The distance bin is of length 50 m. The unit of intensity λ is per meter. The equation numbers corresponding to the binned SINR MD and success probability are given in the parentheses in the legends.

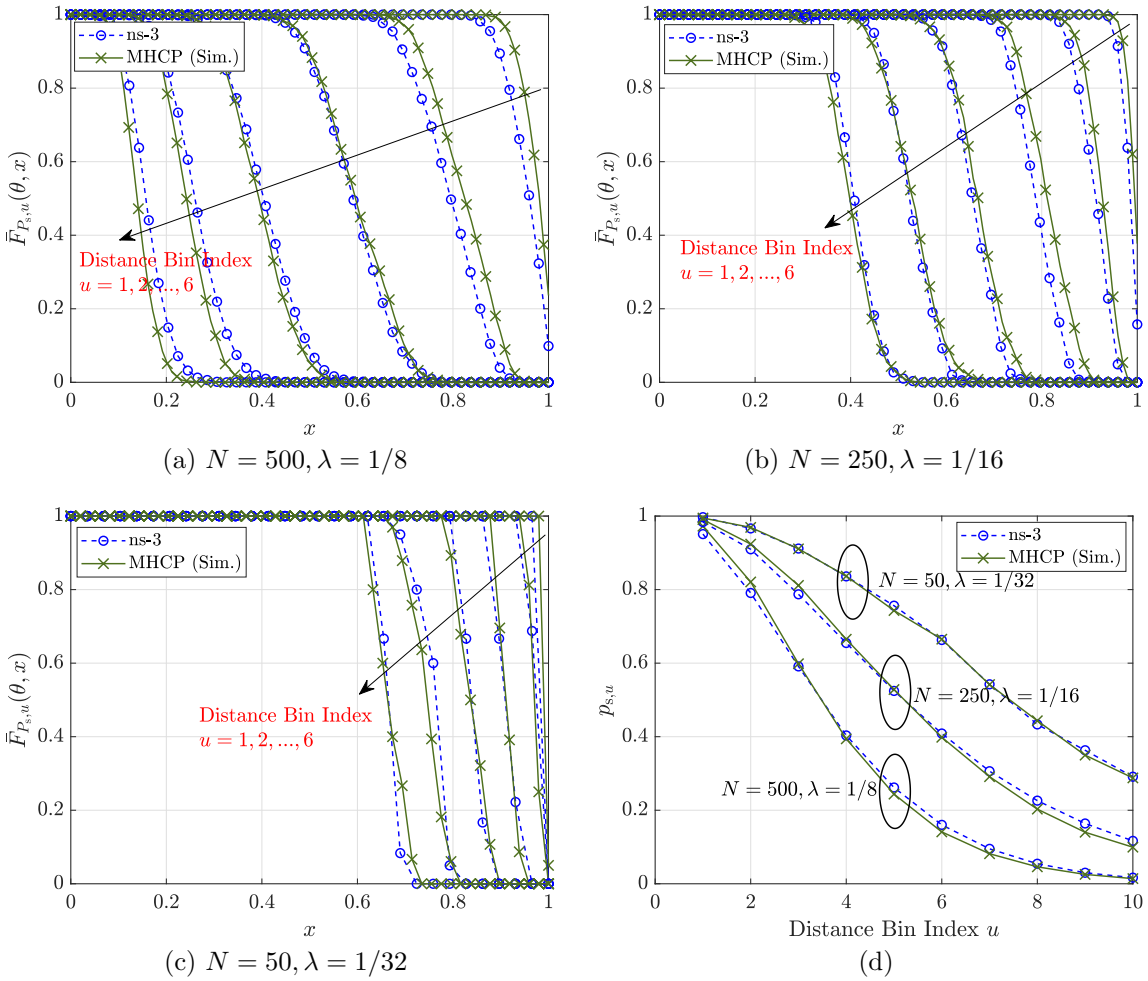

(a) $N = 500, \lambda = 1/8$ (b) $N = 250, \lambda = 1/16$

(c) $N = 50, \lambda = 1/32$ (d)

Figure 5.5: ns-3 vs. MHCP. Figs. (a)-(c) show the binned SINR MD and (d) shows the binned success probability for different traffic intensities and bin indices. The distance bin is of length 50 m. The hard-core distance r_{M} that approximates ns-3 are 425.1 m, 718.3 m, and 1349.7 m for $\lambda = 1/8, 1/16$, and $1/32$ per meter, respectively.

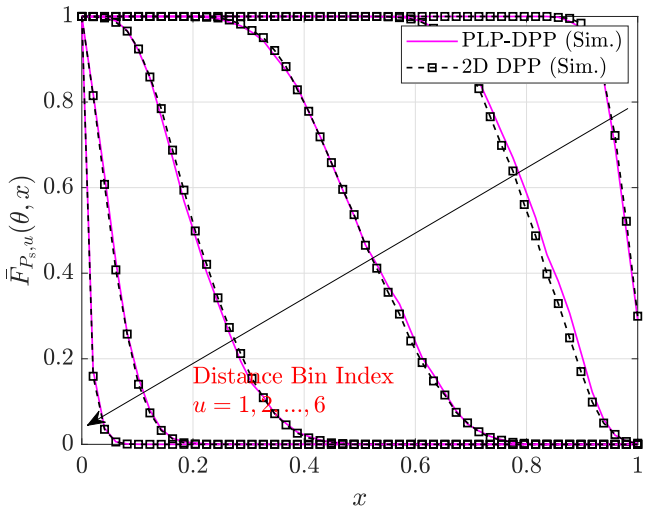

(a)

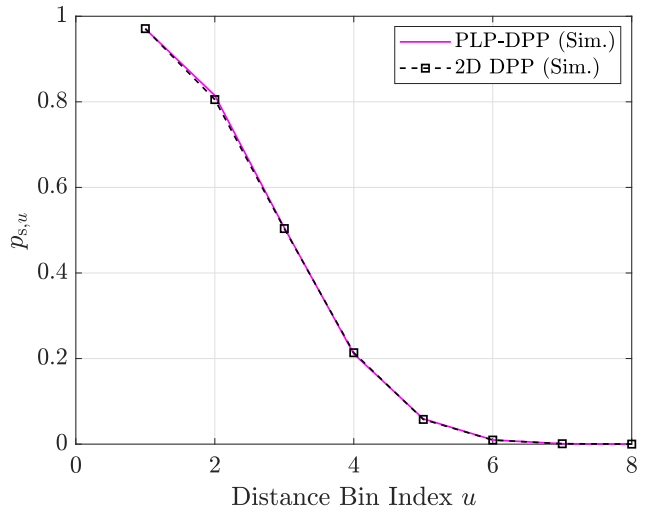

(b)

Figure 5.6: PLP-PPP vs. 2D DPP. Figs. (a) and (b) show the binned SINR MD and success probability, respectively. The distance bin is of length 50 m. $\alpha = 2.5$. $N = 1000$. Similarity matrix is Gaussian with $\sigma = 100$, $\nu = -1.8526$. The rest of the parameters are given in Table 5.1.

pressions up to the conditional success probability with the challenge of finding the appropriate kernel K.

Remark 5.5. *The 2D DPP can effectively capture the distance distribution between the transmitters as in the DPP placed on a PLP. Hence, we need not explicitly consider the street geometry as in the case of PPP-based vehicle location modeling. This remark is also applicable to the repulsion exhibiting hard-core processes such as the MHCP.*

5.9 Conclusions

The determinantal point processes can model the soft and adaptable repulsiveness between the transmitters. The structure of the DPPs permits the evaluation of the performance metrics through a mix of simulation and analysis, unlike the MHCP. Though the MHCP can model the transmitter point process by strictly restricting the minimum distances between the transmitters, it is intractable. We showed that the DPP is a better and more accurate model than the MHCP and analytically tractable PPP through DSRC simulations in ns-3 for different vehicle densities.

The main takeaway is the answer to the question 'should we model the streets in 2D vehicular networks?' If we model the transmitter point process by a PPP, the street geometry cannot be neglected since a 2D PPP cannot model the transmitters clustered along the streets as in street-based vehicular networks. In this case, the transdimensional Poisson point process can be used to model the vehicular networks as they are simpler than the complicated street-based vehicular networks and yet provide tight approximations to them. On the other hand, if we use a DPP to model the transmitter point process, the street geometry can be safely omitted as the DPPs select the transmitters based on the distances between them such that they exhibit repulsion.

CHAPTER 6

SUMMARY AND FUTURE WORK

6.1 Summary

High reliability is a key requirement in safety-oriented vehicular communications, where a vehicle broadcasts safety messages to the intended recipients such as other vehicles, roadside units, or pedestrians. Reliability is defined as the probability that a receiver can successfully decode the message sent by a transmitter. It depends on the locations of the transmitter, receiver and interferers, and the wireless medium. To obtain insights into the reliability, we first need to model the key actors in vehicular communications. To this end, we use mathematical tools such as point and line/stick processes from stochastic geometry to model vehicle locations. They provide crisp insights into the network behavior and complement large-scale simulations/experiments.

Poisson point processes (PPPs) have been widely used to model locations of base stations in cellular networks. The reasons are: (i) they provide a lower bound to the coverage probability—the probability of a cellular user successfully connecting to a base station—evaluated in the real-world cellular networks; (ii) they are the most tractable point processes; (iii) non-Poisson point processes such as hard-core processes that can provide higher accuracy than PPPs are highly intractable. However, the use of PPPs to model vehicle locations is debatable. Unlike base stations, vehicles are located on the streets that possess a certain geometry.

To assess the significance of the street geometry, we first studied a square grid vehicular network with vehicles on each street independently forming 1D PPPs of

some intensity. Each vehicle transmits independently with a certain probability p as in the ALOHA MAC scheme. Transmitters on each street also form a PPP with the intensity scaled by p. The street-based vehicular network behaves differently from a pure PPP-based vehicular network except at the asymptotic regimes of data rate. The reason is that the street system allows vehicles to be clustered along the streets unlike the complete random placement of vehicles in PPPs.

With the evidence favoring the need for modeling the street geometry, we developed a general framework for modeling and analysis of vehicular networks. The spatial models in this framework can characterize streets of different lengths and orientations, and involve intersections and T-junctions. For instance, Poisson line processes (PLPs) can model streets of infinite lengths with different orientations inherently forming intersections. Poisson stick processes (PSPs) can model streets of finite varying lengths with different orientations forming intersections. Poisson lily-pond model (PLM) is a variant of PSPs with sticks forming T-junctions. These models facilitate the reliability analysis of vehicles located at intersections/T-junctions. This is of critical concern as almost 50% of the accidents occur at intersections. The expressions for the reliability of the vehicles located at intersections/T-junctions and non-intersections/T-junctions can be used to study the interplay between the street density, vehicle intensity, data rate, and the location of the vehicle.

The street systems, and, in turn, the spatial models, vary with geographical regions. One might wonder whether there is a need to model each of them. Not necessarily. We introduced the notion of equivalence which helps us to find the street systems that behave the same way qualitatively. We need only a representative class of models that can be used to analyze a larger set of street systems. For instance, a PSP-based vehicular network is equivalent to PLP-based and PLM-based vehicular networks under a certain mapping of system parameters, *i.e.,* if we have the reliability for the PSP-based vehicular network, we can use it to evaluate the reliability for

PLP-based and PLM-based vehicular networks.

The complete characterization of street systems makes analytical expressions unwieldy despite the use of PPPs to model vehicle locations on streets. We proposed a transdimensional Poisson point process (TPPP) that considers only the geometry of the streets passing through the receiver of interest and models the rest of the vehicles using a 2D PPP. Such a simplification resulted in a tremendous increase in tractability yet providing tight approximations to the complete street-based vehicular networks. In particular, the success probability in the TPPP differs from the PLP-based vehicular network by a maximum of only about -14 dB. The TPPP provides good approximations not only in terms of success probability but also in its fine-grained version, the meta distribution (MD) of the signal-to-interference ratio (SIR).

The SIR MD answers questions such as *what fraction of the links can satisfy a target data rate of* 10 *Kbps with a probability of at least* 0.99*?*, whereas the success probability answers questions such as *what fraction of the links can support a target data rate of* 10 *Kbps?* The former provides insights into fairness among the links while the latter focuses only on the average. Using the SIR MD for the TPPP, we devised a congestion control scheme that determines the optimum transmit probability such that the fraction of the links can achieve the target data rate with a certain minimum guarantee. The success probability-based congestion control scheme is inadequate to alleviate network congestion, especially when the transmitter-receiver links exhibit significant variance in terms of reliability, as the success probability does not guarantee that a certain fraction of the links achieves the desired reliability.

Lastly, we explored a middle route between the street-based vehicular networks with transmitters on streets forming PPPs independently and hard-core processes that guarantee a minimum distance between the transmitters. In particular, we study determinantal point processes (DPPs) that belong to the family of soft-core

point processes. Here, transmitters are jointly selected such that there exists soft and adaptable repulsiveness between transmitter locations, which is very much the case in real-world vehicular networks. Such selection obviates the need for street geometry. The structure of DPPs defined on discrete spaces does not facilitate a complete analysis but a simalysis, a blend of simulation and analysis. We found that DPPs can tightly approximate the system-level simulations in terms of the binned SINR MD, that answers questions such as *what fraction of the links within the distance range of* 100-200 *meters can satisfy a target data rate of* 10 *Kbps with a probability of at least* 0.99*?* The binned SINR MD provides insights into the reliable broadcast range.

There exists a trade-off between using PPPs and DPPs for vehicular network modeling. The PPPs guarantee exact analysis albeit with loose approximations to system-level simulations, while DPPs guarantee high accuracy with a simalysis. For modeling and analyzing 2D vehicular networks, one could use the TPPPs with partial street geometry or DPPs forgoing the entire street geometry.

6.2 Future Directions

Analyzing DPP Parameters Fitting the transmitter point process in system-level simulations to DPPs involves optimizing multiple parameters. So far we have shown that a DPP can accurately fit system-level simulations for different vehicle intensities. An interesting extension would be to mathematically formulate the relation between a MAC scheme, vehicle intensity, and DPP parameters. One way to accomplish this is to train a regression model with parameters learned by fitting DPPs to system-level simulations for different vehicle intensities and MAC parameters and predict the parameters for desired vehicle intensity and MAC parameters.

Congestion Control using DPPs Congestion control deals with the trade-off between the number of transmissions and the number of successful broadcast links. The

latter increases with the former. However, as the number of transmissions increases beyond a certain limit, congestion occurs. The goal here is to find the parameters of the DPP that would maximize the number of successful broadcast links.

DSRC vs. NR-V2X The vehicular technologies DSRC and NR-V2X use different mechanisms to select concurrent transmitters. Also, they employ different coding schemes. It will be of interest to analyze (i) whether the performance differences between the DSRC and NR-V2X are merely due to different coding schemes? (ii) whether the DSRC and NR-V2X systems are equivalent, *i.e.,* if we know the behavior of DSRC, can we deduce/approximate the behavior of NR-V2X?

APPENDIX A

PROOFS OF CHAPTER 3

A.1 Proof of Lemma 3.4

To prove Lemma 3.4, we make use of [31, Prop. 6.2], which asserts the following: *There exist $a, b \geq 0$, such that the complementary cumulative distribution function (CCDF) of the half-lengths H in the lilypond model can be bounded as*

$$1 - F_H(h) \leq a \exp(-bh^2), \quad h \geq 0. \tag{A.1}$$

Our goal is to find a tight approximation. By the properties of the cumulative distribution function, $a \geq 1$. However, $a > 1$ makes the bound (A.1) loose for small h, which implies that $a = 1$ is the natural choice. This reduces the bound (A.1) to the CCDF of the Rayleigh distribution. Fig. A.1 fits the CCDF and PDF of the half-lengths to that of the Rayleigh distribution. We observe that the upper bound on the CCDF is loose for small values of h. Instead of choosing a value for b that provides an upper bound, we approximate the CCDF of the half-lengths with an appropriate value for b that minimizes the gap between the empirical and theoretical CCDFs. It follows from the Rayleigh approximation that the mean half-length is $\mathbb{E}[H] \approx \sqrt{\pi/4b}$. The value of b is found by equating $\mathbb{E}[H]$ to the empirical mean of the half-lengths.

Next, we study the relation between b and μ. Suppose we scale the PLM by an arbitrary factor $\nu > 0$. Then the street intensity μ is scaled by $1/\nu^2$ and the half-lengths of the sticks are scaled by ν, inversely proportional to $\sqrt{\mu}$. As the PLM

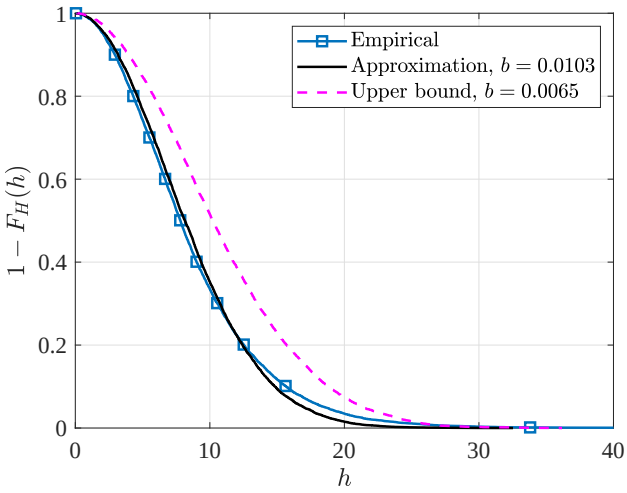

(a)

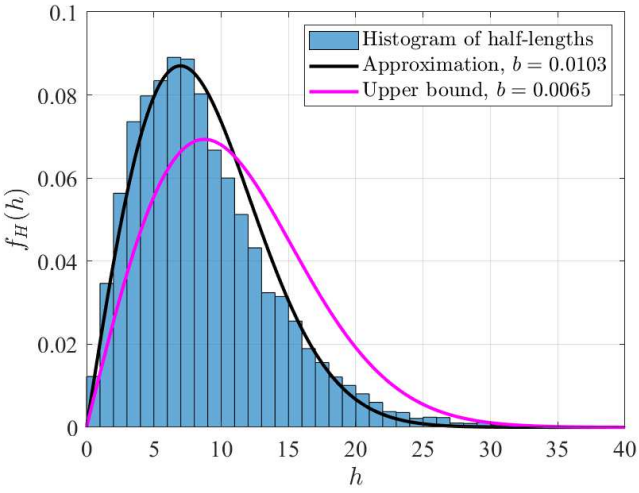

(b)

Figure A.1: Fitting the (a) CCDF and (b) PDF of the half-lengths to that of the Rayleigh distribution. $\mu = 0.01$.

retains its lilypond nature with scaling, the mean of the scaled half-lengths H' is scale-invariant, *i.e.,* $\sqrt{\pi/4b'} \approx \mathbb{E}[H'] = \mathbb{E}[\nu H] \approx \sqrt{\nu^2\pi/4b}$. This implies that $b' = b/\nu^2$, and thus b scales with μ.

A.2 Proof of Lemma 3.5

For the typical vehicle at the origin, the probability that its nearest neighbor is at a distance greater than r, $1 - F_R(r)$, is given by

$$\begin{aligned}
1 - F_R(r) &= \mathbb{E}\Big[\prod_{z\in\mathcal{V}^m} \mathbb{1}\{z \notin b(o,r)\}\Big] \\
&\overset{(a)}{=} \mathbb{E}\Big[\prod_{z\in\mathcal{V}_o^m} \mathbb{1}\{z \notin b(o,r)\}\Big]\mathbb{E}\Big[\prod_{z\in\mathcal{V}_!} \mathbb{1}\{z \notin b(o,r)\}\Big] \\
&= \mathbb{E}\Big[\prod_{k=1}^{\lceil m/2\rceil}\prod_{z\in V_k} \mathbb{1}\{z \notin b(o,r)\}\Big]\mathbb{E}\Big[\prod_{k>\lceil m/2\rceil}\prod_{z\in V_k} \mathbb{1}\{z \notin b(o,r)\}\Big] \\
&\overset{(b)}{=} \underbrace{\mathbb{E}\Big[\prod_{k=1}^{\lceil m/2\rceil}\mathbb{E}\Big[\prod_{z\in V_k} \mathbb{1}\{z \notin b(o,r)\}\Big]\Big]}_{1-F_{R,\mathcal{V}_o^m}(r)}\underbrace{\mathbb{E}\Big[\prod_{k>\lceil m/2\rceil}\mathbb{E}\Big[\prod_{z\in V_k} \mathbb{1}\{z \notin b(o,r)\}\Big]\Big]}_{1-F_{R,\mathcal{V}_!}(r)},
\end{aligned} \tag{A.2}$$

where (a) and (b) exploit the independence of the 1D PPPs.

The contact distance distribution $G_R(r)$ is the probability of finding a vehicle within a distance r from an arbitrary location in the plane, say the origin. No streets pass through or contain the origin a.s. This implies that $G_R(r)$ is defined with respect to $\mathcal{V}$, which is equivalent in distribution to $\mathcal{V}^m \setminus \mathcal{V}_o^m = \mathcal{V}_!$. Hence $G_R(r) = F_{R,\mathcal{V}_!}(r)$.

A.3 Proof of Lemma 3.6

Using the probability generating functional (PGFL) of the PPP, we can express $1 - F_{R,\mathcal{V}_!}(r)$ in (A.2) as

$$1 - F_{R,\mathcal{V}_!}(r) = \exp\left(-2\mu \int_0^{\pi} \int_0^{r} (1 - \exp(-2\lambda\sqrt{r^2 - u^2}))\mathrm{d}u\mathrm{d}v(\varphi)\right),$$
$$\stackrel{(a)}{=} \exp\left(-2\mu \int_0^{r} (1 - e^{-2\lambda\sqrt{r^2-u^2}})\mathrm{d}u\right), \tag{A.3}$$

where (a) follows from the independence between u and φ and the fact that $\int_{\mathbb{R}} \mathrm{d}v(\varphi) = 1$ for the OG-PPP/PLP-PPP. Since the vehicle locations follow a 1D PPP, with respect to the streets that pass through the origin, we have $1 - F_{R,\mathcal{V}_o^m}(r) = (e^{-2\lambda r})^{m/2}$.

A.4 Proof of Theorem 3.1

The probability that there are no vehicles on a stick $S(y, \varphi, h)$ within a distance r from the origin is $\exp(-\lambda|S(y, \varphi, h) \cap b(o, r)|_1)$. We derive $|S(y, \varphi, h) \cap b(o, r)|_1$ as follows: The midpoint y is denoted as (γ, ϕ) in polar coordinates. Using (3.5), we can express the points on a stick $S(y, \phi, h)$ of length $2h$ as $(\gamma\cos\phi + u\cos\varphi, \gamma\sin\phi + u\sin\varphi)$, $u \in (-h, h)$. Then the squared distance between a point on $S(y, \phi, h)$ and the origin is $\gamma^2 + u^2 + 2\gamma u\cos(\phi - \varphi)$. The points of intersection of $S(y, \varphi, h)$ on $b(o, r)$ are at distances $u_1, u_2 = |-\gamma\cos(\phi - \varphi) \pm \sqrt{r^2 - \gamma^2\sin^2(\phi - \varphi)}|$ from the midpoint of the stick. They follow from solving

$$\gamma^2 + u^2 + 2\gamma u\cos(\phi - \varphi) = r^2 \tag{A.4}$$

with respect to u. For a stick $S(y, \varphi, h)$ to intersect $b(o, r)$, y must be within $b(o, r+h)$. We consider two cases—$y \in b(o, r)$, and $y \in b(r, r + h)$:

1. $\boldsymbol{y \in b(o, r)}$: Let $|S(y, \varphi, h) \cap b(o, r)| \triangleq \ell_1$ for $y \in b(o, r)$. When

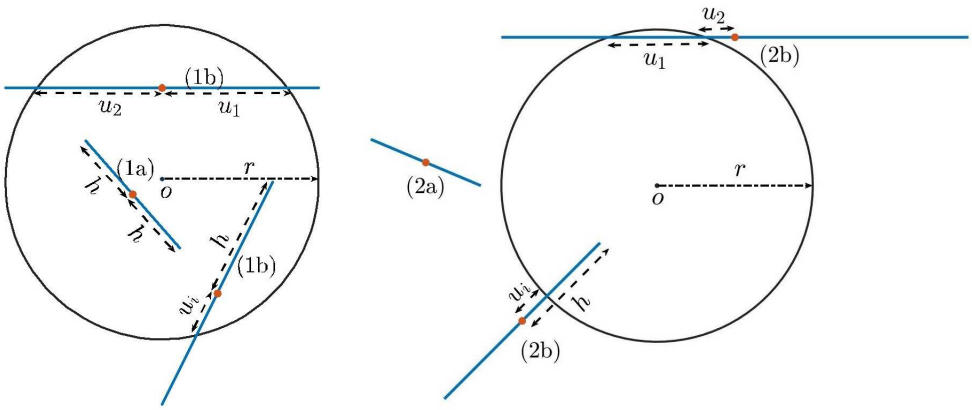

Figure A.2: Realizations corresponding to cases (1a), (1b), (2a), and (2b). The midpoints of the streets are highlighted using filled '$\circ$'. The points of intersection of the street on $b(o,r)$ are at distances u_i, $i \in \{1,2\}$, from the midpoint of the street. u_i in the cases (1b) and (2b) refers to u_1 or u_2.

a. $S(y,\varphi,h) \cap b(o,r) = S(y,\varphi,h)$: The stick lies within $b(o,r)$. Then $\ell_1(\gamma,\phi,\varphi) = 2h$.

b. $S(y,\varphi,h) \cap b(o,r) \subset S(y,\varphi,h)$: The stick is not fully contained in $b(o,r)$. For a stick that passes through $b(o,r)$, $\ell_1(\gamma,\phi,\varphi) = u_1 + u_2$. For a stick with only one endpoint in $b(o,r)$, $\ell_1(\gamma,\phi,\varphi) = u_1 + h$ or $h + u_2$.

Summarizing the above cases, we write $\ell_1(\gamma,\phi,\varphi) = \min(u_1,h) + \min(u_2,h)$.

2. $\boldsymbol{y \in b(r, r+h)}$: Let $|S(y,\varphi,h) \cap b(o,r)| \triangleq \ell_2$ for $y \in b(r, r+h)$. When

a. $S(y,\varphi,h) \cap b(o,r) = \emptyset$: The stick does not intersect $b(o,r)$. Then $\ell_2(\gamma,\phi,\varphi) = 0$.

b. $S(y,\varphi,h) \cap b(o,r) \subset S(y,\varphi,h)$: For a stick that passes through $b(o,r)$, $\ell_2(\gamma,\phi,\varphi) = |u_1 - u_2|$. For a stick with only one endpoint in $b(o,r)$, $\ell_2(\gamma,\phi,\varphi) = |u_1 - h|$ or $|h - u_2|$.

Thus, $\ell_2(\gamma,\phi,\varphi) = |\min(u_1,h) - \min(u_2,h)|$. Then the probability of not finding a vehicle on $S(y,\varphi,h)$ within $b(o,r)$ is $\exp(-\lambda\ell(\gamma,\phi,\varphi))$, where $\ell(\gamma,\phi,\varphi) = \ell_1(\gamma,\phi,\varphi)\mathbb{1}_{\gamma \le r} + \ell_2(\gamma,\phi,\varphi)\mathbb{1}_{r<\gamma\le r+h}$. Fig. A.2 illustrates the above cases.

For the typical vehicle's street to pass through or end at the origin, its midpoint must belong to $b(o,h)$. The midpoint of the typical vehicle's street of half-length h is at a distance $\gamma \in [0,h]$ from the origin. Using the above results and the decomposition

of the nearest-neighbor distance distribution in Lemma 3.5, we can write $1 - F_{R,\mathcal{V}_o^m}(r)$ and $1 - F_{R,\mathcal{V}_!}(r)$ as

$$1 - F_{R,\mathcal{V}_o^m}(r) = \mathbb{E}\Bigg[\prod_{k=1}^{m/2} \mathbb{E}\Bigg[\prod_{z\in V_k} 1\{z \notin b(o,r)\}\Bigg]\Bigg]$$
$$\stackrel{(a)}{=} \Bigg[\int_0^\infty \frac{1}{h} \int_0^h \exp(-\lambda \ell(\gamma,0,0))\tilde{f}_H(h)\mathrm{d}\gamma\mathrm{d}h\Bigg]^{m/2}, \tag{A.5}$$

$$1 - F_{R,\mathcal{V}_!}(r) = \exp\Bigg(-\frac{\mu}{\pi}\int_0^\infty\int_0^\pi\int_0^{2\pi}\int_0^{r+h} \exp(-\lambda\ell(\gamma,\phi,\varphi))\gamma f_H(h)\mathrm{d}\gamma\mathrm{d}\phi\mathrm{d}\varphi\mathrm{d}h\Bigg), \tag{A.6}$$

respectively, by applying the PGFL of the PPP.

Note that (a) in (A.5) follows from the facts that (i) the rotation of the typical vehicle's streets around the typical vehicle does not change u_1, u_2, and hence we can set $\phi = \varphi = 0$, and (ii) $m/2$ streets are independent. Substituting (A.5) and (A.6) in (3.9), we obtain (3.10).

A.5 Proof of Proposition 3.1

By (3.4), we can express the points on $L(x,\varphi)$ as $(x\cos\phi - u\sin\phi, x\sin\phi + u\cos\phi)$, $u \in \mathbb{R}$. Let x refer to the kth-nearest point in Φ_1 from the origin. Then V_k denotes the point process of vehicles on $L(x,\phi)$ (see Section 3.1.5). The Laplace transform of the interference $\mathcal{L}_{I_x}(s)$ from the vehicles on $L(x,\varphi)$ to the typical vehicle at the origin is

$$\mathcal{L}_{I_x}(s) = \mathbb{E}\Bigg[\prod_{z\in V_k} \mathbb{E}_{g_z}\left[\exp\left(-sg_z\|z\|^{-\alpha}B_z\right)\right]\Bigg]$$
$$= \mathbb{E}\Bigg[\prod_{z\in V_k: B_z=1} \frac{1}{1+s\|z\|^{-\alpha}}\Bigg] \tag{A.7}$$
$$\stackrel{(a)}{=} \exp\Bigg(-\lambda p\int_{-\infty}^{\infty} \frac{1}{1+\left(\frac{x^2+u^2}{s^\delta}\right)^{1/\delta}}\mathrm{d}u\Bigg)$$

$$\stackrel{(b)}{=} \exp\left(-\lambda p s^{\delta/2} \int_{\frac{x^2}{s^\delta}}^{\infty} \frac{1}{(1+v^{1/\delta})\sqrt{v-\frac{x^2}{s^\delta}}} \mathrm{d}v \right), \tag{A.8}$$

where $\delta = 2/\alpha$, (a) substitutes $\|z\|_2 = \|(x\cos\phi - u\sin\phi, x\sin\phi + u\cos\phi)\|_2$ and the PGFL of the PPP. λp is the intensity of the active transmitters for which $B_z = 1$, $z \in V_k$. (b) is due to the change of variable $v = \frac{x^2+u^2}{s^\delta}$.

We learned from (3.14) that the success probability is the product of the Laplace transforms of the interference I_o^m and I_{r}, which we derive below.

Laplace Transform of I_o^m: The Laplace transform of the interference from V_0 to the typical general vehicle (order 2) can be obtained by setting $x = 0$ in (A.8), *i.e.,*

$$\mathcal{L}_{I_o^2}(s) = \exp(-2\lambda p s^{\delta/2}\Gamma(1+\delta/2)\Gamma(1-\delta/2)). \tag{A.9}$$

For the typical intersection vehicle (order 4), as two streets pass through the origin, $\mathcal{V}_o^4 = V_0 \cup V_1$ (see Sec. 3.1.5). Then $\mathcal{L}_{I_o^4}(s)$ can be written as in (A.7) as

$$\begin{aligned}\mathcal{L}_{I_o^4}(s) &= \mathbb{E}\left[\prod_{z\in V_0\cup V_1 : B_z=1} \frac{1}{1+s\|z\|^{-\alpha}} \right] \\ &\stackrel{(c)}{=} \left(\mathbb{E}\left[\prod_{z\in V_0 : B_z=1} \frac{1}{1+s\|z\|^{-\alpha}} \right] \right)^2, \end{aligned} \tag{A.10}$$

which is the square of the success probability of the typical general vehicle given in (A.9). (c) results from V_0 being identically distributed as V_1.

Laplace Transform of I_{r}: The aggregate Laplace transform of the interference from the vehicles on all the streets that do not pass through the typical vehicle is given by

$$\begin{aligned}\mathcal{L}_{I_{\mathrm{r}}}(s) &= \mathbb{E}\left[\prod_{z\in\mathcal{V}_{\mathrm{r}}} \mathbb{E}_{g_z}\left[\exp\left(-s g_z \|z\|^{-\alpha} B_z \right) \right] \right] \\ &\stackrel{(e)}{=} \mathbb{E}\left[\prod_{k>m/2} \mathbb{E}\left[\prod_{z\in V_k : B_z=1} \frac{1}{1+s\|z\|^{-\alpha}} \right] \right] \end{aligned} \tag{A.11}$$

$$\stackrel{(f)}{=} \exp\bigg(-\mu \int_0^{\pi} \int_{-\infty}^{\infty} (1-\mathcal{L}_{I_x}(s))\,\mathrm{d}x\,\mathrm{d}\nu(\varphi)\bigg)$$
$$\stackrel{(g)}{=} \exp\bigg(-\mu \int_{-\infty}^{\infty} (1-\mathcal{L}_{I_x}(s))\,\mathrm{d}x\bigg), \tag{A.12}$$

where (e) follows from $\mathcal{V}_{\mathrm{r}} = \cup_{k>m/2} V_k$ and the fact that V_k's are independent 1D PPPs, (f) uses (A.8) and the PGFL of the PPP with respect to x and φ, and (g) results from $\mathcal{L}_{I_x}(s)$ being independent of φ, and $\int_{\mathbb{R}} \mathrm{d}\nu(\varphi) = 1$. Substituting (A.9), (A.10), and (A.12) in (3.14), we obtain (3.15).

A.6 Proof of Proposition 3.2

Using (3.5), we can denote the points on a stick $S(y,\phi,h)$ of length $2h$ as $(\gamma\cos\phi + u\cos\varphi, \gamma\sin\phi + u\sin\varphi)$, $u \in (-h,h)$. The midpoint of the street that passes through the typical vehicle is at a signed distance $W \sim \mathcal{U}(-h,h)$ from the origin. Then the endpoints of the street are at signed distances $-W-h$, and $-W+h$ to the origin. As in (A.7), the Laplace transform of the interference I_o^2 for the typical general vehicle can be written as

$$\mathcal{L}_{I_o^2}(s) = \mathbb{E}\bigg[\prod_{z\in\mathcal{V}_o : B_z=1} \frac{1}{1+s\|z\|^{-\alpha}}\bigg]$$
$$\stackrel{(a)}{=} \mathbb{E}_{H,W}\bigg[\exp\bigg(-\lambda p \int_{-W-H}^{-W+H} \frac{1}{1+\left(\frac{u}{s^{\delta/2}}\right)^{2/\delta}}\mathrm{d}u\bigg)\bigg] \tag{A.13}$$
$$\stackrel{(b)}{=} \mathbb{E}_{H,W}\bigg[\exp\bigg(-\lambda p s^{\delta/2} \int_{(-W-H)s^{-\delta/2}}^{(-W+H)s^{-\delta/2}} \frac{1}{1+v^{2/\delta}}\mathrm{d}v\bigg)\bigg], \tag{A.14}$$
$$\stackrel{(c)}{=} \int_0^{\infty} \frac{1}{2h} \int_{-h}^{h} \exp\bigg(-\lambda p s^{\delta/2} \int_{(-w-h)s^{-\delta/2}}^{(-w+h)s^{-\delta/2}} \frac{1}{1+v^{2/\delta}}\mathrm{d}v\bigg) \tilde{f}_H(h)\mathrm{d}w\,\mathrm{d}h, \tag{A.15}$$

where $\delta = 2/\alpha$, (a) substitutes $\|z\|_2 = \|(u\cos\varphi, u\sin\varphi)\|_2$ and applies the PGFL of the PPP, and (b) results from the change of variable $v = \frac{u}{s^{\delta/2}}$. (c) evaluates the expectation with respect to H using $\tilde{f}_H(h)$ rather than $f_H(h)$ based on Lemma 3.3. As two streets pass through the typical intersection vehicle and the point processes

on them are independent, the corresponding Laplace transform of the interference is the square of the success probability of the typical general vehicle given in (A.15) similar to (A.10).

A.7 Proof of Proposition 3.3

This proof uses the same notation as in Appendix A.6. Let $\mathcal{A} \triangleq \mathbb{R}^+ \times [0, 2\pi) \times [0, \pi) \times \mathbb{R}^+$ and $a = (\gamma, \phi, \varphi, h) \in \mathcal{A}$. From Section 3.1.5, we have V_k, $k > m/2$, denoting the point process of vehicles on the kth street $S(\gamma, \phi, \varphi, h)$ that does not pass through the origin. The Laplace transform of the interference $\mathcal{L}_{I_a}(s)$ from the vehicles on $S(\gamma, \phi, \varphi, h)$ is given by

$$\begin{aligned}\mathcal{L}_{I_a}(s) &= \mathbb{E}\Big[\prod_{z\in V_k: B_z=1} \frac{1}{1+s\|z\|^{-\alpha}}\Big] \\ &\overset{(a)}{=} \exp\bigg(-\lambda p \int_{-h}^{h} \frac{1}{1+\frac{(\gamma^2+u^2+2\gamma u\cos(\phi-\varphi))^{1/\delta}}{s}} \mathrm{d}u\bigg), \end{aligned} \tag{A.16}$$

where (a) applies the PGFL of the PPP and $\|z\|_2 = \|(\gamma\cos\phi + u\cos\varphi, \gamma\sin\phi + u\sin\varphi)\|_2$. Using (A.11), (A.16), and applying PGFL with respect to midpoints, orientations and half-lengths, we write the Laplace transform of the interference from $\mathcal{V}_{\mathrm{r}}$ as

$$\begin{aligned}\mathcal{L}_{I_{\mathrm{r}}}(s) &= \mathbb{E}\Big[\prod_{k>m/2} \mathbb{E}\Big[\prod_{z\in V_k: B_z=1} \frac{1}{1+s\|z\|^{-\alpha}}\Big]\Big] \\ &= \exp\bigg(-\frac{\mu}{\pi}\int_{\mathcal{A}} (1-\mathcal{L}_{I_a}(s))\gamma \tilde{f}_H(h)\mathrm{d}\mathcal{A}\bigg), \end{aligned} \tag{A.17}$$

where $\mathrm{d}\mathcal{A} = \mathrm{d}\gamma\mathrm{d}\phi\mathrm{d}\varphi\mathrm{d}h$.

A.8 Proof of Proposition 3.4

Success Probability of the Typical General Vehicle in the PLM-PPP We learned from Conjecture 1 that the probability of finding the n-th nearest neighbor closer is higher in the PSP-PPP than in the PLM-PPP. Consequently, the success probability of the typical general vehicle in the PLM-PPP is lower bounded by that in the PSP-PPP. As this inference is based on a conjecture, we present the result for the success probability of the typical general vehicle in the PLM-PPP as an approximation rather than a bound. By (3.12) and (3.14), we have

$$\begin{aligned} p_2^{\mathrm{PLM-PPP}} &= \mathcal{L}_{I_o^2+I_!}^{\mathrm{PLM-PPP}}(s) \\ &\approx \mathcal{L}_{I_o^2}^{\mathrm{PSP-PPP}}(s)\mathcal{L}_{I_!}^{\mathrm{PSP-PPP}}(s) \mid_{f_H(h)=\hat{f}_H(h)} . \end{aligned} \tag{A.18}$$

Success Probability of the Typical T-junction Vehicle in the PLM-PPP We have $\mathcal{V}_o^3 = V_0 \cup V_1$, where V_0 denote the vehicles on the street that passes through the origin, and V_1 denote the vehicles on the street with one endpoint at the T-junction. The success probability of the typical T-junction vehicle (order 3), $p_3^{\mathrm{PLM-PPP}}$, is given by

$$\begin{aligned} p_3 &= \mathbb{E}\left[\prod_{\substack{z\in V_0\cup V_1:\\ B_z=1}} \frac{1}{1+s\|z\|^{-\alpha}} \prod_{\substack{z\in \mathcal{V}_!:\\ B_z=1}} \frac{1}{1+s\|z\|^{-\alpha}}\right] \\ &\overset{(a)}{\approx} \mathbb{E}\left[\prod_{\substack{z\in V_0\cup \mathcal{V}_!:\\ B_z=1}} \frac{1}{1+s\|z\|^{-\alpha}}\right]\mathbb{E}\left[\prod_{\substack{z\in V_1:\\ B_z=1}} \frac{1}{1+s\|z\|^{-\alpha}}\right] \\ &\overset{(b)}{\approx} \mathcal{L}_{I_o^2}^{\mathrm{PSP-PPP}}(s)\mathcal{L}_{I_!}^{\mathrm{PSP-PPP}}(s)\mathbb{E}\left[\prod_{\substack{z\in V_1:\\ B_z=1}} \frac{1}{1+s\|z\|^{-\alpha}}\right] \\ &\overset{(c)}{=} \mathcal{L}_{I_o^2}^{\mathrm{PSP-PPP}}(s)\mathcal{L}_{I_!}^{\mathrm{PSP-PPP}}(s)\int_0^\infty \exp\left(-\lambda p s^{\delta/2}\int_0^{2hs^{-\delta/2}} \frac{1}{1+v^{2/\delta}}\mathrm{d}v\right)\hat{f}_H(h)\mathrm{d}h, \end{aligned} \tag{A.19}$$

where (a) assumes independence between V_1 and $V_0 \cup \mathcal{V}_!$, and (b) follows from (A.18).

The integral expression in (c) can be derived similarly to (A.14) using the detail that for the street whose one endpoint is a T-junction at the origin, its other endpoint is at a distance $2H$ from the origin. $\hat{f}_H(h)$ is the approximated density of the half-length of the street that ends at a T-junction.

A.9 Proof of Lemma 3.8

We can approximate $\mathcal{L}_{I_{\mathrm{r}}}(\theta D^{\alpha})$ (A.17) using Taylor's series as $\theta \to 0$ as

$$\mathcal{L}_{I_{\mathrm{r}}}(\theta D^{\alpha}) \sim 1 - \frac{\theta\mu\lambda p}{\pi} \int_0^{\infty}\int_0^{\pi}\int_0^{2\pi}\int_0^{\infty}\int_{-h}^{h} \left(\frac{D^2}{\gamma^2+u^2+2\gamma u\cos(\phi-\varphi)}\right)^{1/\delta} \gamma \tilde{f}_H(h)\mathrm{d}u\mathrm{d}\gamma\mathrm{d}\phi\mathrm{d}\varphi\mathrm{d}h$$
$$= 1 - \Theta(\theta). \tag{A.20}$$

Using (A.13) and (A.20), as $\theta \to 0$, the outage probability can be written as

$$\lim_{\theta\to 0} 1 - p_m = 1 - \lim_{\theta\to 0} \mathbb{E}_{H,W}\left[\exp\left(- \lambda p s^{\delta/2} \int_{(-W-H)s^{-\delta/2}}^{(-W+H)s^{-\delta/2}} \frac{1}{1+v^{2/\delta}}\mathrm{d}v\right)\right]^{m/2}$$
$$\overset{(a)}{=} 1 - \mathbb{E}_{H,W}\left[1 - \lambda p s^{\delta/2} \int_{(-W-H)s^{-\delta/2}}^{(-W+H)s^{-\delta/2}} \frac{1}{1+v^{2/\delta}}\mathrm{d}v\right]^{m/2}, \tag{A.21}$$

where (a) interchanges the limit and expectation (by the monotone convergence theorem), and applies the Taylor's theorem inside the expectation. We can further simplify (A.21) as $\theta \to 0$ as

$$1 - p_m \overset{(b)}{\sim} 1 - \mathbb{E}_{H,W}\left[1 - \frac{\lambda p s^{\delta/2}}{2} \int_{(-W-H)^2 s^{-\delta/2}}^{(-W+H)^2 s^{-\delta/2}} \frac{1}{(1+u^{1/\delta})\sqrt{u}}\mathrm{d}u\right]^{m/2} \tag{A.22}$$
$$\overset{(c)}{=} K_{\alpha}\lambda p s^{\delta/2}, \tag{A.23}$$

where (b) follows from the change of variable $u = v^2$, and (c) results from the integral in (A.22) evaluating to a constant K_α as $\theta \to 0$. Note that K_α depends on α.

A.10 Proof of Lemma 3.9

Consider a model $\mathcal{V}'$ formed by mapping all the points on each stick to its midpoint. The expected number of active transmitters on each stick is $2\lambda p\mathbb{E}[H]$. Since the midpoints follow a 2D PPP of intensity μ, $\mathcal{V}'$ forms a non-simple 2D PPP with density $2\mu\lambda p\mathbb{E}[H]$. It can be seen as a marked point process whose ground process is a 2D PPP of intensity μ and the marks $2\lambda p\mathbb{E}[H]$ refer to the multiplicity of the points. Let $\mathbb{M}$ define the mapping from $\mathcal{V}$ to $\mathcal{V}'$. Using (3.6) and (3.7), the success probability of the typical vehicle in the PSP-PPP can be expressed as

$$p_m^{\text{PSP}-\text{PPP}} = \mathbb{P}\bigg(g > D^\alpha \sum_{z\in\mathcal{V}} g_z \|\theta^{-1/\alpha} z\|^{-\alpha} B_z\bigg).$$

Similarly, the success probability of the typical vehicle in $\mathcal{V}'$ is written as

$$p_m^{\mathcal{V}'} = \mathbb{P}\bigg(g > D^\alpha \sum_{z\in\mathcal{V}} g_z \|\theta^{-1/\alpha} \mathbb{M}(z)\|^{-\alpha} B_z\bigg).$$

For sticks of half-length h, $|\|z\| - \|\mathbb{M}(z)\|| \le \|z - \mathbb{M}(z)\| \le h < \infty$. Then

$$|\|\theta^{-1/\alpha} z\| - \|\theta^{-1/\alpha}\mathbb{M}(z)\|| \to 0 \quad \text{as} \quad \theta \to \infty. \tag{A.24}$$

Then $p_m^{\text{PSP}-\text{PPP}} \to p_m^{\mathcal{V}'}$ as $\theta \to \infty$. The order m of the typical vehicle is irrelevant as the mapping $\mathbb{M}$ does not distinguish an intersection from a non-intersection. The success probability $p_m^{\mathcal{V}'}$ is obtained by substituting $\lambda_2 = 2\mu\lambda p\mathbb{E}[H]$ in (3.11).

APPENDIX B

PROOFS OF CHAPTER 4

B.1 Proof of Theorem 4.1

By (3.7) and (4.1), the conditional success probability can be expressed as

$$\begin{aligned} P_m^{\mathrm{PLP-PPP}}(\theta) &= \mathbb{P}(g > \theta D^\alpha I \mid I, \mathcal{V}) \\ &= \mathbb{E}_I[\exp(-\theta D^\alpha I) \mid \mathcal{V}] \\ &\overset{(a)}{=} \prod_{z\in\mathcal{V}} \left(\frac{p}{1+s\|z\|^{-\alpha}} + 1 - p\right)^b, \end{aligned} \tag{B.1}$$

where $s = \theta D^\alpha$, and (a) is obtained by averaging over ALOHA and fading. Then

$$\begin{aligned} M_{b,m}^{\mathrm{PLP-PPP}} &= \mathbb{E}[P_m(\theta)^b] \\ &= \mathbb{E}\Big[\prod_{z\in\mathcal{V}} \left(\frac{p}{1+s\|z\|^{-\alpha}} + 1 - p\right)^b\Big] \\ &\overset{(b)}{=} \underbrace{\mathbb{E}\Big[\prod_{z\in\mathcal{V}_o^m} \left(\frac{p}{1+s\|z\|^{-\alpha}} + 1 - p\right)^b\Big]}_{M_{b,m}^o} \underbrace{\mathbb{E}\Big[\prod_{z\in\mathcal{V}_!} \left(\frac{p}{1+s\|z\|^{-\alpha}} + 1 - p\right)^b\Big]}_{M_{b,m}^!}, \end{aligned} \tag{B.2}$$

where (b) follows from the independence of the 1D PPPs. $M_{b,m}^o$ and $M_{b,m}^!$ are the b-th moments with respect to the point processes $\mathcal{V}_o^m$ and $\mathcal{V}_!$. We have

$$\begin{aligned} M_{b,m}^o &\overset{(c)}{=} \exp\left(-2\lambda \int_0^\infty \left[1 - \left(\frac{p}{1+su^{-\alpha}} + 1 - p\right)^b\right] \mathrm{d}u\right) \\ &= \exp\left(-2\lambda \int_0^\infty \left[1 - \left(1 - \frac{ps}{u^\alpha + s}\right)^b\right] \mathrm{d}u\right) \end{aligned}$$

$$\stackrel{(d)}{=} \exp\bigg(-\lambda\delta \int_0^\infty \bigg[1 - \bigg(1 - \frac{ps}{v+s}\bigg)^b\bigg] v^{\delta/2-1} \mathrm{d}v\bigg), \tag{B.3}$$

where (c) applies $\|z\| = |(-u\sin\varphi, u\cos\varphi)|_2$, and the probability generating functional (PGFL) of the PPP and (d) is the result of substituting $v = u^\alpha$. Similarly, we can derive $M^!_{b,m}$ as

$$\begin{aligned} M^!_{b,m} &= \mathbb{E}\bigg[\prod_{z\in\mathcal{V}_!} \bigg(\frac{p}{1+s\|z\|^{-\alpha}} + 1 - p\bigg)^b\bigg] \\ &\stackrel{(e)}{=} \mathbb{E}\bigg[\exp\bigg(-\lambda \int_{\mathbb{R}} \bigg[1 - \bigg(\frac{p}{1+sg(t,u)^{-\alpha}} + 1 - p\bigg)^b\bigg] \mathrm{d}u\bigg)\bigg] \\ &\stackrel{(f)}{=} \exp\bigg(-2\mu \int_0^\infty (1 - G_b(t)) \mathrm{d}t\bigg), \end{aligned} \tag{B.4}$$

where $g(t,u) = t^2 + u^2$, $\|z\| = \|(t\cos\varphi - u\sin\varphi, t\sin\varphi + u\cos\varphi)\|_2$ in (e), (f) follows from the PGFL of the PPP, and

$$\begin{aligned} G_b(t) &= \exp\bigg(-2\lambda \int_0^\infty \bigg[1 - \bigg(\frac{p}{1+s(t^2+u^2)^{-\alpha}} + 1 - p\bigg)^b\bigg] \mathrm{d}u\bigg) \\ &= \exp\bigg(-2\lambda \int_0^\infty \bigg[1 - \bigg(1 - \frac{ps}{(t^2+u^2)^{1/\delta} + s}\bigg)^b\bigg] \mathrm{d}u\bigg) \\ &\stackrel{(g)}{=} \exp\bigg(-\lambda\delta \int_{t^{2/\delta}}^\infty \bigg[1 - \bigg(1 - \frac{ps}{v+s}\bigg)^b\bigg] \frac{v^{\delta-1}}{\sqrt{v^\delta - t^2}} \mathrm{d}v\bigg) \qquad \text{(B.5)} \\ &= \exp(-\lambda\delta F_b(t)), \qquad \text{(B.6)} \end{aligned}$$

where (g) follows from the change of the variable $v^2 = t^2 + u^2$. Note that $G_b(0) = M^o_{b,m}$. Using the binomial expansion, $F_b(t)$ can be expanded as [34]

$$F_b(t) = \sum_{k=1}^\infty \binom{b}{k} (ps)^k (-1)^{k+1} \int_{t^{2/\delta}}^\infty \frac{v^{\delta-1}}{(v+s)^k \sqrt{v^\delta - t^2}} \mathrm{d}v. \tag{B.7}$$

For $t = 0$, (B.6) reduces to

$$G_b(0) = \exp\bigg(- 2\lambda\theta^{\delta/2} D \frac{\pi\delta/2}{\sin(\pi\delta/2)} \sum_{k=1}^{\infty} \binom{b}{k} \binom{\delta/2-1}{k-1} p^k \bigg)$$
$$= \exp\bigg(- 2\lambda D \theta^{\delta/2} \Gamma(1+\delta/2)\Gamma(1-\delta/2) \mathfrak{D}_b(p, \delta/2) \bigg), \tag{B.8}$$

where $\mathfrak{D}_b(p, \delta/2) = \sum_{k=1}^{\infty} \binom{b}{k}\binom{\delta/2-1}{k-1} p^k = pb\,{}_2F_1(1-b, 1-\delta/2; 2; p)$. Substituting (B.8) for $M^o_{b,m}$ and (B.4) in (B.2), we obtain the result in Theorem 4.1.

B.2 Proof of Corollary 4.2

Corollary 4.2 states that the variance of the conditional success probabilities tends to zero as $p \to 0$ while λp is set to a constant C. By (B.2), the moment $M_{b,m}$ can be expressed as $M_{b,m} = M^o_{b,m} M^!_{b,m}$. The first term inside the exponential function in (4.6) refers to $M^o_{b,m}$ and the second term is $M^!_{b,m}$. $\mathfrak{D}_b(p, \delta/2) = p$ for $b = 1$ and $2p + (\delta/2 - 1)p^2$ for $b = 2$. Thus $M^o_{2,m} = (M^o_{1,m})^{2+(\delta/2-1)p}$. By (B.4), $M^!_{2,m} = \exp(-2\mu \int_0^{\infty} (1 - G_2(t)\mathrm{d}t)$, where

$$G_2(t) = \exp\bigg(- \lambda\delta \int_{t^{2/\delta}}^{\infty} \bigg[1 - \bigg(1 - \frac{ps}{v+s}\bigg)^2\bigg] \frac{v^{\delta-1}}{\sqrt{v^\delta - t^2}} \mathrm{d}v \bigg). \tag{B.9}$$

As $p \to 0$ with $\lambda p = C$, we have

$$\lim_{\substack{p\to 0 \\ \lambda p = C}} M^!_{2,m} = \exp\bigg(- 2\mu \lim_{\substack{p\to 0 \\ \lambda p = C}} \int_0^{\infty} (1 - G_2(t))\mathrm{d}t \bigg)$$
$$\overset{(a)}{=} \exp\bigg(- 4\mu\lambda\delta ps \int_{t^{2/\delta}}^{\infty} \frac{v^{\delta-1}}{(v+s)\sqrt{v^\delta - t^2}} \mathrm{d}v + o(p^2) \bigg)$$
$$\overset{(b)}{\approx} \exp\bigg(- 4\mu \lim_{\substack{p\to 0 \\ \lambda p = C}} \int_0^{\infty} (1 - G_1(t))\mathrm{d}t \bigg)$$
$$= (M^!_{1,m})^2, \tag{B.10}$$

where (a) applies Taylor's series and (b) follows from (B.5). Now, we are ready to

evaluate the variance $M_{2,m} - M_{1,m}^2$ of the conditional success probability.

$$\begin{aligned} M_{2,m} - M_{1,m}^2 &= (M_{1,m}^o)^{2+(\delta/2-1)p} M_{2,m}^! - (M_{1,m}^o M_{1,m}^!)^2 \\ &= (M_{1,m}^o)^2((M_{1,m}^o)^{(\delta/2-1)p} M_{2,m}^! - (M_{1,m}^!)^2). \end{aligned} \tag{B.11}$$

By (B.10), as $p \to 0$ with $\lambda p = C$, (B.11) reduces to

$$\lim_{\substack{p\to 0 \\ \lambda p = C}} (M_{1,m}^o M_{1,m}^!)^2((M_{1,m}^o)^{(\delta/2-1)p} - 1) = 0.$$

B.3 Proof of Theorem 4.3

We note that the first term in the product (4.7) with $m = 2$ is the success probability of the typical vehicle in the 1D PPP given by (4.9) with $b = 1$. For the typical intersection user, $m = 4$, as two independent 1D PPPs pass through the origin. Consequently, as $0 \le p_{\mathrm{s}} \le 1$, the success probability of the typical vehicle in the PLP-PPP is upper bounded by that of the 1D PPP.

As $\theta \to 0$, the first term in (4.7) can be approximated using Taylor's series as $1 - m\lambda p D\theta^{\delta/2}\Gamma(1+\delta/2)\Gamma(1-\delta/2)$. Applying Taylor's series to the second term in (4.7), we get

$$\begin{aligned} &\lim_{\theta\to 0} \exp\left(-2\mu \int_0^\infty \left(1 - \exp\left(-\lambda p D\theta^{\delta/2} \int_{\frac{t^2}{R^2\theta^\delta}}^\infty \frac{1}{(1+v^{1/\delta})\sqrt{v - \frac{t^2}{R^2\theta^\delta}}} \mathrm{d}v\right)\right) \mathrm{d}t\right) \\ &\approx 1 - 2\mu\lambda p D\theta^{\delta/2} \int_0^\infty \int_{\frac{t^2}{R^2\theta^\delta}}^\infty \frac{1}{(1+v^{1/\delta})\sqrt{v - \frac{t^2}{R^2\theta^\delta}}} \mathrm{d}v\, \mathrm{d}t \\ &= 1 - o(\theta^{\delta/2}), \end{aligned}$$

since $\frac{t^2}{R^2\theta^\delta} \to \infty$ as $\theta \to 0$. Then we can express $p_{\mathrm{s}}^{\mathrm{PLP-PPP}}$ as

$$1 - p_{\mathrm{s}}^{\mathrm{PLP-PPP}} \sim m\lambda p D\theta^{\delta/2}\Gamma(1+\delta/2)\Gamma(1-\delta/2), \quad \theta \to 0. \tag{B.12}$$

Similarly, we can approximate (4.9) with $b = 1$ as

$$1 - p_{\mathrm{s}}^{\Phi_d} \sim c_d \lambda_d D^d \theta^{\delta'} \Gamma(1+\delta')\Gamma(1-\delta'), \quad \theta \to 0. \tag{B.13}$$

Setting $\delta/2 = \delta' = 1/\alpha$ *i.e.,* $d = 1$ ($m = c_1 = 2$), and $\lambda p = \lambda_1$ in (B.12), we obtain (B.13), which refers to a 1D PPP or a single street. For the typical intersection user, $m = 4$.

B.4 Proof of Theorem 4.4

Intuitively, as $\theta \to \infty$, for SIR $> \theta$, there should not be any interferers in a large disk around the user. It follows from (4.13) that the pair correlation function $g^{\mathrm{PLP-PPP}}(r) \to 1$ as $r \to \infty$, exhibiting a Poisson network-like behavior. Hence the PLP-PPP behaves like a 2D PPP as $\theta \to \infty$. A rigorous proof follows.

Let G_u denote an orthogonal grid with the locations of the lines $u \in \mathbb{Z}$, *i.e.,* u is the x-intercept or y-intercept of the line. The vehicles on each line form a 1D PPP. One way of obtaining such a model is to start with a 2D PPP Φ_2 and quantize one of the coordinates of the points with equal probability (Definition 2.2). Similarly, we can generate the PLP-PPP from a 2D PPP.

In the PLP-PPP, the locations of the streets are characterized by x, which follows a 1D PPP Φ_1 of intensity μ. This implies that the distances between the points in Φ_1 are exponentially distributed. With each x, there is an associated orientation φ i.i.d. on $[0, \pi)$. Then, by rotating the lines in the orthogonal grid with exponential spacing G_e, we can obtain the PLP-PPP. However, direct mapping from Φ_2 to G_e would result in an inhomogeneous distribution of points on the streets.

Let $\mathcal{M} : \Phi_2 \to \mathcal{V}_u \to \mathcal{V}$ define the mapping from a 2D PPP to the PLP-PPP, where $\mathcal{V}_u$ and $\mathcal{V}$ denote the locations of the transmitters in G_u and the PLP-PPP, respectively. We order the streets based on their perpendicular distances to the origin.

By $\Phi_2 \to \mathcal{V}_u$, the points on Φ_2 are translated to G_u through the quantization process described above. The mapping $\mathcal{V}_u \to \mathcal{V}$ involves two steps: 1) The points on the ith street on the grid G_u are translated to the ith street on the grid G_e. 2) Each line is rotated independently such that φ is i.i.d. on $[0, \pi)$.

From (3.6) and (3.7), the success probability is given by

$$p_m^{\text{PLP}-\text{PPP}} = \mathbb{P}\bigg(g > D^\alpha \sum_{z \in \mathcal{V}} g_z \|\theta^{-1/\alpha} z\|^{-\alpha} B_z\bigg). \tag{B.14}$$

Using the mapping function $\mathcal{M}$, we can express (B.14) as

$$p_m^{\text{PLP}-\text{PPP}} = \mathbb{P}\bigg(g > D^\alpha \sum_{z \in \Phi_2} g_z \|\theta^{-1/\alpha} \mathcal{M}(z)\|^{-\alpha} B_z\bigg). \tag{B.15}$$

The success probability of the typical vehicle in Φ_2 is

$$p_{\text{s}}{}^{\Phi_2} = \mathbb{P}\bigg(g > D^\alpha \sum_{z \in \Phi_2} g_z \|\theta^{-1/\alpha} z\|^{-\alpha} B_z\bigg). \tag{B.16}$$

The mapping $\Phi_2 \to \mathcal{V}_u$ displaces each point by at most $1/2$ as $u \in \mathbb{Z}$. Since the exponential distribution has a finite variance and the PLP is isotropic, the mapping $\mathcal{V}_u \to \mathcal{V}$ translates the points in $\mathcal{V}_u$ only by a finite distance. Then, by the Cauchy-Schwarz inequality, $|\|z\| - \|\mathcal{M}(z)\|| \leq \|z - \mathcal{M}(z)\| < \infty$. Multiplying by $\theta^{-1/\alpha}$, we obtain

$$|\|\theta^{-1/\alpha} z\| - \|\theta^{-1/\alpha} \mathcal{M}(z)\|| \to 0 \quad \text{as} \quad \theta \to \infty. \tag{B.17}$$

Applying (B.17) to (B.15) and (B.16), we infer that the interference experienced by the typical general/intersection user in the PLP-PPP tends to that of in a 2D PPP as $\theta \to \infty$. Note that the type of user does not matter since the mapping does not affect the points of Φ_2 as $\theta \to \infty$, *i.e.*, there is no difference between a general user and an intersection user. Hence the success probability in the PLP-PPP tends to

that in Φ_2 with intensity $\lambda p \mu$ (Lemma 3.1).

APPENDIX C

PROOFS OF CHAPTER 5

C.1 Proof of Lemma 5.1

We can express the mean number of points as

$$\begin{aligned}\mathbb{E}|\mathcal{X}| &= \mathbb{E}\left[\sum_{i=1}^{N} \mathbb{1}(y_i \in \mathcal{X})\right] \\ &= \sum_{i=1}^{N} \mathbb{E}[\mathbb{1}(y_i \in \mathcal{X})] \\ &= \sum_{i=1}^{N} \mathbb{P}(\{y_i\} \subseteq \mathcal{X}) \\ &\overset{(a)}{=} \sum_{i=1}^{N} K_{ii} = \operatorname{tr}(K) \overset{(b)}{=} \sum_{i=1}^{N} \frac{\varepsilon_i}{1+\varepsilon_i},\end{aligned}$$

where (a) follows from Definition 5.1 and (b) follows from the eigendecomposition of K. $\operatorname{tr}(K)$ denotes the trace of K.

C.2 Proof of Lemma 5.2

The matrix K can be written in terms of blocks as $K = \begin{bmatrix} K_A & K_C^T \\ K_C & K_D \end{bmatrix}$. Without loss of generality, we assume $A = \{x_1\}$ and $D = \mathcal{X} \setminus A$. The conditional marginals of observing D given A has been observed are given by

$$\mathbb{P}(D \subseteq Y \mid A \subseteq Y) = \frac{\mathbb{P}(A \cup D \subseteq Y)}{\mathbb{P}(A \subseteq Y)}$$

$$\stackrel{(a)}{=} \frac{\det(K_{A\cup D})}{\det(K_A)}$$
$$\stackrel{(b)}{=} \det(K_D - K_C K_A^{-1} K_{C^T}),$$

where (a) follows from Definition 5.1 and (b) uses the Schur complement of K. Then, $D \mid A \sim \mathrm{DPP}(K_D - K_C K_A^{-1} K_{C^T})$.

BIBLIOGRAPHY

1. S. S. Kalamkar and M. Haenggi. The spatial outage capacity of wireless networks. *IEEE Transactions on Wireless Communications*, 17(6):3709–3722, Jun. 2018.

2. Technical report, Association for safe international road travel. URL `https://www.asirt.org/safe-travel/road-safety-facts/`.

3. J. Harding, G. Powell, R. Yoon, J. Fikentscher, C. Doyle, D. Sade, M. Lukuc, J. Simons, and J. Wang. Vehicle-to-vehicle communications: Readiness of V2V technology for application. Technical report, 2014. URL `https://rosap.ntl.bts.gov/view/dot/27999`.

4. M. Haenggi. *Stochastic Geometry for Wireless Networks*. Cambridge University Press, 2012.

5. H. ElSawy, E. Hossain, and M. Haenggi. Stochastic geometry for modeling, analysis, and design of multi-tier and cognitive cellular wireless networks: A survey. *IEEE Communications Surveys Tutorials*, 15(3):996–1019, Mar. 2013.

6. Z. Tong, H. Lu, M. Haenggi, and C. Poellabauer. A stochastic geometry approach to the modeling of DSRC for vehicular safety communication. *IEEE Transactions on Intelligent Transportation Systems*, 17(5):1448–1458, May 2016.

7. K. Koufos and C. P. Dettmann. Mean and variance of interference in vehicular networks with hardcore headway distance. *IEEE Transactions on Wireless Communications*, 17(12):8330–8341, Oct. 2018.

8. J. P. Jeyaraj and M. Haenggi. Reliability analysis of V2V communications on orthogonal street systems. In *2017 IEEE Global Communications Conference (GLOBECOM)*, Singapore, Dec. 2017.

9. J. P. Jeyaraj and M. Haenggi. Nearest-vehicle communication in regular street systems. In *2018 IEEE 88th Vehicular Technology Conference (VTC-Fall)*, Chicago, USA, Aug. 2018.

10. C. Jiang, H. Zhang, Z. Han, Y. Ren, V. C. M. Leung, and L. Hanzo. Information-sharing outage-probability analysis of vehicular networks. *IEEE Transactions on Vehicular Technology*, 65(12):9479–9492, Dec. 2016.

11. J. P. Jeyaraj and M. Haenggi. Cox models for vehicular networks: SIR performance and equivalence. *IEEE Transactions on Wireless Communications*, 20(1): 171–185, Jan. 2021.

12. J. P. Jeyaraj and M. Haenggi. A transdimensional Poisson model for vehicular networks. In *2019 IEEE Global Communications Conference (GLOBECOM)*, Waikoloa, HI, USA, Dec. 2019.

13. J. P. Jeyaraj, M. Haenggi, A. H. Sakr, and H. Lu. The transdimensional Poisson process for vehicular network analysis. *IEEE Transactions on Wireless Communications*, 2021. Early Access.

14. M. Haenggi. Simalysis: Symbiosis of simulation and analysis. *Stogblog by M. Haenggi*, Oct. 2020. URL `https://stogblog.net/2020/10/15/simalysis-symbiosis-of-simulation-and-analysis/`.

15. Y. Jeong, J. W. Chong, H. Shin, and M. Z. Win. Intervehicle communication: Cox-Fox modeling. *IEEE Journal on Selected Areas in Communications*, 31(9): 418–433, Sep. 2013.

16. B. Błaszczyszyn, P. Mühlethaler, and Y. Toor. Stochastic analysis of ALOHA in vehicular ad hoc networks. *Annals of Telecommunications*, 68(1):95–106, 2013.

17. A. Al-Hourani, R. J. Evans, S. Kandeepan, B. Moran, and H. Eltom. Stochastic geometry methods for modeling automotive radar interference. *IEEE Transactions on Intelligent Transportation Systems*, 19(2):333–344, Feb. 2018.

18. M. J. Farooq, H. ElSawy, and M. Alouini. A stochastic geometry model for multi-hop highway vehicular communication. *IEEE Transactions on Wireless Communications*, 15(3):2276–2291, Nov. 2016.

19. M. Giordani, M. Rebato, A. Zanella, and M. Zorzi. Coverage and connectivity analysis of millimeter wave vehicular networks. *Ad Hoc Networks*, 80:158–171, 2018.

20. E. Steinmetz, M. Wildemeersch, T. Q. S. Quek, and H. Wymeersch. A stochastic geometry model for vehicular communication near intersections. In *2015 IEEE Globecom Workshops*, San Diego, CA,USA, Dec. 2015.

21. Q. Cui, N. Wang, and M. Haenggi. Vehicle distributions in large and small cities: Spatial models and applications. *IEEE Transactions on Vehicular Technology*, 67(11):10176–10189, Nov. 2018.

22. P. Crucitti, V. Latora, and S. Porta. Centrality in networks of urban streets. *Chaos: An Interdisciplinary Journal of Nonlinear Science*, 16(1):0151131–0151139, Mar. 2006.

23. V. V. Chetlur and H. S. Dhillon. Coverage analysis of a vehicular network modeled as Cox process driven by Poisson line process. *IEEE Transactions on Wireless Communications*, 17(7):4401–4416, Jul. 2018.

24. F. Morlot. A population model based on a Poisson line tessellation. In *2012 International Symposium on Modeling and Optimization in Mobile, Ad Hoc and Wireless Networks (WiOpt)*, pages 337–342, May 2012.

25. C. Choi and F. Baccelli. An analytical framework for coverage in cellular networks leveraging vehicles. *IEEE Transactions on Communications*, 66(10):4950–4964, Oct. 2018.

26. V. V. Chetlur and H. S. Dhillon. Coverage and rate analysis of downlink cellular vehicle-to-everything (C-V2X) communication. *IEEE Transactions on Wireless Communications*, 19(3):1738–1753, Mar. 2020.

27. V. V. Chetlur and H. S. Dhillon. Success probability and area spectral efficiency of a VANET modeled as a Cox process. *IEEE Wireless Communications Letters*, 7(5):856–859, Oct. 2018.

28. C. Choi and F. Baccelli. Poisson Cox point processes for vehicular networks. *IEEE Transactions on Vehicular Technology*, 67(10):10160–10165, Oct. 2018.

29. M. N. Sial, Y. Deng, J. Ahmed, A. Nallanathan, and M. Dohler. Stochastic geometry modeling of cellular V2X communication over shared channels. *IEEE Transactions on Vehicular Technology*, 68(12):11873–11887, Dec. 2019.

30. F. Voss, C. Gloaguen, F. Fleischer, and V. Schmidt. Distributional properties of Euclidean distances in wireless networks involving road systems. *IEEE Journal on Selected Areas in Communications*, 27(7):1047–1055, Sep. 2009.

31. D. J. Daley, S. Ebert, and G. Last. Two lilypond systems of finite line-segments. *Probability and Mathematical Statistics*, 36(2):221–246, 2016.

32. P. Parker and R. Cowan. Some properties of line segment processes. *Journal of Applied Probability*, 13(1):96–107, 1976.

33. W. E. Stein and R. Dattero. Sampling bias and the inspection paradox. *Mathematics Magazine*, 58(2):96–99, 1985.

34. M. Haenggi. The meta distribution of the SIR in Poisson bipolar and cellular networks. *IEEE Transactions on Wireless Communications*, 15(4):2577–2589, Apr. 2016.

35. M. Haenggi. Meta distributions—Part 1: Definition and examples. *IEEE Communications Letters*, 25(7):2089–2093, July. 2021.

36. M. Haenggi. Meta distributions—Part 2: Properties and interpretations. *IEEE Communications Letters*, 25(7):2094–2098, July. 2021.

37. N. Deng and M. Haenggi. The energy and rate meta distributions in wirelessly powered D2D networks. *IEEE Journal on Selected Areas in Communications*, 37 (2):269–282, Feb. 2019.

38. K. Koufos and C. P. Dettmann. The meta distribution of the SIR in linear motorway VANETs. *IEEE Transactions on Communications*, 67(12):8696–8706, Sep. 2019.

39. M. Abdulla and H. Wymeersch. Fine-grained vs. average reliability for V2V communications around intersections. In *2017 IEEE Globecom Workshops (GC Wkshps)*, Singapore, Dec. 2017.

40. X. Liu and A. Jaekel. Congestion control in V2V safety communication: Problem, analysis, approaches. *MDPI Electronics*, 8(5):540, May 2019.

41. D. Stoyan, W. S. Kendall, and J. Mecke. *Stochastic geometry and its applications*. John Wiley & Sons, 1987.

42. X. Zhang and M. Haenggi. The performance of successive interference cancellation in random wireless networks. *IEEE Transactions on Information Theory*, 60(10):6368–6388, Oct. 2014.

43. B. Błaszczyszyn, M. K. Karray, and H. P. Keeler. Wireless networks appear Poissonian due to strong shadowing. *IEEE Transactions on Wireless Communications*, 14(8):4379–4390, Aug. 2015.

44. M. Noor-A-Rahim, Z. Liu, H. Lee, G. G. M. N. Ali, D. Pesch, and P. Xiao. A survey on resource allocation in vehicular networks. *IEEE Transactions on Intelligent Transportation Systems*, 2020. Early Access.

45. M. H. C. Garcia, A. Molina-Galan, M. Boban, J. Gozalvez, B. Coll-Perales, T. Şahin, and A. Kousaridas. A tutorial on 5G NR V2X communications. *IEEE Communications Surveys Tutorials*, 23(3):1972–2026, Feb. 2021.

46. K. Koufos and C. P. Dettmann. Performance of a link in a field of vehicular interferers with hardcore headway distance. *IEEE Transactions on Intelligent Transportation Systems*, 2020. Early Access.

47. ns-3 network simulator. `https://www.nsnam.org/`. Accessed: Aug. 2021.

48. A. Borodin. Determinantal point processes. 2009. URL `https://arxiv.org/abs/0911.1153`.

49. F. Lavancier, J. Møller, and E. Rubak. Determinantal point process models and statistical inference. *Journal of the Royal Statistical Society: Series B (Statistical Methodology)*, 77(4):853–877, Dec. 2014.

50. N. Deng, W. Zhou, and M. Haenggi. The Ginibre point process as a model for wireless networks with repulsion. *IEEE Transactions on Wireless Communications*, 14(1):107–121, Jun. 2015.

51. Y. Li, F. Baccelli, H. S. Dhillon, and J. G. Andrews. Statistical modeling and probabilistic analysis of cellular networks with determinantal point processes. *IEEE Transactions on Communications*, 63(9):3405–3422, Jul. 2015.

52. A. Kulesza and B. Taskar. *Determinantal Point Processes for Machine Learning*. Now Publishers Inc., 2012.

53. B. Błaszczyszyn and H. P. Keeler. Determinantal thinning of point processes with network learning applications. In *2019 IEEE Wireless Communications and Networking Conference (WCNC)*, Marrakesh, Morocco, Apr. 2019.

54. B. Błaszczyszyn, A. Brochard, and H. P. Keeler. Coverage probability in wireless networks with determinantal scheduling. In *2020 18th International Symposium on Modeling and Optimization in Mobile, Ad Hoc, and Wireless Networks (WiOPT)*, Volos, Greece, Jun. 2020.

55. C. Saha and H. S. Dhillon. Machine learning meets stochastic geometry: Determinantal subset selection for wireless networks. In *2019 IEEE Global Communications Conference (GLOBECOM)*, Waikoloa, HI, USA, Dec. 2019.

56. A. M. Voicu, L. Simić, and M. Petrova. Modelling large-scale CSMA wireless networks. In *2021 IEEE Wireless Communications and Networking Conference (WCNC)*, Nanjing, China, May 2021.

57. S. Sharafkandi, G. Bansal, J. B. Kenney, and D. H. C. Du. Using EDCA to improve vehicle safety messaging. In *2012 IEEE Vehicular Networking Conference (VNC)*, Seoul, South Korea, Nov. 2012.

58. M. Malinverno, F. Raviglione, C. Casetti, C. Chiasserini, J. Mangues-Bafalluy, and M. Requena-Esteso. A multi-stack simulation framework for vehicular applications testing. In *Proceedings of the 10th ACM Symposium on Design and Analysis of Intelligent Vehicular Networks and Applications*, DIVANet '20, Alicante, Spain, Nov. 2020.

59. H. S. Dhillon, R. K. Ganti, F. Baccelli, and J. G. Andrews. Modeling and analysis of k-tier downlink heterogeneous cellular networks. *IEEE Journal on Selected Areas in Communications*, 30(3):550–560, Mar. 2012.

60. S. S. Kalamkar and M. Haenggi. Simple approximations of the SIR meta distribution in general cellular networks. *IEEE Transactions on Communications*, 67 (6):4393–4406, Feb. 2019.

61. A. Borodin and E. M. Rains. Eynard-Mehta theorem, Schur process, and their Pfaffian analogs. *Journal of Statistical Physics*, 121(3–4):291–317, Nov. 2005.

62. J. B. Hough, M. Krishnapur, Y. Peres, and B. Virág. Determinantal processes and independence. *Probability Surveys*, 3:206–209, May 2006.

63. T. Shirai and Y. Takahashi. Random point fields associated with certain Fredholm determinants II: Fermion shifts and their ergodic and Gibbs properties. *The Annals of Probability*, 31(3):1533–1564, Jul. 2003.